Development and Performance Analysis of Thin Film Semi-Transparent Solar Photovoltaic Window System

Ph.D. Thesis

Sankar Barman
ID No. 2014REN9507

CENTRE FOR ENERGY AND ENVIRONMENT
MALAVIYA NATIONAL INSTITUTE OF TECHNOLOGY JAIPUR

August 2018

Dedicated to my elder brother

Naba Kumar Barman

Development and Performance Analysis of Thin Film Semi-Transparent Solar Photovoltaic Window System

Submitted in

fulfilment of the requirements for the degree of

Doctor of Philosophy

by

Sankar Barman

ID:2014REN9507

Under the supervision of

Dr.-Ing Jyotirmay Mathur

Professor
Centre for Energy and Environment
MNIT Jaipur

Dr. Sanjay Mathur

Professor
Centre for Energy and Environment
MNIT Jaipur

CENTRE FOR ENERGY AND ENVIRONMENT

MALAVIYA NATIONAL INSTITUTE OF TECHNOLOGY JAIPUR

August 2018

DECLARATION

I, Sankar Barman, declare that this thesis titled, **"Development and Performance Analysis of Thin Film Semi-Transparent Solar Photovoltaic Window System"** and the work presented in it, are my own. I confirm that:

- This work was done wholly or mainly while in candidature for a research degree at this university.
- Where any part of this thesis has previously been submitted for a degree or any other qualification at this university or any other institution, this has been clearly stated.
- Where I have consulted the published work of others, this is always clearly attributed.
- Where I have quoted from the work of others, the source is always given. With the exception of such quotations, this thesis is entirely my own work.
- I have acknowledged all main sources of help.
- Where the thesis is based on work done by myself, jointly with others, I have made clear exactly what was done by others and what I have contributed myself

Date:

Sankar Barman
ID:2014REN9507

CERTIFICATE

This is to certify that the thesis entitled " **Development and Performance Analysis of Thin Film Semi-Transparent Solar Photovoltaic Window System**" being submitted by **Sankar Barman (2014REN9507)** is a bonafide research work carried out under our supervision and guidance in fulfilment of the requirement for the award of the degree of **Doctor of Philosophy** in the Department of **Centre for Energy and Environment**, Malaviya National Institute of Technology Jaipur, India. The matter embodied in this thesis is original and has not been submitted to any other University or Institute for the award of any other degree.

Place: Jaipur
Date:

Dr.-Ing Jyotirmay Mathur
Professor
Centre for Energy and Environment
MNIT Jaipur

Dr. Sanjay Mathur
Professor
Centre for Energy and Environment
MNIT Jaipur

ACKNOWLEDGMENT

This thesis would not have come to its completion without the support and encouragement of numerous people. At this stage, I would like to take the opportunity to express my gratitude to all those people who made this thesis possible and an unforgettable experience for me directly or indirectly.

At this moment of accomplishment, first and foremost, I would like to acknowledge, with a deep sense of heartfelt gratitude to my supervisors, **Prof. Jyotirmay Mathur,** Professor and **Dr. Sanjay Mathur**, Associate Professor at Centre for Energy and Environment. This work would not have been possible without their guidance, support and encouragement. Under their guidance, I have overcome successfully many difficulties and learned a lot. Despite being very busy, they reviewed my thesis progress, gave their valuable suggestions and made corrections even during late hours. Their persistent courage and opinion will always inspire me, and I hope to continue to work with these noble thoughts. I can only say proper thanks to them through my future activities.

I am extremely indebted and thankful to **Dr. Amartya Chowdhury,** Assistant Professor at Centre for Energy and Environment, for his guidance throughout my journey of the research. He provided the valuable suggestions in planning my research work at the initial stages. He constantly encouraged and supported me in all possible ways.

I also appreciate and heartily thank all other faculty members of Centre for Energy and Environment, MNIT Jaipur. I am thankful to my fellow research scholars **Dr. Rajesh Chedwal, Dr. Sanjay, Shashank Vyas, Mayank Bhatnagar, Partha Das, Prateek Srivastava, Priyam Tewari, Avinash Kumar, Ranaveer Singh, Shitanshu Sapre, Mayank Vyas and Falti Teotia** who were always there when I really needed. Thanks don't seem sufficient, but it is said with appreciation and respect to them for their support, care, understanding and valuable friendship.

I am very fortunate to have the opportunity to work in the Center for Building Energy Research and Development (**CBERD**) project funded by the Indian Ministry of Science

and Technology and U.S. Department of Energy and administered by Indo-US Science and Technology Forum in India.

I am thankful to all technical, non-technical staff of **CBERD** project and Centre for Energy and Environment, MNIT Jaipur namely **Kamlesh Jagratwal**, **Dharmendera Kumawat, Sunita Sharma, Sanjay Chettri, Yasin Khan, Deepak Sharma, Abhishek Sharma, Rajendera Prasad and Narendra Sharma** for supporting and helping me throughout the research work.

I am also thankful to all the people who have knowingly and unknowingly helped me in the successful completion of this thesis.

Last but not least, I would like to pay high regards to my **family** for their inspiration and motivation throughout my work and lifting me uphill this phase of life. I owe everything to them. I am grateful to my wife **Pranati Medhi Barman** for her understanding and moral support: and my daughter **Nitashree Barman**. I appreciate my wife for her patience, encouragement and the pains taken during the whole journey.

ABSTRACT

The Indian building sector accounts for about one-third of the total energy consumption in the country. The energy demand of the country is envisaged to increase with the growth of the economy, urbanization and living standard. Further, to meet the energy demands, India largely depends upon imported fossil fuels. Burning of fossil fuels adversely affect the environment. Therefore, given the importance of energy in today's scenario, it is imperative and urgent to find some alternative solutions for buildings which lead to efficient use of energy as well as less dependent on the fossil fuels without compromising the occupant's comforts.

The Semi-Transparent Photovoltaic (STPV) module integrated into the vertical envelope of a building can play a significant role in managing the energy demand of that building. However, the performance of an STPV system is subjected to different factors like amount of incident radiation, Angle of Incidence (AOI), type of incident spectrum, and the cell operating temperature. Also, the optimal opto-thermal characteristics of STPV module for window application changes with the climate of the installed location. Therefore, a serious need was felt to investigate the performance of thin film STPV module integrated window systems under various design and operating conditions by using a simplified approach.

Cadmium Telluride (CdTe) based STPV module was selected to explore the goals of the present research. Using the chosen STPV module with one Low-e and clear glass, four double pane window configurations were investigated. Two different modes of ventilation strategies were also considered to evacuate the hot air from the window cavity. Initially, the measured material characteristics were processed in the software like Optics6 and WINDOW7.3. Subsequently, the whole building simulation was carried out using the 'EnergyPlus' software. The electrical energy generation was calculated by applying the concept of wavelength dependent short-circuit current density and Quantum Efficiency (QE) of the solar cell. An experimental setup built on the campus of Malaviya National Institute of Technology, Jaipur, India was used to validate the simulation model.

In the present research, the energy generation observed to be affected more dominantly by AOI and cell operating temperature. The effect of AOI which is also known as an

angular loss increases significantly for AOI beyond 70^0. Orientation wise, the AOI effect the most in the south. Further, with an increase in STPV module transmittance, the effect of AOI get reduced. For example, compared to the normal incidence, the annual energy reduced by 6.4 and 2.3 kWh/m^2 for STPV module of transmittance 6.0% and 27.5% respectively at Jaipur. Due to a high cell operating temperature, the annual energy generation was observed to be decreased by 4.8%. The conversion efficiency and hence power generation are also affected by the incident radiation. Due to this factor, the energy generation is found to be lowered by 3.0% in the present study. As per effect of the incident spectrum on energy generation is considered, it has been positive for more precipitable water content in the atmosphere. When the effect of all the four parameters is considered, the annual energy generation reduced from 106 kWh/m^2 to 95.3 kWh/m^2 for the window systems with STPV module having 17.7% visible transmittance. This reduction is accounted for 10.0 % per annum.

Among all the proposed window configurations, the cell operating temperature has observed to be minimum for the configuration having Low-e glass in front of the STPV module. However, due to blocking of some useful wavelength along with the non-productive part of the incident radiation, this window configuration generates relatively low electrical energy. Nevertheless, the energy generation has been lowered by only 10.6% against 35.3% reduction in the amount of incident radiation. With the introduction of air flow through the window air cavity, the module temperature decreases. The maximum drop of 3.8^0C has been observed when hot cavity air is ejected into the outside environment. Also, the room temperature was found to be increased by 2^0C in the winter day with a particular airflow strategy.

In the present research, the maximum photovoltaic energy generation has been 119.6 kWh/m^2/yr. This generation occurred with the window system having the least transparent STPV module in the south orientation. As far as the effectiveness of daylighting is considered, it has been more sensitive to module transparency than Window to Wall Ratio (WWR). Similarly, the patterns of cooling and heating demands showed opposite trends in transparency and WWR. Finally, compared to a standard window as per Energy Conservation of Building Code (ECBC) of India, a maximum energy saving of 60.4% has been observed in the present research. However, with the STPV window systems having a reasonable level of VLT and most commonly used WWR (30%), the energy saving is found to be 37.6%.

The findings of the present research suggest that besides the module temperature, the performance of the STPV module integrated window system is influenced by several other factors along with design and operating conditions. Therefore, proper optimization should be undertaken before installing a system in the actual field. The research also showed that there is high energy saving potential of CdTe based STPV module integrated window system in the daytime used buildings of composite climate. Implementation of these systems will help in converting the buildings into low or net-zero energy establishments. Eventually, it will contribute towards achieving the goals of smart and sustainable cities.

TABLE OF CONTENTS

LIST OF FIGURES

LIST OF TABLES

ABBREVIATIONS

Notation	Description
ALEC	Artificial Lighting Energy Consumption
a-Si	Amorphous Silicon
AOI	Angle of Incidence
BIPV	Building Integrated Photovoltaic
BIS	Bureau of Indian Standards
CL	Clear Glass
CTF	Conductive Transfer Function
CdTe	Cadmium Telluride
CIGS	Copper Indium Gallium Diselenide
CRI	Colour Rendering Index
CV(RMSE)	Coefficient of Variation of Root Mean Square Error
EJ	Exa Joules
EQE	External Quantum Efficiency
EVA	Ethylene Vinyl Acetate
ECBC	Energy Conservation Building Code
EPBT	Energy Payback Time
FF	Fill Factor
GHG	Greenhouse Gases
HVAC	Heating Ventilation and Air-Conditioning
HIT	Heterojunction with an Intrinsic Thin layer
IQE	Internal Quantum Efficiency
LBNL	Lawrence Berkeley National Laboratory
LCC	Life Cycle Cost
LCCE	Life Cycle Conversion Efficiency
LCE	Levelized Cost of Energy
MBE	Mean Bias Error
MS	Mild Steel
Mtoe	Million Tone Oil Equivalent
m-Si	Mono-crystalline Silicon
NBC	National Building Code

NERL	National Renewable Energy Laboratory
NOCT	Nominal Operating Cell Temperature
NPV	Net Present Value
PVC	Polyvinyl Chloride
p-Si	Poly-crystalline Silicon
PBT	Payback Time
SHGC	Solar Heat Gain Coefficient
SNL	Sandia National Laboratory
STC	Standard Test Condition
STPV	Semi-Transparent Photovoltaic
VLT	Visible Light Transmittance
WWR	Window to Wall Ratio
XPS	Extruded Polystyrene

NOMENCLATURE

English symbols

Notation	Description	Unit
AM_a	Effective air mass	Unitless
C	Velocity of light	m/sec
d	Glazing thickness	Mm
E_λ	Spectral irradiance at wavelength λ	$Wm^{-2}nm^{-1}$
E	Incident solar irradiance on module,	W/m^2
E_b	Beam component of the incident solar radiation on the module surface	W/m^2
E_{diff}	Diffuse component of the incident solar radiation on the module surface	W/m^2
E_0	Reference solar irradiance on module (1000)	W/m^2
f_d	Fraction of diffuse irradiance used by module	%
$f_1(AM_a)$	Empirically determined polynomial relating the solar spectral influence on Isc to air mass variation over the day	Unitless
$f_2(AOI)$	Empirically determined polynomial relating optical influences on Isc to solar angle-of-incidence	Unitless
h	Plank constant (6.626×10^{-34})	J. Sec
I_{sc}	Short circuit current	A
I_{mp}	Current at maximum power point	A
J_{sc}	Short circuit current density	mA/cm^2
J_0	Dark saturation current density	mA/cm^2
K	Boltzmann constant	W/m^2
k_i	Thermal conductance	$W/m^2/K$
N	Number of glazing layers	Nos
P	Power generation	Watt
P_m	Nominal power	Watt
p_{wat}	Perceptible water content in the atmosphere	Mm
q	Electronic charge	Coulomb
T_m	Module back side temperature	°C

T_c	Cell operating temperature	°C
T_{25}	Standard room temperature (25)	°C
ΔT	Temperature difference between cell and module back surface at an irradiance level of 1000 W/m^2	°C
$T_{\cdot}^{sol}$	Optical transmittance through a window system	%
V_{0c}	Open circuit voltage	Volt
V_{mp}	Voltage at maximum power point	Volt

Greek symbols

Notation	**Description**	**Unit**
ϕ_λ	Photon flux at wavelength λ	m^{-2} sec^{-1}
λ	Incident wavelength	Nm
η	Conversion efficiency	%
$\eta_{T_{25}}$	Conversion efficiency at reference temperature	%
η_{T_C}	Conversion efficiency at actual operating temperature	%
θ_k	Temperature coefficient for maximum power output	% per °C
$\xi(\lambda)$	Wavelength-dependent value of transmittance or reflectance	%
Δ_x	Spectral weighting function	Unitless
Φ	Angle of incidence	(°)
τ_λ	Optical transmissivity	%
ρ_λ	Optical reflectivity	%
α_λ	Optical absorption coefficient	cm^{-1}

CHAPTER 1
INTRODUCTION

1.1 World energy scenario

The global primary energy consumption was 13276.3 Mtoe or 555.85EJ (1EJ=10^{18}J) in 2016 **[1].** This was 1.0% more compared to the previous year's consumption. Fuel wise, oil with 33.28% stood at the top position followed by natural gas with 24.13% of the total consumption. The consumption of coal, nuclear and hydro energies were 28.11%, 4.46%, and 6.86% respectively. In the total energy consumption, the renewable sources of energy contributed the least (3.16%). However, some estimates show that in the renewable energy category, the solar radiation reaching the Earth surface alone has the potential to meet the existing demand 10,000 times more **[2].** By 2050, the projected primary energy demand of the world is 1000EJ or more **[3].**Moreover, as per the International Energy Agency (IEA), the solar photovoltaic sector will contribute around 11% of the expected world electricity supply by that time. In 2050, the expected installed capacity of the photovoltaic plant is estimated at 3000 GW with 4500 TWh electricity generation per annum. **Figure 1-1** shows the expected electricity generation by the photovoltaic technology in the four market segments in the three decades to come. The figure also shows the projected share of the electricity generated by photovoltaic technology into the global electricity supply.

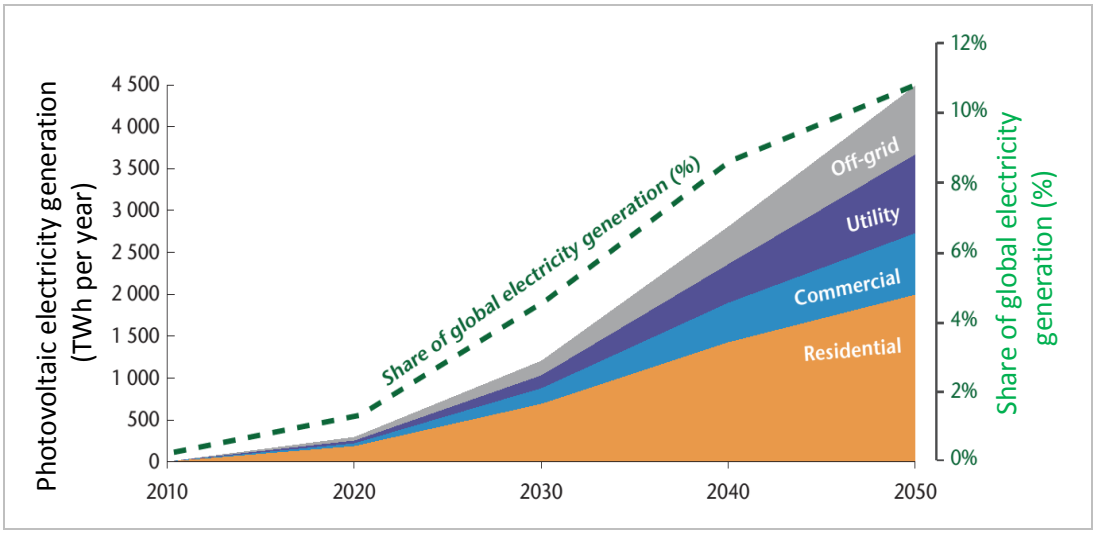

Source: IEA, Solar Photovoltaic Energy, Technology Roadmap

Figure 1-1: Expected electricity generation by solar photovoltaic technology in different segments

1.2 Energy consumption in building

Worldwide, the building sector accounts for about 40% of global energy consumption **[4].** In India, the building sector consumes 33 % of the total energy usage **[5].** In terms of electricity, the Indian building sector accounts for 30% of total electricity consumption (8% commercial, 22% residential) **[6]. Figure 1-2,** shows the electricity used in different activities in the residential and commercial buildings of India. With the growth of the economy, it can be envisaged that the demand for energy in the building sector will increase rapidly. An estimation of Bureau of Energy Efficiency (BEE) India, show that by 2030 the constructed floor area of Indian building sector is expected to increase by fivefold compared to 2005. The rising energy consumption per unit area and the addition of huge new floor area demanded the aggressive energy efficiency measures in the Indian building sector.

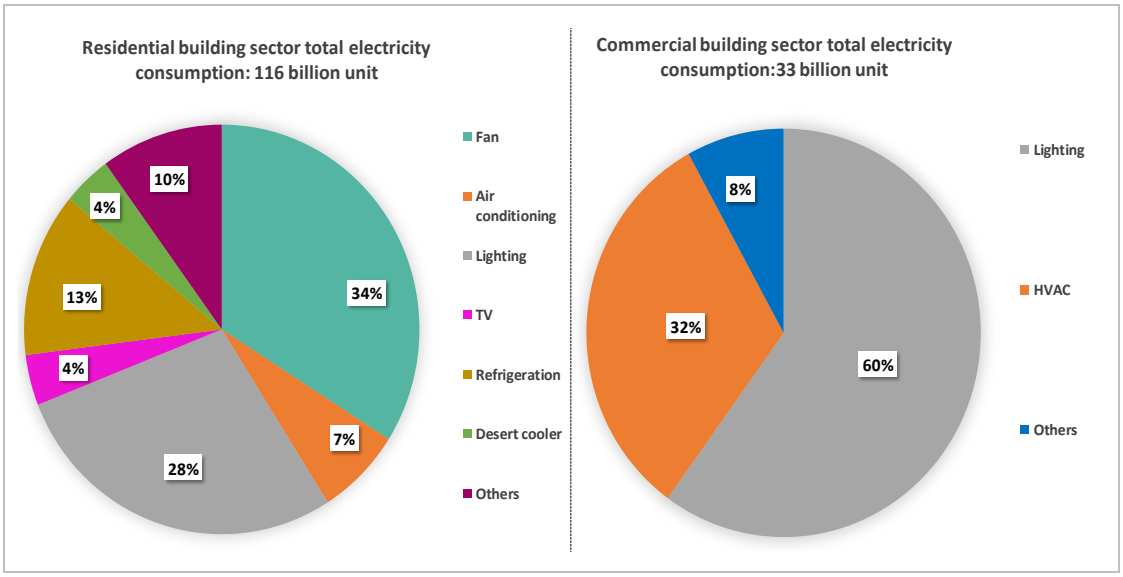

Figure 1-2: Electricity consumption in the building sector of India [7]

1.3 Window of a building

Natural daylighting is crucial for comfort and efficient working environment. Building windows have an important role in maintaining this natural daylighting along with view and fresh air for occupants **[8].** The windows also have an important role in maintaining the building energy load and the aesthetics. According to the American Society of Heating, Refrigerating and Air-Conditioning Engineers (ASHRAE) (2009), the performance of a window is characterized by three properties namely (a) U-value of the window assembly, (b) Solar Heat Gain Coefficient (SHGC) and (c) Visible Light Transmittance (VLT) through the window. These three parameters along with air leakage and condensation resistance are also necessary for energy performance labeling

of a window system by National Fenestration Rating Council (NFRE). The above three parameters are also important in determining the effect of the window on the building interior's lighting and thermal conditions through simulation by using the software like 'EnergyPlus.'

A window system with appropriate size, orientation and glazing type provides the best energy balance and natural lighting. The U-value determines the heat loss or gain through a window. **Figure 1-3** shows the U-value of most commonly used window systems and the IEA recommended values for the world as well as to achieve the goals of ZEB. In several regions of the world, clear glass (CG) with the poorly insulated frame is used in the window. The U-value of these window ranges from 4.5 to 5.6 W/m^{2}K.

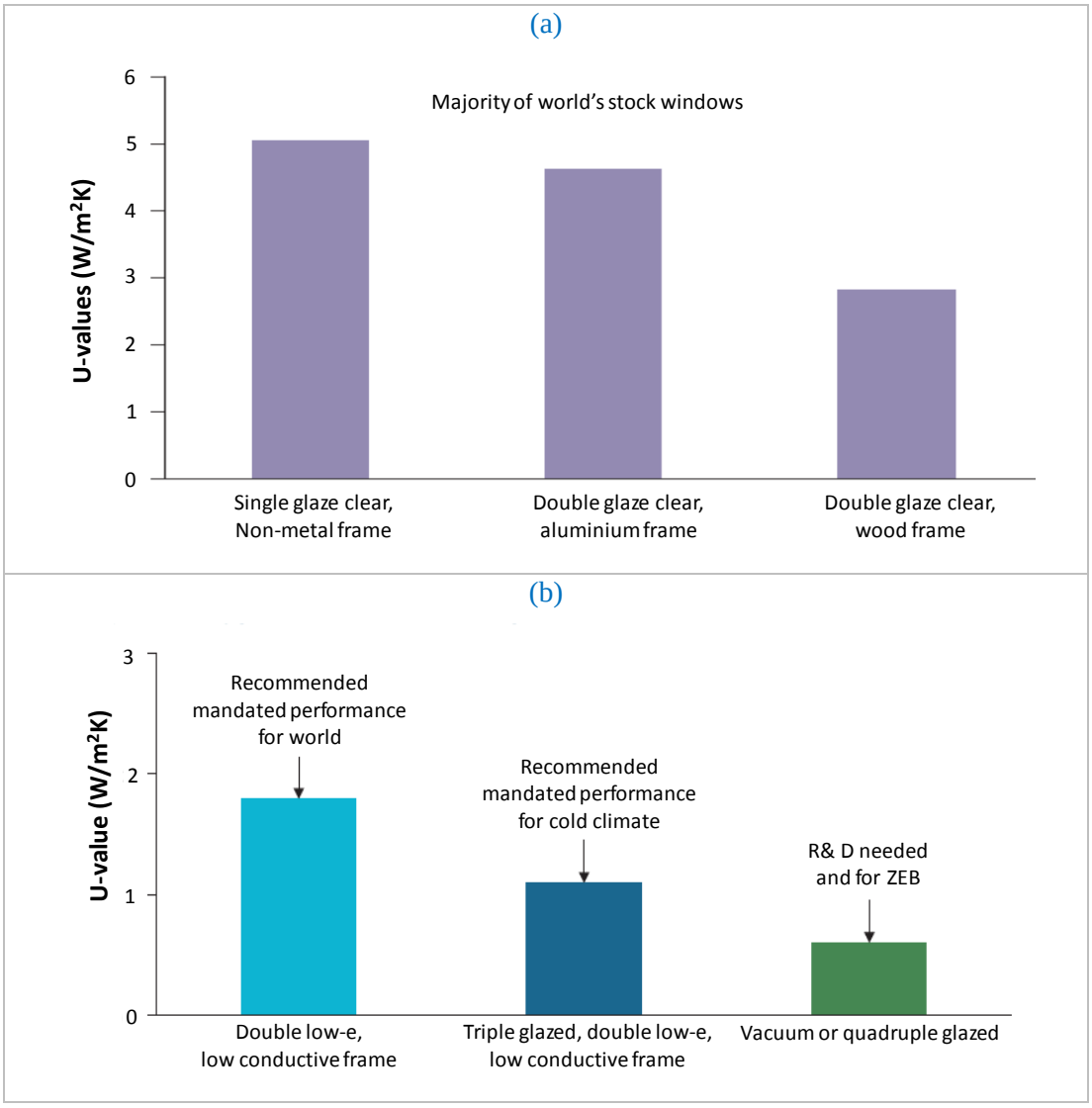

Source: IEA, Energy Efficient Building Envelopes

Figure 1-3: U-value of window (a) commonly used; (b) recommended for the world, cold climate and net-zero energy building

Several countries in Economic Co-operation and Development (OECD) region have achieved the low U-value window by using the Low-e coated glass and low conductive frame. However, much R&D will need to be conducted to achieve the targeted window U-values recommended for Zero Energy Buildings (ZEB).

1.4 Building Integrated Photovoltaic (BIPV) system

Energy positive or ZEBs are need of the present time. In the recent past, these types of buildings have become a reality through innovative design, use of energy efficient technologies and the integration of solar and other renewable energy technologies in the building **[9].** The literature also revealed that the Building Integrated Photovoltaic (BIPV) systems have an important role to play towards achieving the goal of ZEB in the years to come **[10-11].** The importance of integrations of solar photovoltaic systems in buildings have also been emphasized in the recently published Energy Conservation Building Code (ECBC)-2017 of India. The code recommended meeting at least 4% of the total electric load by solar or other renewable energy in the advanced buildings called super ECBC buildings **[12].**

In a building, photovoltaic modules can be attached or integrated in the form of the rooftop power plant, façade/window, window overhang, and skylight. Among different BIPV systems, the Semi-Transparent Photovoltaic (STPV) systems have gained the intense attention of researchers in recent times **[13-14].** Application of STPV module embedded window reduces the off-site electricity demand and yet allow daylight to enter the occupant area **[15].** Further, the STPV integrated window systems maintain or improve the primary purposes of a window compared to a conventional system. **Figure 1-4** shows the working of the STPV window in comparison to the conventional window.

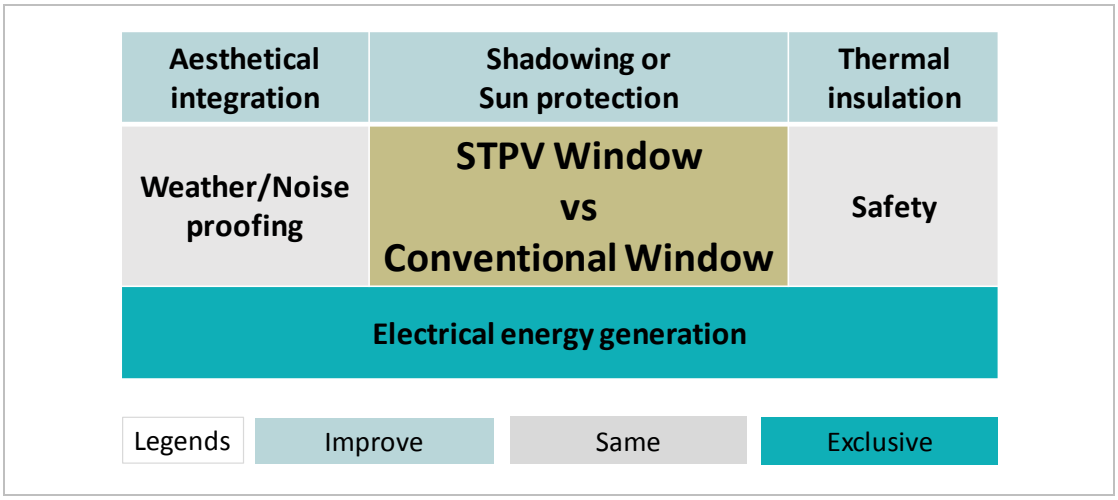

Figure 1-4: Comparison of STPV and conventional window's working

Figure 1-5 shows an application of ventilated photovoltaic façade in a public library of Spain. The installed photovoltaic capacity is 20kWp, and it produces 20,000 kWh energy per annum.The façade has a 150 mm cavity. In the summer the hot cavity air is naturally ventilated into the outdoor environment. During the winter season, the hot air is used to warm the fresh intake through a heat recovery system. The installation delivered an overall photovoltaic/thermal efficiency of 62% in the seven months of monitoring.

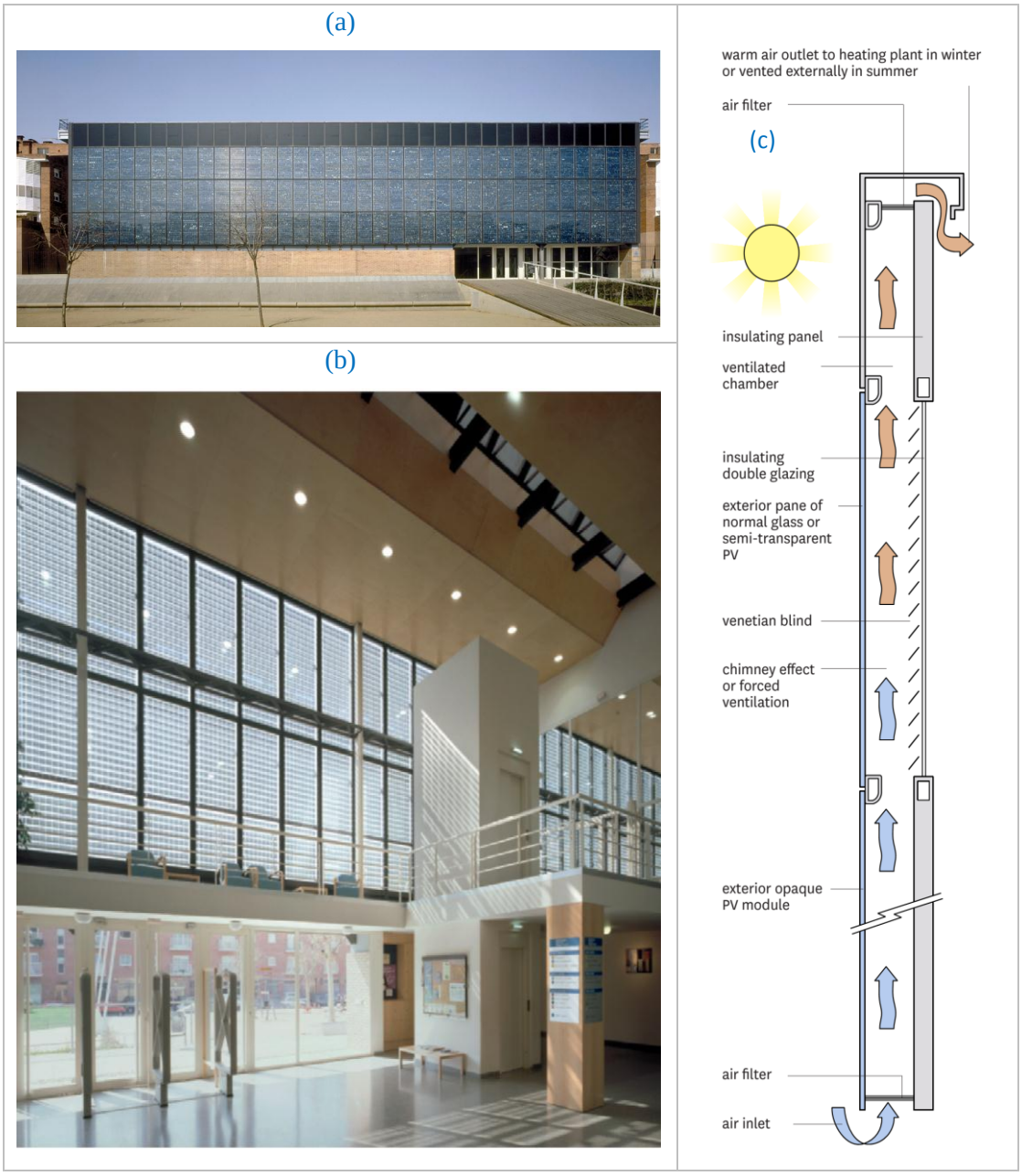

Source: Building Integrated Photovoltaics/ a Handbook by S. Roberts & N. Guariento, 2009

Figure 1-5: Application of ventilated photovoltaic façade (a) View from south, (b) Interior view compared to clear glazing, (c) Schematic of the ventilation process

The effect of the STPV module based window system on building energy load is a complex issue. While it needs to generate energy it also requires to transmit daylight. Like any other photovoltaic module, the performance of STPV also depends on the place of installation, design and operating conditions **[16].** Moreover, the part of solar radiation which is absorbed but not converted into electrical energy leads to increases in STPV module's temperature and releases heat into the surrounding. The release of heat into the occupant area leads to an increase in buildings cooling demand. On the other hand, due to constraint at the material level, a wide range of the solar spectrum doesn't convert into useful electrical energy. Therefore, special care needs to be taken in the selection and design of the STPV module based window system.

1.5 Types of solar photovoltaic cells

Various photovoltaic technologies have been developed in the recent time. The technologies differ with respect to the cell material, manufacturing process, energy yield and so forth. The application of diverse manufacturing process requires a different amount of energy to produce unit area of the modules. Moreover, the dissimilar conversion efficiency among the technologies leads to the generation of a varied amount of energy per unit area. Each technology has its limitations and advantages. The involvement of separate amount of material and energy along with the yield lead to a different payback period for each technology. A simplified classification of the available photovoltaic technologies is given in **Figure 1-6.**

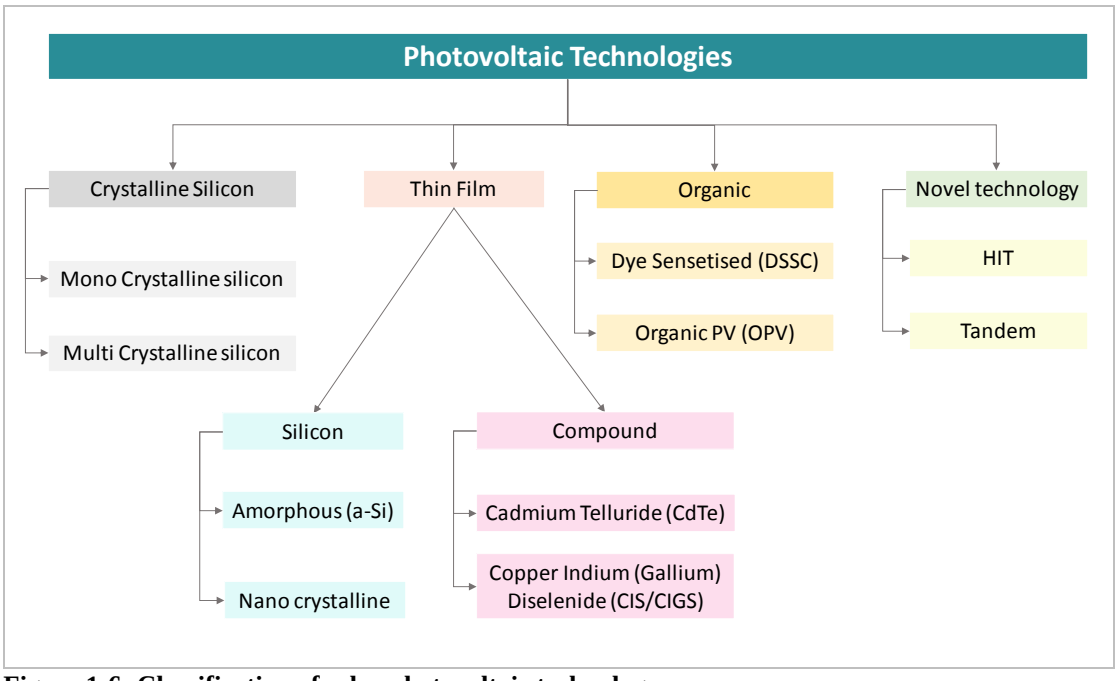

Figure 1-6: Classification of solar photovoltaic technology

The thin film semi-transparent photovoltaic (STPV) modules are preferred over the crystalline-based modules for window applications. This is mainly due to penetration of uniform daylighting through the semi-transparent STPV modules. The organic photovoltaic modules also possess the good potential for the building applications, but these are yet to be commercialized at the large scale. In the present study, Cadmium Telluride (CdTe) based thin film STPV modules have been used to carry all the proposed investigations. Some advantages of this material are described in section **3.3.**

1.6 Origin and objectives of the present research

For energy, India heavily depends on imported oil. Every year millions of Rupees are spent to meet the energy demands of the country. Moreover, the burning of fossil fuel like oil adversely affects the environment in different ways **[17].** Therefore, there is need of the hour to save energy in all sectors of the society. The building sector consumes a significant amount of energy. However, this sector has enormous energy saving potential **[6].** In the building sector, a large amount of energy can be saved by changing the building construction, climate-sensitive design, use of locally appropriate material and operations. Solar photovoltaic module based system can play a significant role in this regards.

However, with growth in the economy, the high-rise buildings are increasing at a fast rate. The roof areas of these buildings are negligible in comparison to other envelope parts. Moreover, some portion of the roof area is required to install an air conditioning plant, water tanks, and so forth. Therefore, the major available options for STPV system in these buildings are the facades/windows **[18].** On the other hand, the window is an important element of a building in terms of their energy load, visual comfort and fresh air for the occupants. Therefore, cutting-edge research is needed for the optimal design and operation of the STPV module integrated window system.

Further, the literature review revealed that the optimal characteristics of the STPV module for window application changes with the climate of the installed location. On the other hand, India is a large country. There are significant variations of climate within the country. However, very few works have been carried on semi-transparent photovoltaic window system with respect to the Indian climate. Also, the performance of a semi-transparent photovoltaic integrated window is affected by the parameters like amount of incident radiation, type of incident spectrum, cell temperature and the angle of incidence. A simplified approach which includes the effect of all these parameters on

the performance of the vertical semi-transparent photovoltaic system is rare to find in the literature.Moreover, the prevention of the primary cause of the increase in cell temperature of a photovoltaic module in case of building application has rarely been discussed in the literature. These research gaps encouraged to perform a study on the STPV integrated window systems in the Indian climatic context. The objectives of the present research are mentioned below.

I. ***Development of double pane window system using semi-transparent photovoltaic module***
II. ***Performance analysis of semi-transparent photovoltaic module based double pane window system under different operating conditions***

Various design and operating conditions of STPV module integrated window systems have been investigated in the present study. Some of the variables are mentioned below.

- Double pane window systems with change are the position of the cavity with respect to the STPV module
- Ventilated air cavity between the two window panes: Change in mode of ventilation
- Variation in STPV module characteristic: Change in STPV module Transparency
- Effect of location and orientation
- Effect of Angle of incidence
- Variation in Window to Wall Ratio (WWR)

1.7 Scope of the present thesis

The motivation for working on STPV integrated window system can range from global to the national level or from institutions to the individual level. At the global or national level, the reduction of GHG emissions can be a motivational force while for an institution or individual lowering the electricity bill as well as better thermal comfort can be the motivational causes. However, the primary goals of this study are to evaluate the performance of the STPV integrated window system in terms of energy generation and energy savings in buildings under different design and operating conditions.

1.8 Assumptions considered in the present thesis

The results of the present thesis have been achieved under various assumptions for the simplification of the problem. The major assumptions are listed below.

a. The building is exposed to the solar radiation and atmospherics wind in all the sides without any obstacles from the nearby constructions
b. Temperature difference between cell and module back surface at an irradiance level of 1000 W/m^2 is 3^0C **[19]**
c. The temperature coefficient of maximum power remains constant for all temperature
d. Reflection or transmission is the same for all wavelengths for a particular angle
e. Energy generation of the STPV modules due to diffuse solar radiation are independent of the angle of incidence
f. There is no loss in energy generation due to soiling on the window surfaces
g. There is no mismatch among the STPV modules either in electrical or optical terms
h. There is no degradation of the STPV modules electrical performance within a year
i. The generated energy is always drawn at the maximum power point

1.9 Organization of the present thesis

The thesis contains five chapters, the references to the relevant work and one appendix. The highlights of the chapters are described below.

Chapter 1: This chapter presents the concept of STPV module integrated window systems and the problem statement.

Chapter 2: The relevant theories and approaches used by different researchers in the study of STPV integrated systems have been included in Chapter 2. Different system design and operation of STPV systems, their energy saving potential, and cost-benefit analysis presented in the literature have been discussed with some example. In the end, this chapter contains the identified research gap and the objectives of the present research.

Chapter 3: This chapter explains the methodology applied to achieve the objectives of the present research. The research approach, the selected materials, and their characterization have been included in this chapter. Various simulation software used in the study and details of the experimental investigations have also been discussed in Chapter 3.

Chapter 4: The findings of the present research and related scientific background have been described in Chapter 4. The findings have been described in four different categories. The categories are

1. Impact of different key factors on the energy generation in window integrated STPV module
2. Effect of angle of incidence on energy generation in window integrated STPV module
3. Effect of window configurations and airflow strategies on the performance of STPV module integrated window systems
4. Effect of STPV module integrated window systems on lighting and air conditioning loads

Chapter 5: This is the last chapter of the thesis. This chapter summarizes the findings of the present research, the contribution of the thesis and the future research scope in the STPV module integrated window systems.

CHAPTER 2
LITERATURE REVIEW

2.1 Preamble

Building integrated photovoltaic system generates electricity at the place of consumption. In this kind of system, the photovoltaic module also plays the role as part of the building envelope **[20].** In the recent past, the STPV module integrated window systems have become popular among the researchers **[21].** An STPV integrated window systems considerably reduce direct solar heat gain **[22].** In other words, the STPV modules use in window or façade also work as a shading device in a building **[23-24].** This feature further enhances the potential benefits of STPV integrated window system. Among different photovoltaic modules, the thin film STPVs are preferred for window/façade in a building. This is mainly because of better daylight performance and aesthetic appearance of thin film modules **[25].**

The performance analysis of the STPV integrated window system needs various interdisciplinary concepts. The concept of Sun-Earth geometry, the photovoltaic science, the science of building cooling and heating, the idea of daylight penetration inside the building are some of the important areas need to analyze the STPV integrated window systems. In this chapter, a review of the recently published literature relevant to the present research has been presented. In the review, the selected literature have been investigated with respect to the following categories.

- Performance determining parameters and their effect
- System design and operation
- Energy saving potential
- Cost-benefit analysis

The categorical descriptions are followed by a summary of the review. In the end, this chapter contains the identified research gaps and the objectives of the present research.

2.2 Performance determining factors and their effect

The performance of a solar photovoltaic system is affected by various interdependent factors. Some of the important factors are the temperature of module & ambient air,

place of installation, incident radiation & spectrum, Angle of Incidence (AOI) & tilt angle, orientation or surface azimuth, shading, soiling, and so forth. Another set of factors which affected the performance of photovoltaic systems are module's optical, thermal and electrical properties, type of material and cell area in the module. The performance is also affected due to wiring, string diode, partial shading, dirt accumulation, low & inhomogeneous radiation, cell mismatch, MPPT and system failure **[26].** In the following subsection, some of the factors and related research findings have been explained in brief.

2.2.1 Module temperature

Fill factor and conversion efficiency of the photovoltaic module decrease with an increase in the cell temperature **[27].** These dependencies eventually reduce the power generation capacity of the photovoltaic module. Depending on the type of the photovoltaic module, the range in the reduction of annual energy generation is 5% to 8% due to high operating cell temperature **[28].** The reduction in power generation per degree rise in cell temperature is represented by the temperature coefficient of maximum power (θ_k). The value of θ_k, changes with the material used to make the solar cell. Several researchers have calculated the value of θ_k at the cell/module as well as at the systems level **[29-37].** The findings of the above researchers suggest that the value of θ_k changes in the range of 0.0026 per ^{0}C to 0.0045 per ^{0}C depending upon the photovoltaic material or the systems, Various correlations for temperature dependent photovoltaic conversion efficiency have also been proposed in the literature**[38-44].** However, the temperature of photovoltaic modules in an STPV window system varies with design and operating conditions. This variation demands the assessment of module temperature for a particular design or application. In case of building application, the assessment of module temperature is also important due to their influence on the heat transfer into the occupant area.

Park K. E. et al. **[45]** conducted an experimental investigation of STPV module temperature and the related effect on power generation in building the application. They found that color of STPV module's and the property of the back glass are the determining factors for module temperature due to their significant role in the absorption or transmission of the incident radiation. A reduction of 0.52% in power generation per degree rise in cell temperature is reported in the study.

Armstrong S. et al. **[46]** proposed a model by considering different atmospheric condition, material, and mounting structure. Jones D. et al. **[47]** also proposed a transient model for the module temperature. In both the studies, the module temperature is found to be changed with the different atmospheric features such as wind speed and incident solar radiation. For example, the module temperature changes from 15.62^0C to 15.56^0C when the wind speed increases from 0.77m/sec to 2.14 m/sec **[46] .**

The effect of packing factor on the cell temperature of the roof-integrated photovoltaic module has been studied by Vats K. et al. **[48]** using the analytical method. They considered six types of photovoltaic modules, m-Si, p-Si, a-Si, CdTe, CIGS, and HIT. In the analysis, the cell temperature is observed to be reduced by 10^0C for m-Si, a-Si, and HIT modules with a decrease in packing factor by 49%. For the similar change in packing factor, the reduction in cell temperature has been 11^0C in case of p-Si, CdTe, and CIGS modules. Similarly, Kamthania D. et al. **[49]** compared the cell temperature of opaque and STPV modules using numerical analysis. In the study, they observed higher cell temperature in case of the opaque module than that of the STPV module due to heat retention by the cell.

Figure 2-1: Crystalline Si photovoltaic modules with different packing factors [48]

A photovoltaic module contains different layers. The cell which is the active part of the module remains sandwiched in between the glass, Ethylene Vinyl Acetate (EVA), and tedlar. However, the sandwich structure prevents the direct measurement of cell

temperature in the actual working conditions. Nayak S. et al. **[50]** through an experimentally validated analytical method developed the models to calculate the temperature of different layers of a photovoltaic module. They observed that the cell temperature remains higher than the back side tedlar layer by 3–4^{0}C.

The formula for operating cell temperature developed by Sandia National Laboratory (SNL) is widely used in the photovoltaic research. Nominal Cell Operating Temperature (NOCT) is another widely used standard. D'Orazio M. et al. **[51]** compared the experimental values of cell temperature with these two standards. For this purpose, they conducted an experimental observation on cell temperature of the roof-mounted photovoltaic module. Three different configurations, roof integrated with & without ventilation and rack-mounted, have been considered in the experiment. Subsequently, the measured temperatures were compared with the predicted values by NOCT and SNL methods. They observed that for the rack mounted systems both NOCT and SNL methods could predict the temperature quite accurately. On the other hand, for the integrated systems with and without ventilation ducts between the module and insulation, the SNL could predict more closely to the experimental results.

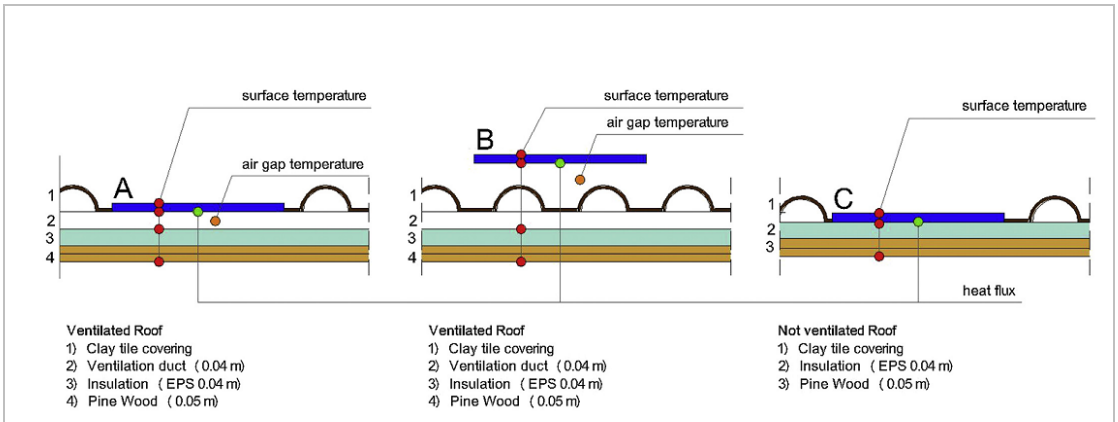

A, Roof integrated with ventilation; B, Rack mounted; C, Roof integrated without ventilation

Figure 2-2: Experimental setup for temperature measurement of roof-mounted photovoltaic modules in different configurations [51]

For example, the RMSE values between the observed and predicted average cell temperature with NOCT and SNL are ±6.3 and ±4.3 respectively for the integrated system without any ventilation. In the present study, we have used the SNL equation for calculating the cell operating temperature from the simulated module backside temperature.

2.2.2 Local climate, incident spectrum, and level of incident radiation

The local climatic conditions such as water vapor, cloud, and so forth determine the air mass. In most of the locations in the world, the air mass remains more than unity **[52].** The air mass and hence the spectral characteristics of solar radiation changes with time and geographical location. Further, a solar cell material cannot absorb the whole spectrum of the incident radiation. Moreover, some part of the absorbed radiation cannot generate useful charge carriers inside the material. The spectral response of the material is used to measure the consequences of the above parameters. It is also known as Quantum Efficiency (QE) of the cell. The photovoltaic module's responses to the incident spectrum vary depending upon the type of the cell material. For example, modules with a cell of a-Si material are more sensitive to incident spectrum than that of the p-Si due narrow working wavelength range **[53-54].**

Water vapor is virtually transparent for wavelength range which is effective for CdTe photovoltaic module **[55].** The transmittance of water vapor remains almost 100% between 320nm to 800nm with a slight dip at 715nm to 725nm wavelength. Consequently, the conversion efficiency of CdTe module in the monsoon and post-monsoon seasons are more compared to the other seasons. However, mere high conversion efficiency does not ensure more power generation from a photovoltaic module. High conversion efficient module with more incident solar radiation resulted in more power generation. In the real operating condition, the amount of incident radiation changes from location to location and state of the receiving surface. Li D.H.W et al. **[56]** proposed an approach to calculate the solar radiation values on different surfaces considering the available sky irradiance data. Further, Aaditya G. et al. **[57]** conducted an experimental study on the performance of the roof-integrated photovoltaic system in the temperate climate of (Bengaluru) India. In the study, they found that besides the cell material and mounting method, the performance of the photovoltaic system is influenced by incident solar irradiance along with ambient temperature. Li D.H.W. et al. **[58]** in their experimental study on efficiency characterization of roof-integrated photovoltaic systems also observed that the high incident radiation with lower operating temperature produces more energy in the winter compared to the summer season.

Therefore, besides analyzing the data provided by the manufacturer, performance assessment of photovoltaic system in real operating condition are necessary to know the

economic potential **[59].** The performance analysis in a local climatic condition established the suitability of a given photovoltaic technology in that location **[60].** The performance study of STPV window/façade system in a particular place is also required to build confidence among the designer and architecture. It helps in applying the energy assessment tools in the new smart buildings. Chae Y.T. et al. **[16]** evaluated the energy performance of the STPV window in six cities of USA. They concluded that besides power conversion efficiency, the place of installation and opto-thermal properties are also determining factors for STPV integrated system performance. For instance, they observed a variation of 27.4% in annual energy generation with the change in place of installation.

2.2.3 Angle of incidence and tilt angle

For a given geographical location, the Sun position keep changing throughout the day and night. For this reason, the solar radiation strikes at a different angle of incidence (AOI) on a static surface. However, in the laboratory, the radiation is maintained at normal incidence during the characterization of photovoltaic modules. On the other hand, the reflection as well as transmission of surface changes with AOI. Therefore, when a photovoltaic module is installed in the actual field, the deviation of solar radiation from the normal incidence incur a loss in the energy generation. This loss is known as an optical or angular loss. It is measured with respect to the energy generation at the normal incident. Two factors contribute to this loss of energy generation. The factors are the cosine effect and the optical characteristics of the module surface **[61].** Orientation, latitude and local climatic characteristics are the determining factors for this optical or angular loss of photovoltaic energy generation **[62].** In a tropical country, the solar radiation mostly incident at a higher angle on the building facades in a tropical country. Therefore, the loss of energy generation due to the angle of incidence becomes significant in the case of BIPV vertical systems such as window/façade.

Martin N. and Ruiz J.M. have studied the effect of AOI on photovoltaic module energy generation using analytical model **[62-64].** Three different versions of a model have been proposed to calculate the AOI effect depending upon the type of data available to the users. In some earlier research also the AOI got emphasis in the calculation of photovoltaic module performance **[65-66].**

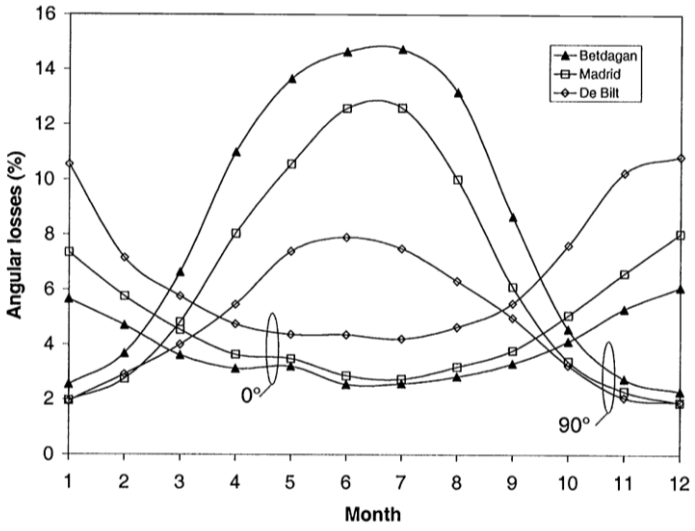

Figure 2-3: Monthly angular losses of a standard m-is solar module at different places (latitudes) installed at 0^0 and 90^0 tilt angle [62]

To measure the effect of AOI on photovoltaic module performance, the International Electrotechnical Commission (IEC) has proposed a procedure in IEC 61853-2 standard **[67].** One of the major statement of this standard is that for a flat glass superstrate modules the value of a flat glass-air interface can be used without performing the AOI test **[68].** The SNL has also developed a procedure to check the effect of AOI on non-glass or non-planar photovoltaic modules **[19].** An empirically determined polynomial relating optical influences on short circuit current has been proposed in the SNL procedure. The polynomial is given below **[19].**

$$I_{SC} = (I_{SCO} \times f_1(AM_a)) \times \{(E_b \times f_2(AOI) + f_d \times E_{diff})/E_0\} \times \{1 + \alpha_{Isc} \times (T_c - T_{25})\} \quad (1)$$

Where,

E_b, Beam component of the incident solar radiation on the module surface, (W/m^2); E_{diff}, Diffuse component of the incident solar radiation on the module surface, (W/m^2); f_d, Fraction of diffuse irradiance used by the module, it is generally assumed to be 1 for flat-plate modules. ; E_0, Reference solar irradiance (1000 W/m^2) with the standard spectrum; AM_a, Absolute air mass; T_c, Cells operating temperature (^0C); T_{25}, room temperature (^0C); $f_1(AM_a)$, Empirically determined polynomial relating the solar spectral influence on Isc to air mass variation over the day; $f_2(AOI)$, Empirically

determined polynomial relating optical influences on Isc to solar angle-of-incidence (AOI).

The value of $f_2(AOI)$ is determined using the following polynomial.

$$f_2(AOI) = b_0 + b_1.(AOI) + b_2.(AOI)^2 + b_3.(AOI)^3 + b_4.(AOI)^4 + b_5.(AOI)^5 \quad (2)$$

Where, $b_0$to b_5 are the empirically-determined coefficient establishing the rate at which module short-circuit current changes with AOI

Subsequently, Knisely B. et al. **[69]** have experimentally found similar results for five different photovoltaic module technology. Fanney A. H. et al. **[70]** presented a procedure for the characterization of different BIPV panels. Among the many parameters, the researchers have also investigated the effect of AOI on energy generation by applying the SNL's empirical model. Their findings indicate that the effect of AOI above 60^0 could be severe to the photovoltaic energy generation. Similar observations have also been drawn in another work of the same researchers **[71].** Significant reflection losses have been observed with AOI beyond 50^0 for a particular photovoltaic module by Fanni L. et al. **[72].** Further, in the indoor calorimetric hot box experiment, Chen F. et al. **[73]** detected as high as 50% reduction in power generation of the semi-transparent photovoltaic module at 60^0 AOI compared to the normal incidence. Significant loss in energy generation at a higher incident angle has also been noticed in a field study by Song J. H. et al. **[74].**

Song J. H. et al. **[74]** have analyzed the effect of tilt angle on power generation potential of photovoltaic modules using TRANSYS simulation and experiment. At the considered location, the tilt angle $30^0$is found to provide the best power generation. Further, a significant decrease in power generation has been observed for tilt angle above 70^0. The effect of the tilt angle on the surface temperature has been experimentally studied by Yoon J. H. et al. **[13].** STPV and clear glass double pane window at 0^0, 30^0 and 90^0 tilt angles have been considered in the investigation. They noticed that in the summer daytime, the innermost surface temperature remains lower by 1^0C in case of STPV window than that of the clear glass. While in the winter night, the temperature of the same surface has been higher by 2^0C for the STPV window. Further, in the winter season, the surface temperature is observed to be increased rapidly

for vertical window due to more incident radiation. Similarly, in the summer season, the horizontal window showed the rapid increase of surface temperature.

The amount of solar radiation received by photovoltaic modules also depends upon the tilt angle of the module. Elminir H. et al**. [75]** experimentally found that the photovoltaic modules received maximum solar radiation during the winter and summer season at different tilt angles. In the winter season, the optimum tilt angle is 15^0 more than the local latitude. In the summer season, the optimum tilt angle is found to be 15^0 less than the local latitude.

2.2.4 Orientation and WWR

A building receives the various amount of solar radiation in different orientations. This difference in incident solar radiation affects the amount of energy generation from a photovoltaic module. Orientation wise the south facing window generates the maximum energy **[74].** It occurs due to more incident radiation on the south-facing window. The power generation decreases when the window orientation changes from south to the east and west. However, in the case of BIPV application, the orientations other than the south are not completely forbidden. It has been observed that in the tropical country like Singapore, the orientation which doesn't receive direct solar radiation also processes the good potential for vertical STPV window **[76].** Effect of orientation on power generation of façade integrated BIPV (a-Si) system has also been investigated by Yoon J. H. et al. **[77].** For this purpose, they conducted a long-term experiment (2 years) on a BIPV system installed in an institutional building.

Figure 2-4: Application of thin-film Photovoltaic module in institution building, (a) building front view, (b)part of the building having Photovoltaic modules [77]

In the experiment, they found lower energy generation than the expected value due to the constraint in surface azimuth angle (w. r. to south 50^0) and shading effect by the other part of the building. However, with removing the effect of azimuth angle and shading in the ESPr simulation, they observed an improvement of 47% in the energy generation. In the present research, it has been assumed that the building is exposed to solar radiation in all directions without any shadow from the neighboring buildings.

Saleh M. A. et al. **[52]** proposed a theoretical model for the variation of heat gain with the orientation of window. They subsequently proposed that both cooling and heating loads can be controlled by adjusting the orientation of a window with a time of the day. The orientation and WWR are interdependent. In a cooling demand country like India, small WWR is preferred in the orientation which receives higher solar radiation. However, to get more energy from the STPV integrated window, larger WWR is preferable. Therefore, the WWR need to be optimized by considering the overall energy performance. Yun G. Y et al. **[78]** studied different area of clear glass and opaque photovoltaic module integrated window using ESPr simulation software. Based on the findings of the study, they concluded that the optimum WWR changes with building location as well as with applied insulation and heat gain from the artificial lighting. In the EnergyPlus simulation study, Xu S. et al. **[79]** observed that STPV modules with higher cell area are suitable for the buildings with deep room and large WWR. The optimum WWR also changes with the transparency of the window glazing. Miyazaki T. et al. **[80]** investigated the relationship between transparency and WWR of photovoltaic module integrated window systems with reference to energy performance. They found that STPV window with 50% WWR and 40% module transparency provide the best energy result. Therefore, in the present work, the WWR has been changed from 20% to 50%. Similarly, the range of VLT considered in the present study is 7.0% to 32.7%.

2.2.5 Photovoltaic cell/module characteristics

STPV module's optical, electrical and thermal characteristics play a major role in the energy performance of a BIPV system. Various researchers have studied these features from a different point of view.

Moralejo-V F. J. et al. **[81]** carried an optical characterization of different photovoltaic modules regarding transmissivity and reflectivity at normal as well as inclined

incidence. They found that the STPV module's transparency is less dependent upon the cell material than the laminated material. Degradation of the laminated material influences the transmissivity of the STPV module though it does not affect the CRI inside the room. They also observed that the front reflection is dominated by the property of the glass. The presence of metal contact leads to higher reflection in case of the back surface. They also proposed that the angular optical properties of STPV modules are more important than the normal incidence in the evaluation of STPV integrated systems.

Transparent Conducting Oxides (TCO) is an integral part of STPV modules. However, the thickness of the TCO layer influences the transparency of the module. Lim J. W. et al. **[82]** developed a-Si: H and a-SiGe: H solar cells with a varying thickness of TCO and studied them with respect to transparency and conversion efficiency. Between the two cell types, a-SiGe: H showed better conversion efficiency but lower transparency. However, they proposed that by changing the Ge content, the transparency can be managed.Further, thick TCO absorbs more radiation and reduces the module transparency. For good transparency, the proposed optimum thickness of TCO is 300 to 500nm. Study on module transparency and their related effect on STPV module performance have also got emphasis in some other research **[25, 83-84].** Olivieri L. et al. **[83]** studied the performance of STPV glazing with transparency from 10% to 40%. The decrease in electrical outputs with module transparency has been observed in the survey. However, they concluded that the transparency is not the sole electrical output determining factor. Kapsis K. et al**. [84]** investigated the role of module transparency in the study of the potential benefits of STPV window in the commercial building. They noticed that the STPV module with 10% visible transmittance provided the best overall energy performance. The effect of module transparency on energy saving potential of STPV double pane ventilated window have also been investigated by Chow T. T. et al. **[25].** For this purpose, they developed an energy balance model and found that the module transparency between 45% to 55% delivered the best electricity savings.

Solar cell thickness and the surface property are determining factors for the electrical, optical and thermal performance of BIPV systems. Chae Y. T. et al. **[16]** developed three a-Si: H semi-transparent solar cell of different thickness with and without texturization. Subsequently, they carried the electrical and thermal performance for all the cells in a mid-size office building in six different cities in the USA. WINDOW and

EnergPlus software have been used for the parametric analysis. Besides electrical properties, the performance of the solar cells is also observed to be affected by the place of installation, primary energy used, environmental impact, etc. Therefore, they concluded that the solar cell customized as per the applied location delivers the best results in BIPV applications.

Lighting color has a significant role in the visual comfort and aesthetic. In the case of thin film STPV module, the material, and the cell thickness determines the color of the light passing through the window. Selj J. H. et al. **[85]** developed solar cells of various colors by depositing multiple layer Anti-Reflection Coating (ARC) and studied the behavior of the light passes through them. Lynn N. et al. **[86]** experimentally investigated the Colour Rendering Index (CRI) of different a-Si and a micro-morph solar module regarding visual comfort and aesthetic. In the investigation, the CRI of a-Si modules has found to be above 90 for all AOI while for the micro-morph module it is less than 90. They also proposed that CRI could be one of the determining factors in choosing the STPV module for the application in a building.

SHGC is one of the major factors which determine the thermal performance of glazing. It dominates the total heat ingress through the photovoltaic window **[87].** However, this property changes from module to module and with the working scenario. Kuhn T. E. et al. **[88]** at Fraunhofer, Germany, developed a procedure to calculate the g-value of STPV window glazing using the calorimetric facility. They noticed that in the measurement of angle-dependent SHGC the movement of the light source or the sample gives the same values. Calorimetric measurement of SHGC has also been carried out in some other research **[73, 89].** Chen F. et al. **[73]** observed that the reduction in SHGC become rapid for AOI above 45^0 and it can be as high as 20%. They also noticed that the SHGC decreases with the connection of load in the STPV systems. Further, Olivieri L. et al. **[89]** observed that the SHGC changes depending upon the state of working on the STPV module. The SHGC of the same photovoltaic module reduces by 11% when it works at maximum power point (MPP) instead of a short circuit current condition. Along with the SHGC, the U-value also plays a significant role in the thermal performance analysis of ventilated photovoltaic façade/window. Infield D. et al. **[90]** proposed four theoretical formulae for U value and g-value splitting them into two components. The U-value has been divided into the recovered loss coefficient (U_{vent}) and transmission loss coefficient (U_{trans}). Similarly, the g-value has been divided into

the constant transmission coefficient (g_{trans}) and indirect solar gains to the ventilation (g_{vent}). The parameters are shown in **Figure 2-5**.

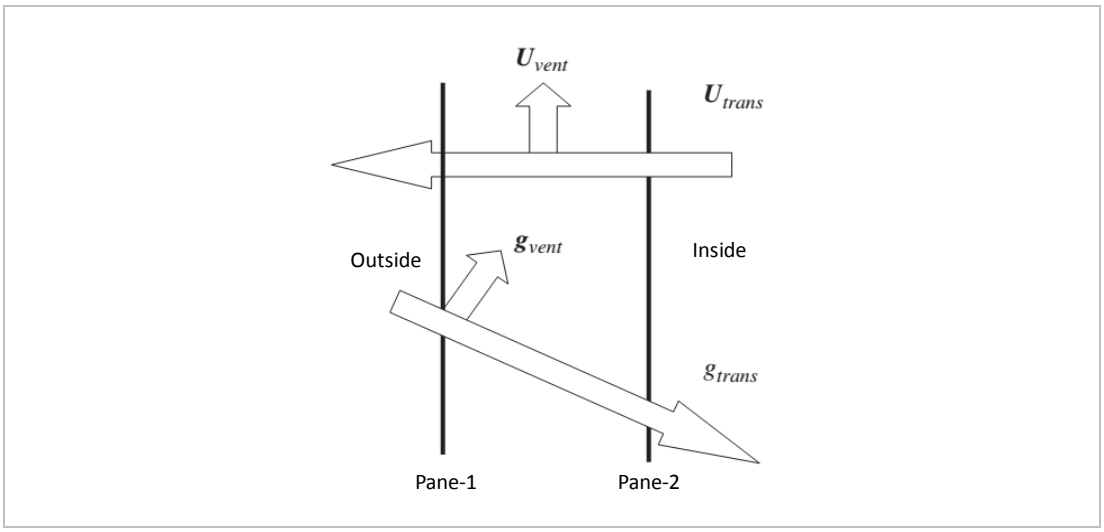

Figure 2-5: Energy flow of a ventilated façade [90]

Software like WINDOW and THERM are also used to calculate the U-value and g values of STPV modules. Chen F. et al. **[91]** found similar values of heat transfer in calorimetric hot box measurement as calculated by WINDOW and THERM software. Further, among various characteristics of the STPV module, the cell area affects the most in the heat transfer through the module **[87]**. The dominant role of cell area on the heat transfer through the STPV module has also been observed by Xu S. et al. **[79]**

2.3 Effect of STPV façade/window system design and operation

When the STPVs are used as the external envelope of a building, there is a high possibility of overheating in the system. The application of the STPV module as a window also changes the perception of comfort regarding thermal and visual **[92].** Further, a significant amount of heat loss/gain is associated with single pane STPV window. These eventually interfere with the occupant's thermal comfort or building energy load. Therefore, some strategies are necessary for STPV window structure to prevent it from overheating and also to avoid the critical heat loss/gain through the window. In this context, double pane STPV window structures with an air cavity have found to be worthy of the findings of various research **[93-98].** The findings of the above research work along with various system designs, operation strategies, and related conclusions have been discussed briefly in the following sub-sections.

2.3.1 Façade/Window system design

The STPV façade/window design affects the electrical & thermal performance as well as the life of the systems. With respect to thermal performance, a considerable amount of radiative heat transfer occurs when a single layer photovoltaic module is used as a window. However, this problem can be reduced significantly by designing a double pane window system with a Low-e glass at the back of the photovoltaic module **[99].** He W. et al. **[100]** investigated the effectiveness of double pane a-Si window system vis-à-vis a single pane window using experimental and CFD simulation. They observed similar electrical conversion efficiency in both the cases but much lower innermost surface temperature in case of the double glazed system. The innermost surface directly affects the occupant's thermal comfort. A lower innermost surface in summer season helps in keeping a lower room air temperature. It also provides the better thermal comforts or leads to lower cooling demand. In the numerical analysis, Han J. et al. **[101]** observed 5^0C less room temperature with STPV double pane window compared to the clear glass window. Further, in the thermodynamic analysis, Agarwal B. et al. **[102]** observed that the BIPVT systems delivered better overall performance compared to BIPV systems. Further, compared to the single clear glass and Low-e glass window an energy savings of 25.3% and 10.7% respectively have been observed with STPV double pane system by Wang M. et al. **[93].**

Vast K. et al. **[103]** analytically carried the performance analysis of STPV and opaque photovoltaic module integrated double layer façade and roof with and without air duct. The analysis was conducted for the cold climatic condition of Srinagar, India. In this climatic condition, a large amount of energy is required for space heating purpose. Among all the systems design, the STPV double pane structure showed the most effective results in maintaining higher room temperature. In the typical winter day, Kamthania D. et al. **[49]** also observed a higher room temperature (5 to 6^0C) compared to the ambient with a double pass photovoltaic façade.

The effectiveness of BIPV system changes with the applied module technology. Vats K. et al. **[104]** studied six different photovoltaic modules integrated into the roof of a building with respect to energy and exergy performance. From the overall exergy and energy point of view, the HIT type photovoltaic module made of a-Si and c-Si showed the best result. While for the space heating purpose, the a-Si photovoltaics has been the more favorable. Technology wise Luminescent Solar Concentrators (LSC) also

provided superior results compared to the conventional photovoltaic modules for BIPV application **[105].**

Further, in the case of a double pane STPV system, the thickness of the air cavity influences the amount of heat transfer **[98-106].** In the numerical analysis, Han J. et al. **[106]** found that an air cavity of thickness 60-80 mm resulted in the minimum heat transfer. The air cavity thickness also plays a significant role in determining the flow rate of the naturally ventilated air. **[107].** The energy consumption by the fan and other cooling devices also changes with the cavity thickness of a double pane STPV system **[21].**

2.3.2 Façade/Window system operation

In the literature, various studies have found to be focused on releasing the hot air from the window cavity to the outdoor environment or making the system an insulating entity **[13, 21, 83, 93, 96, 99, 101, 106, 108].** Some studies have also attempted to use the hot air in the indoor environment by circulating indoor air through the cavity **[25, 103, 109].** However, the prudent use of ambient air can help in increasing the saving of building energy loads besides enhancing the human productivity. Yun et al. endeavored to use the ambient air for mixing the cavity air with the indoor environment **[78].** Chen Y. et al. **[110]** also studied the application of warm/hot air from the roof-integrated BIPV/T systems into the occupant area. **Figure 2-6** illustrates some of the possible ventilation strategies in case of double pane window systems.

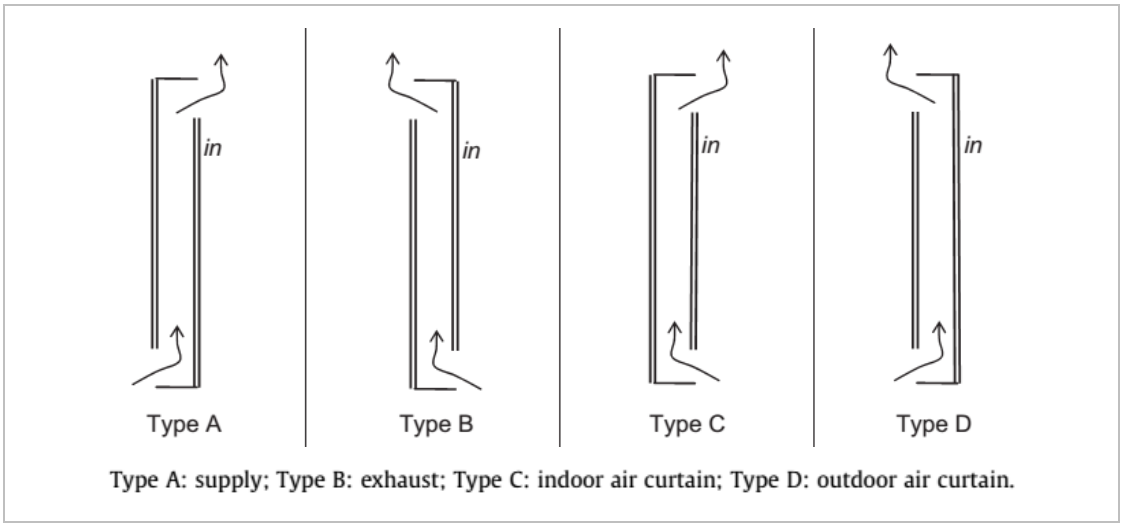

Figure 2-6: Some of the possible ventilation strategies in double pane window [111]

In the ventilation category, both passive as well as active mechanisms have been studied to evacuate the hot air from the cavity of STPV integrated double pane window/façade

systems. Peng J. et al. **[96]** experimentally studied the performance of a double skin façade (DSF) made of STPV module and clear glass with a 400 mm air gap between the two layers. Three different operations namely ventilation, buoyancy-driven ventilation, and non-ventilation have been considered in the analysis. The experimental setup used to create different modes of ventilation strategies is shown in **Figure 2-7.**

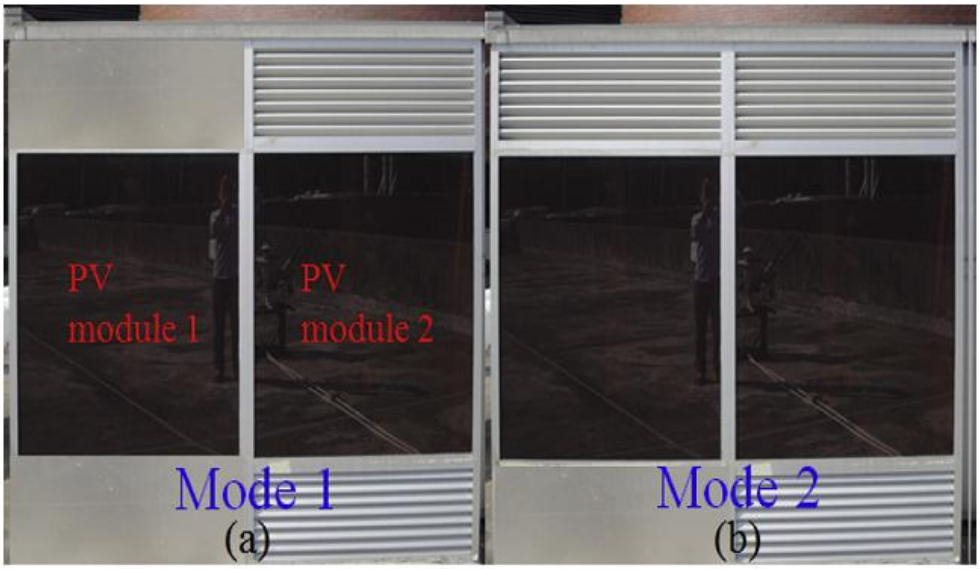

Figure 2-7: Experimental setup to create different mode of ventilation [96]

They observed that the ventilation mode reduced the maximum module temperature and led to the highest power generation. This operation delivered 3% more power generation than the non-ventilated condition. Lowest SHGC has also been observed with the ventilated mode of operation. On the other hand, the non-ventilated mode of operation provided the lowest U-value while it has been the highest in the ventilated mode of operation. Lower heat transfer through STPV DSF with the non-ventilation case has also been observed in another work of the same researchers **[94].**

Cooling of roof-integrated photovoltaic module due to outdoor airflow has been observed by Gan G. et al. **[112].** In the analytical analysis, Dubey S. et al. **[113]** noticed an improvement of 0.66% in conversion efficiency of glass to glass photovoltaic module due to airflow beneath the module. Some researchers have also investigated the effect of water in disseminating the heat from the photovoltaic module. Gaur A. et al. **[114]** achieved an improvement of 7.3% in electrical efficiency by flowing the water on the top of an a-Si module. They also observed that the effect changes with the mass flow rate of the water. Further, Charron R. et al. **[115]** theoretical analyzed the combined

effect of airflow and motorized blind on the performance of double pane photovoltaic façade. They observed an overall efficiency of 60% with the proper arrangement of the blind and the cavity.

In the active (force) mode of operation, the rate of air flow can be adjusted as per the requirement. Kaiser A.S. et al**. [95]** analyzed the performance of photovoltaic module under the force mode of operation. They noticed that the high air velocity in force mode of operation helps in improving the power output of the photovoltaic module. An improvement of 19% in power generation has been observed with air velocity of 6m/sec in force mode operation compared to the natural flow case (0.5 m/sec). They also proposed the semi-empirical formulae for temperature, conversion efficiency and power generation of the photovoltaic module under the force mode of air flow. The force mode of operation also helps in reducing the cooling demand of a building. For example, Chow T.T et al. **[108]** observed an energy saving of 82% in the air conditioning demand with a force-ventilated photovoltaic window compared to single absorptive glazing.

Figure 2-8 illustrates some ventilation strategies investigated in case of double pane window systems.

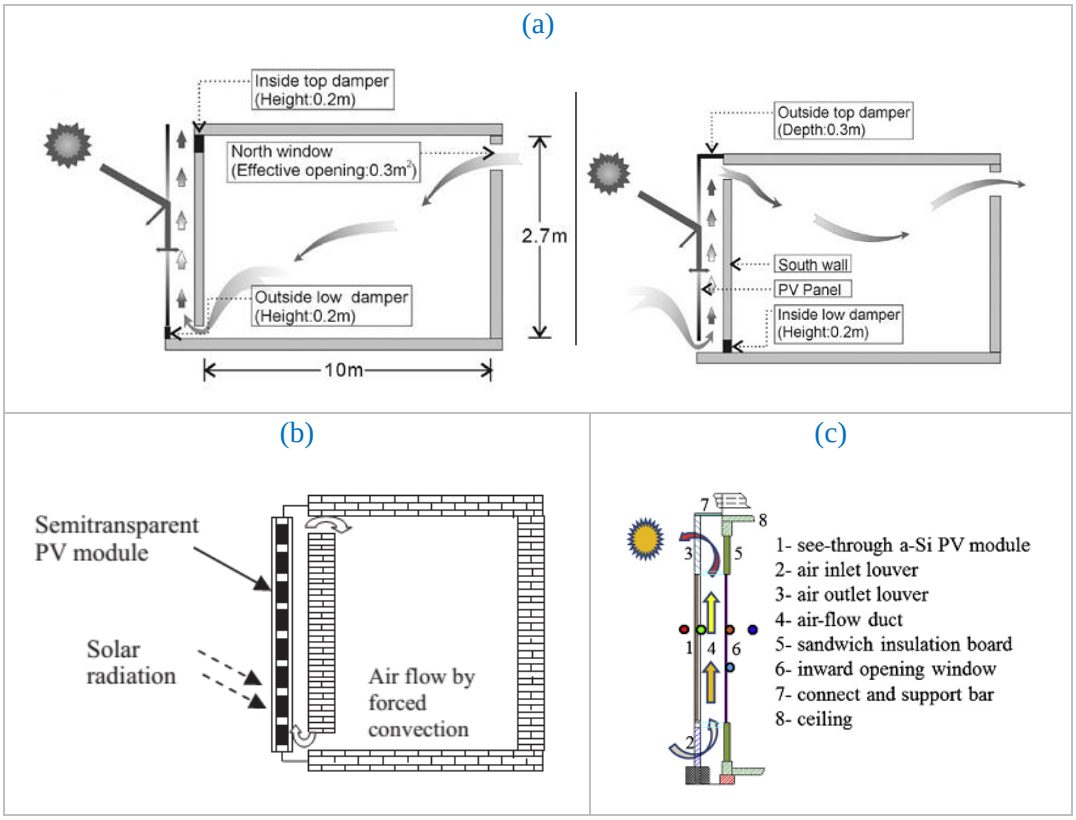

Figure 2-8: Some of the ventilation strategies investigated in the literature (a) Yun G. Y. et al. [78]; (b) Vats K. and Tiwari G.N. [103]; (C) Peng J. et al. [96]

The performance of photovoltaic systems decreases with the accumulation of dust on the module. The problem becomes severe in the arid and semi-arid region. Therefore, the photovoltaic systems need to be clean at regular interval. Water is most commonly used to clean the photovoltaic modules. However, in the arid regions of the middle east water is a limited resource. Therefore, automatic cleaning mechanism such as electrodynamic screens possesses high potential in future **[116].**

2.4 Energy saving potential using BIPV

The generation of energy by the BIPV system at the consumption center nullify the losses incurred in the process of transmission and distribution. Thus the BIPV system saves some amount of energy besides generation. Further, the heat gain through ventilated double pane STPV window is lower than the conventional glazing. The lower heat gains further enhance the energy-saving potential by using the STPV window. In the numerical investigation, Peng J. et al. **[21]** observed up to 50 % less net electricity consumption compared to commonly used glazing system in the cool Mediterranian climate. Miyazaki T. et al. **[80]** presented an energy performance of an STPV integrated building in Japan. With the optimized system, they achieved energy savings up to 54%, compared to the standard model for thermal analysis of Japanese office building. Further, a low room air temperature can be maintained by using ventilated STPV window/facade systems **[97, 106].** The lower room air temperature helps in reducing the energy consumption of the building in a cooling demand country. Chow T. T. et al. **[25]** obtained up to 28% electricity saving in cooling of a typical office building in the tropical climate of Hong Kong. The energy performance of the STPV window is also superior to absorptive glass **[16, 108].** Also, compared to the clear glass the STPV module can block up to 65% heat gain from entering into the occupant area **[117].**

Dinode E. L. et al. **[118]** conducted a theoretical investigation on the energy saving potential of STPV integrated window systems in two Brazilian cities. For this purpose, they developed a model of cell temperature and calculated the energy performance using EnergyPlus simulation software. The results were compared with a Low-e and a clear glass window. They noticed that in the orientation which doesn't receive direct solar radiation, the Low-e double glazed window delivered the best energy performance. However, in the other orientations, the STPV windows showed the better results. Compared to the clear glass window they observed energy saving up to 43% with the STPV window. Ordenes M. et al. **[119]** conducted EnergyPlus simulation to

analyze the impact of the BIPV system on the energy demand of Brazillian multi-family dwellings. In the study, the photovoltaic modules were considered in all the opaque façade of a low-cost building. They found that for 30% time of the year, the photovoltaic modules energy generation suppressed the demand for the considered building. Based on the findings, they also concluded that the energy generation potential of the BIPV system is not negligible at the lower latitude of Brazil. Energy saving potential of STPV systems in the high glazed building of Middle East which experiences harsh climate has been studied by Bahaj A. S. et al. **[120].** The analysis was carried out using TRANSYS simulation for the Burj-al-Arab Tower and Jumeriah beach complex, Dubai. Among different technologies, the thin film photovoltaic showed the most effective in the energy saving. They also concluded that if very high efficient modules are used, the energy generation will exceed the building cooling demand. Further, an estimate shows that the BIPV systems have the potential to meet up to 22% of the total electricity consumption of the European Union (EU) in 2030 **[121].**

WWR of STPV window in a building plays a significant role in the energy-saving. In the high glazed building of tropical climate (Singapore), the energy-saving potential of STPV window increases with WWR **[76].** The increase in energy saving with WWR has also been observed by Olivieri L. et al. **[122]** in the buildings of Madrid which experience the Mediterranean climate. They investigated the energy-saving potential of five different STPV module integrated window using EnergyPlus, PVsyst and COMFEN software. For the reference, they considered glazing with visible transmittance,0.461; g-value,0.473; and U-value,2.783. Compare to the reference glazing; they noticed an energy saving of 18% and 59% with WWR 30% and 88% respectively. Application of solar energy through passive mechanism is another important area for energy saving in the building. In a case study, Lotfabadi P. et al. **[123]** observed up to 30% energy saving in the high-rise building of London by combining the passive and active mechanisms of solar energy utilization.

The above discussion shows that the energy-saving potential of STPV window changes with many factors. Therefore, before installing, the STPV systems need to be optimized properly. However, different optimization methods should be considered depending on the climate of the location and application of the building **[22].**

2.5 Cost-benefit analysis

Both economic and environmental issues are considered in the evaluation of cost-benefit of renewable energy systems **[124].** Due to the involvement of numbers of components such as material, installation, operation & maintenance, fluctuation, and so forth the cost-benefit analysis is a challenging task. In this section, an attempted has been made to summarize the relevant literature focuses on economic, energy and environmental cost-benefit of BIPV systems. Different researchers have investigated the energy and economic aspects of benefits with respect to Energy Payback Time (EPBT), Life Cycle Conversion Efficiency (LCCE), Levelized Cost of Energy (LCE), Payback Time (PBT), Life Cycle Cost (LCC), Net Present Value (NPV). In the environmental head, calculation of reduction in greenhouse gases (GHG) such as CO_2, SOx, and NOx are the prime focus.

2.5.1 Economic and energy payback period

The involvement of many interdependent parameters makes the economic decision of BIPV systems a complex issue. Eiffert P. et al. **[125]** developed a guideline for the selection of BIPV system under the task 7-05:2002, of International Energy Agency (IEA). In the guideline, the methods for investment, design, and sizing of BIPV systems have been proposed. According to the guideline, for investment decision-making in the BIPV sector, all conventional method can be used. However, for designing and sizing a BIPV system, the NPV or LCC provided the more practical outputs. Ng P. K. et al. **[126]** developed a factor for ease of the designer and architectures in selecting the STPV module for building application. They proposed the concept of Net Electricity Benefits (NEB). The NEB is the combination of electricity saving in lighting, electricity consumption for space heating and cooling and energy generation due to photovoltaic effect. They also observed that under certain conditions the cost of some photovoltaic module could be less than the conventional double pane window.

The cost of energy or PBT of STPV systems is a function of many factors. For example, various photovoltaic modules such as mono, multi, and ribbon silicon, and CdTe are available in the market. Each module uses the different raw material. The manufacturing processes are different. The energy yields are also different among the modules. Among the various modules, the CdTe show the least LCE **[127].** It occurs mainly due to low energy requirement in the production of CdTe photovoltaic module. The EPBT is also observed to be minimum for the CdTe module in another research **[97].** Similarly, in

the case of PBT calculation, the parameters like electricity tariff, energy saving, trading of CO_2 have particular importance. With CO_2 trading the PBT of BIPV systems could be 10 years **[128].** In some other works, the PBT of STPV systems has found to be 15 years or at least less than the life of the technology **[129-130].**

Kamthania D. et al. studied the performance of semi-transparent hybrid photovoltaic thermal double pass facades (HPVT-DPF) in different configurations **[131].** They investigated the energy and exergy performance in four weather conditions of Srinagar. The consideration of thermal outputs has found to be effective in reducing the embodied energy payback time of the systems. Also, among various photovoltaic technology, the heterojunction with an intrinsic thin layer (HIT) has found to be advantageous with respect to Electricity Production Factor (EPF), Life Cycle Conversion Efficiency (LCCE) and CO_2 mitigation.

Further, the STPV system saves significant building energy consumption. The energy savings can be as large as three times of generation (1:3) **[132].** Therefore, when the energy saving is considered, the PBT reduce substantially. In a case study, Radhi H. et al. **[132]** found that the EPBT drops from 12-13 to 3- 3.2 years with the consideration of energy saving by the STPV systems in the buildings of UAE. The useful application of the heat generated by the photovoltaic module also improved the economic viability of a BIPV system. Buker M. S. et al. **[133]** conducted a techno-economic analysis of roof-integrated photovoltaic system embedded with polyethylene heat exchanger loop. The polyethylene heat exchanger observed to be effective in saving the waste thermal energy from the system. In the study, the cost of power generation has been calculated to €0.0778 per kWh using the LCC method.

2.5.2 Environmental impact

The environmental concerns are one of the major driving force for the development of renewable energy technologies. With the increase in energy generation from the renewable sources such as solar radiation, the emission of harm full Green-House Gases (GHG) is expected to be reduced significantly **[97].** Another significant contribution of the photovoltaic system is the reduction of hazardous particulate matters **[129].** Therefore, the environmental impact is an essential part of the cost-benefit analysis of STPV systems.

A considerable amount of energy is involved in the manufacturing of photovoltaic modules. As a result, the energy mix of the module manufacturing country has a substantial role in the environmental impact assessment of STPV systems **[126].** The environmental issues and related development also play a significant role in determining the STPV system's PBT **[130].** An extensive analysis of the environmental impact of the most commonly used solar modules has been carried by Peng J. et al. **[97].** The considered solar modules are mono-Si, multi-Si, a-Si CdTe, and CIS. They obtained the least GHG emission for the CdTe module. In case of CdTe module, the GHG emission has been calculated to 10.5–50 gCO_2 equivalents for per unit energy production.

2.6 Summary of literature review

The literature review shows that the double pane STPV window systems have got the immense interest in research towards achieving the low or net zero energy building. Various researchers have investigated these systems from the different point of views. In summary, the important works can be categories as follows

- The modeling, assessment, and effect of different parameters on the energy performance of STPV systems
- Innovative STPV system designs, optimization of WWR, orientations and module characteristics
- Different working scenario for better performances, optimization of the air gap between the panes of the window system
- Economic factors such as cost, payback period and so on involved with STPV systems
- Contribution of STPV systems towards a sustainable environment by reducing the GHG and particulate matters

Finally, the place of installation and local climatic conditions have found to play a significant role in the above aspects. However, hardly any research can be found in terms of Indian climatic context.

2.7 Research gaps identified

The following research gaps have been identified based on the literature review.

I. STPV for best optoelectrical and thermal performance in Indian climatic context has not been reported in the literature

II. The literature discusses the heat dissemination mechanism from the photovoltaic module. However, prevention of the infrared part of the solar spectrum which causes heating has not been significantly explored.

III. Wavelength-based study for energy generation of STPV module used in a building system is not investigated

2.8 Objectives of the research

Based on the research gap mentioned in the previous section, the following objectives have been proposed in the present research.

I. Development of double pane window system using semi-transparent photovoltaic module

II. Performance analysis of semi-transparent photovoltaic module based double pane window system under different operating conditions

Some of the considered design and operating conditions are mentioned below.

- Double pane window systems with change are the position of the cavity with respect to the STPV module
- Ventilated air cavity between the two window panes: Change in mode of ventilation
- Variation in STPV module characteristic: Change in STPV module Transparency
- Effect of location and orientation
- Effect of Angle of incidence
- Variation in Window to Wall Ratio (WWR)

2.9 Chapter summary

This chapter described the issues and theories related to the working of BIPV systems. It also contains the findings of some recently published literature relevant to the present research. The identified research gaps and objectives of the present research have also been included in this chapter.

CHAPTER 3
METHODOLOGY

3.1 Preamble

This chapter describes the methodology adopted to achieve the objectives of the present research. Both theoretical and experimental investigations as part of the research have been explained in the methodology. An overall description of the research approach has been presented at the beginning of the chapter. The research approach is followed by the description of the selected materials and their characterizations. After the material characterization, we moved to the system level and different working scenarios. A brief description of the software used to simulate various parameters have been included in the calculation section. In the end, this chapter discusses the experimental setup and the different instruments used in the experiment. In brief, the methodology has been divided into the following sections.

- Research approach
- Material selection and characterization
- Window configurations and airflow strategies
- Calculation method
- Design of experimental investigation

3.2 Research approach

The present research starts with reviewing the works related to the application of photovoltaic technology in the building sector. Available literature, various BIPV product installed around the world, different company's brochures and pamphlet, etc. were the sources of the review process. The thorough review helped in understanding the application of solar photovoltaic technology in building. It revealed the effectiveness of BIPV product, issues related to the technology and their applications, the market orientation and so on. In the second step, the objectives of the research were finalized based on the findings of the literature review. In setting the objectives, the parameters of immediate as well long-term importance were taken into consideration. The flow of work of the present research is shown in **Figure 3-1.**

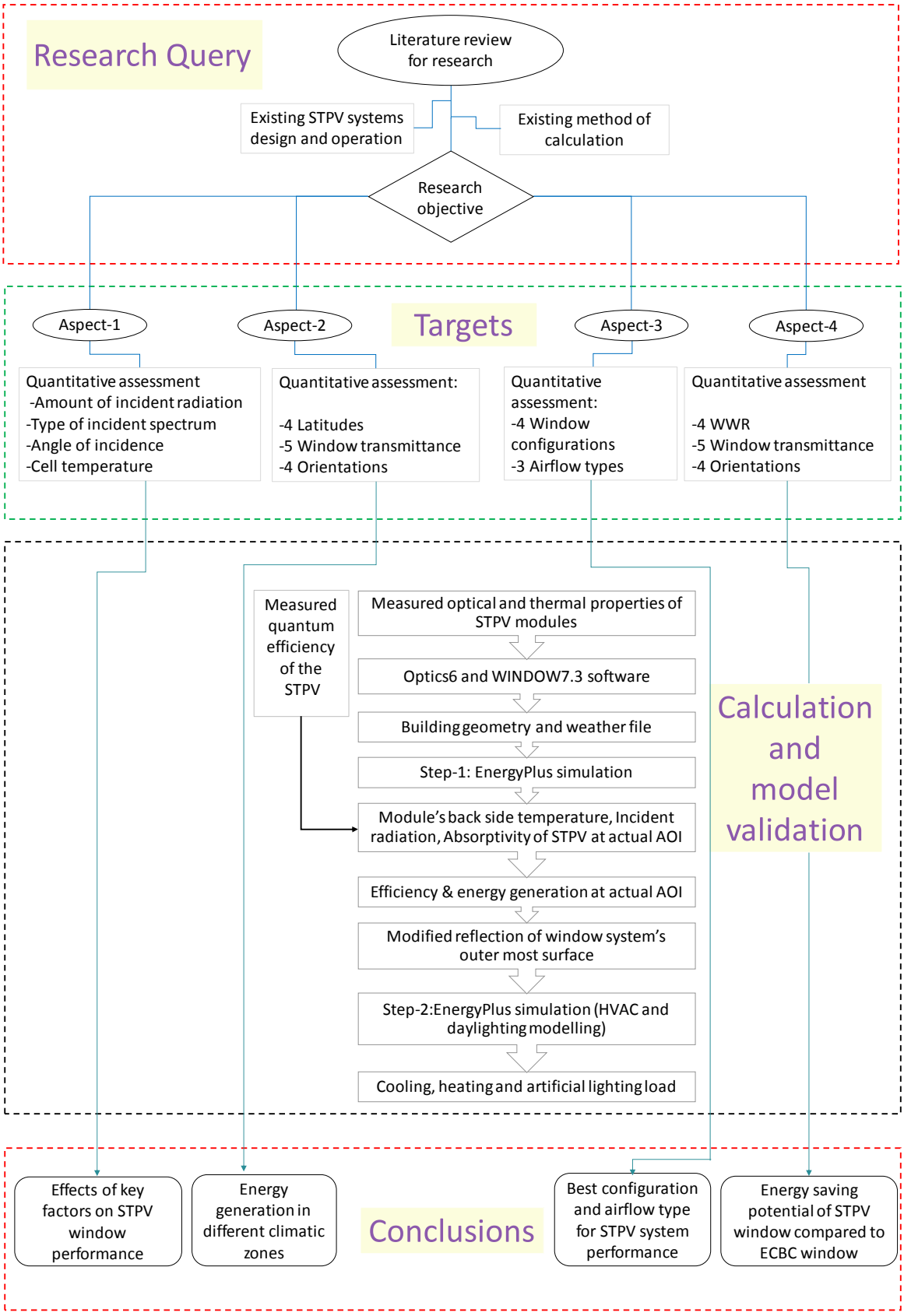

Figure 3-1: Flowchart of the research methodology

Once the objectives were finalized, further investigations were carried for the design of the research. For this purpose, different intermediate parameters were studied and selected to investigate further. The parameters were segregated depending upon their effectiveness and importance in the research process. The design of the research was also used to decide if a parameter would need to be found through simulation or experiment. Subsequently, different experiment and simulations were carried out at the parametric as well as system level. For the simulation, some data were collected from the literature. The validity of the few results was also compared with relevant findings in the available literature. Finally, the conclusions were drawn from the critical analysis of the experimental and simulation findings.

3.3 Material selection and characterization

Thin film semi-transparent solar photovoltaic modules have been selected in the present study. The cells of modules are made of Cadmium Telluride (CdTe). Decent working behavior in diffuse radiation, high material stability, low degradation of conversion efficiency with temperatures, etc. are some of the basic characteristics of CdTe material which make it a natural choice for building applications. Further, the studied location falls in the tropical region as described in section **3.5.2.** High ambient temperature is one of the basic features of this region. This also makes the CdTe material a good choice for the building application in studied location. Five different transparent modules were considered for the detail investigation. In order to separate them, the modules were marked as PV1, PV2, PV3, PV4, and PV5 according to their transparency in ascending order. The photograph of the selected modules is shown in **Figure 3-2.**

Figure 3-2: Photograph of the selected STPV modules

Photovoltaic module directly converts the incident solar radiation into electrical energy. The voltage and current are the basic properties associated with STPV modules. The other set of important parameter which defines the rating of photovoltaic modules are nominal power at Standard Test Condition (STC) and Fill Factor (FF). Instead of the FF, some manufacturers provide current and voltage at maximum power point along with current and voltage at the short and open circuit conditions respectively. Another category of parameters associated with photovoltaic modules rating is the temperature coefficients. Manufacturers provide the temperature coefficients of maximum power, open circuit voltage, and short circuit current. The properties of the considered STPV modules given by the manufacturer are presented in **Table 1.**

Table 1: Properties of the STPV modules at STC (provided by the manufacturer)

Parameters (unit)	**PV1**	**PV2**	**PV3**	**PV4**	**PV5**
Nominal power [Pm] (W)	71.34	63.5	55.68	47.85	43.50
Short circuit current[I_{sc}] (A)	0.880	0.780	0.680	0.590	0.540
Open circuit voltage [V_{oc}] (V)	116.0	116.0	116.0	116.0	116.0
Current at maximum power point [I_{mp}] (A)	0.820	0.730	0.640	0.550	0.500
Voltage at maximum power point [V_{mp}] (V)	87.00	87.00	87.00	87.00	87.00
Efficiency [η] (%)	9.910	8.800	7.730	6.640	6.040
Temperature coefficient of Isc (%/^{0}C)	0.060	0.060	0.060	0.060	0.060
Temperature coefficient of Voc (%/^{0}C)	-0.321	-0.321	-0.321	-0.321	-0.321
Temperature coefficient of Pm (%/^{0}C)	-0.214	-0.214	-0.214	-0.214	-0.214

The STPV modules are meant for building application. Therefore, besides the electrical properties, the optical and thermal characteristics are also equally important. The quantum efficiency is another important parameter for the present research investigation. All these properties are not mandatorily required for the conventional application of the photovoltaic system. These parameters are usually not found with the

manufacturers. Therefore, these characteristics of the selected STPV modules were measured experimentally. Samples of 5×5 cm were prepared to measure the required properties.

3.3.1 Optical characteristics

The optical characteristics were measured using a UV-VIS-NIR spectrophotometer, Lamda750 made by Perkin Elmer, the USA. It is a benchtop, true double beam, double monochromator spectrophotometer having a 60mm integrating sphere. The basic optical design of the integrating sphere is shown in **Figure 3-3.** The availability of the integrating sphere helps in capturing the primary and secondary beams along with the back-reflected radiation. Two detectors are there inside the integrating sphere. The first one is a PbS detector for the UV-VIS range another one is InGaAs for the NIR region.

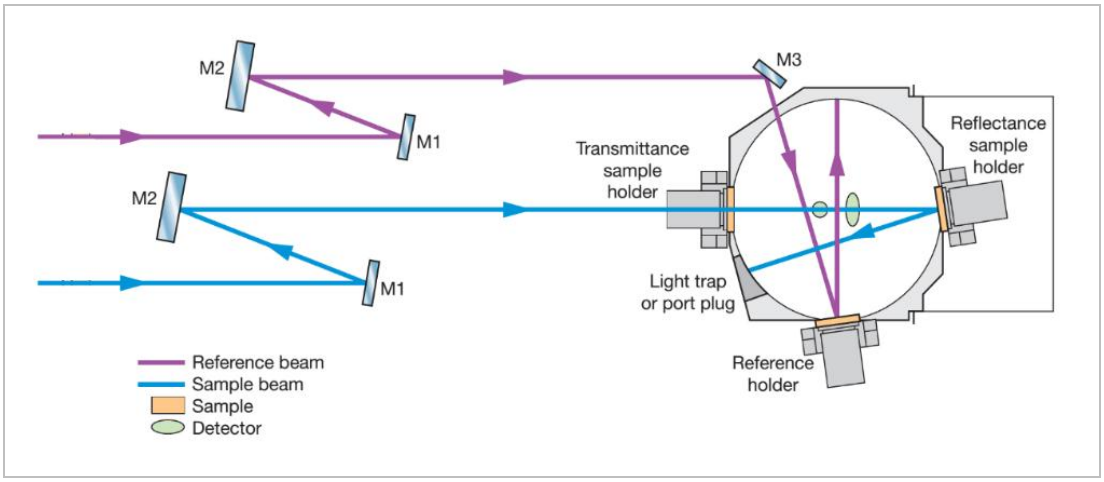

Figure 3-3: Basic optical design of the integrating sphere [134]

In the present research, the transmissivity, and front & back surface reflectivity at normal incidence were measured in the wavelength range from 300nm to 2500nm. **Figure 3-4** presents the measured transmittance characteristics of the selected STPV modules. It shows that for all the STPV module, the transmittance starts at 390 nm wavelength. The value reached the maximum point at 600 nm wavelength and then decreased. At wavelength around 1750nm, the transmittance decreases relatively more rapidly due to the presence of Ethylene Vinyl Acetate (EVA) in the module. For all the considered STPV modules, the transmittance becomes zero after 2300 nm wavelength.

The front reflectance is dominated by the property of the front glass and window layer of the solar cell. Due to this reason, the front reflectance curves of the modules become indistinguishable as shown in **Figure 3-5.**

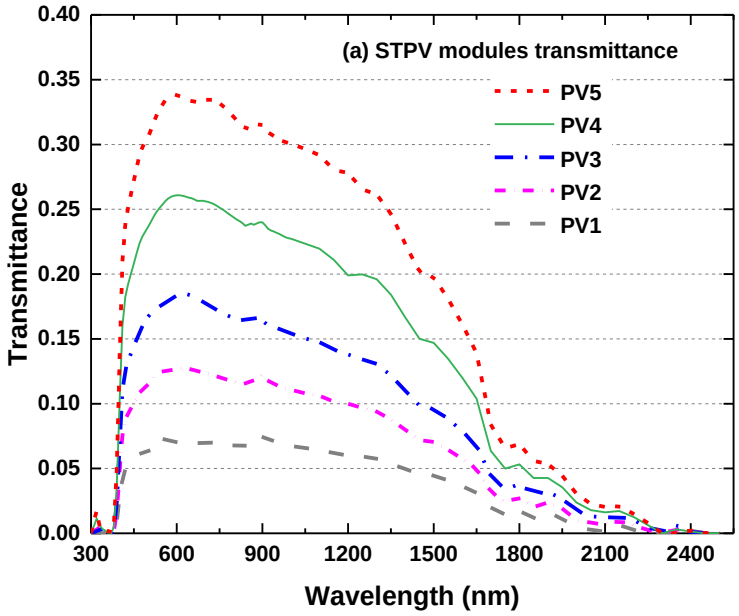

Figure 3-4: Measured transmittance characteristics of the STPV modules

In case of the back surface, besides the glass layer, the silver paste used for electrical connection also contributed to the reflectance. Since the area of the silver paste is the largest in the least transparent STPV module, the back surface reflectance is highest for this module. The presence of EVA on the back side of the modules leads to a rapid decrease of back reflectance in the wavelength range 1700nm to 1800 nm. The back surface reflectance characteristics of the selected STPV modules are shown in **Figure 3-6.**

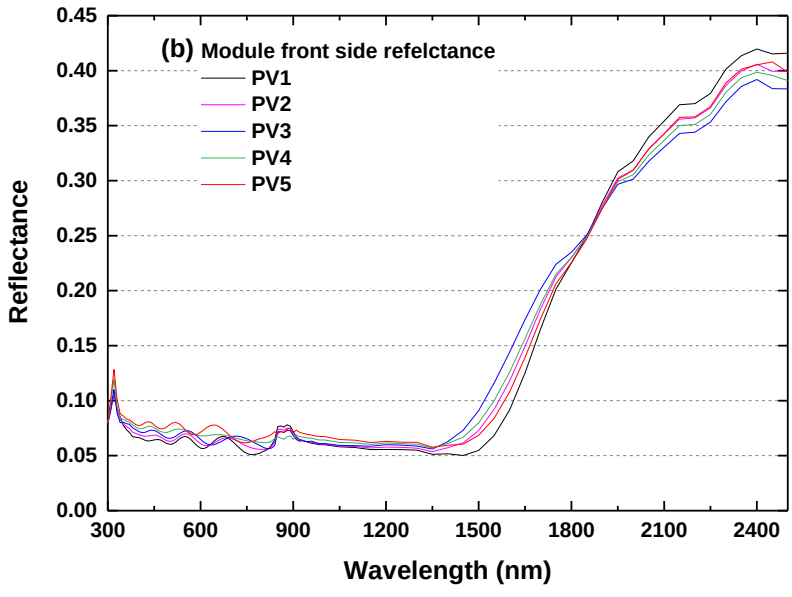

Figure 3-5: Measured front side reflectance characteristics of the STPV modules

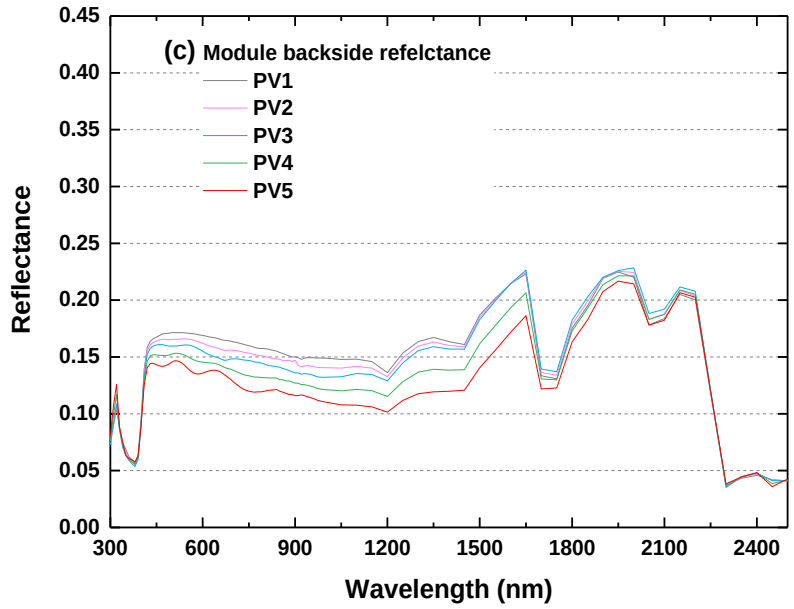

Figure 3-6: Measured backside side reflectance characteristics of the STPV modules

3.3.2 Thermal characteristics

The thermal properties were measured using Hot disk thermal constant analyzer (TPS 500) made by Hot Disk AB, Sweden. This instrument works on Transient Plane Source (TPS) theory. It uses a double spiral sensor supported by Krypton for mechanical protection and electrical insulation. The sensor acts as a source for increasing temperature of the sample as well as a thermo-resistor to record the increase in temperature with time. Quick measurement, a wide range of thermal quantities and high accuracy are the basic advantages of this instrument. In the present research work, the instrument was used to measure the thermal conductivity of the STPV modules using an appropriate sample size.

3.3.3 Opto-electrical characteristics

In the optoelectrical category, we measured the External Quantum Efficiency (EQE) of the selected STPV modules. EQE is the response of a solar cell to the incident spectrum. The EQE is measured without considering the reflection and transmission of the incident radiation. In the present research, the EQE was measured using a setup having Xenon Arc lamp, a monochromator for the self-driven chopper and other accessories. The schematic diagram of the complete setup is shown in **Figure 3-7.** The wavelength of the light generated by the Xenon lamp can be changed in the range of 300 to 1200 nm. The light initially passes through a diffraction grating type monochromator. The

light then focused on the sample with the help of a lens. A chopper is there to nullify the effect of the room lighting. Finally, the photogenerated current at each wavelength is measured by a lock-in amplifier. The short circuit condition is maintained during the observation of quantum efficiency.

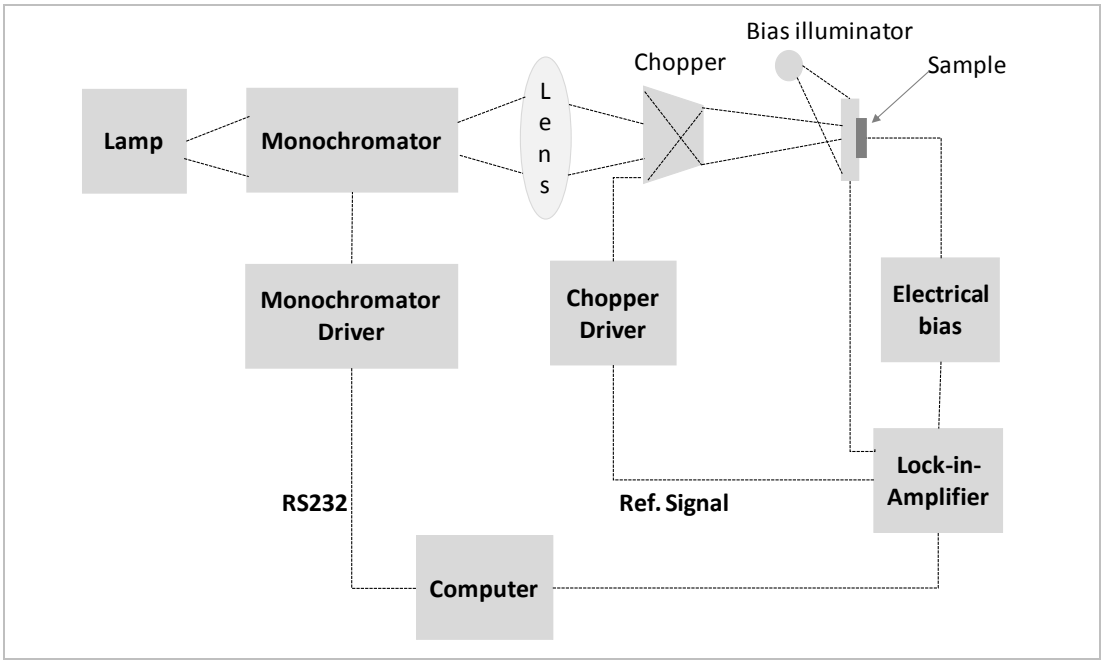

Figure 3-7: Schematic layout of the quantum efficiency measurement setup

The measured EQE of the considered STPV modules is shown in **Figure 3-8.** The graph shows that the spectral response of the selected STPV modules starts from the wavelength 340nm. The transmissivities of the selected modules are different. Therefore, the modules absorb a different amount of solar radiations. The different absorptions become distinct in the EQE after 350nm wavelengths.

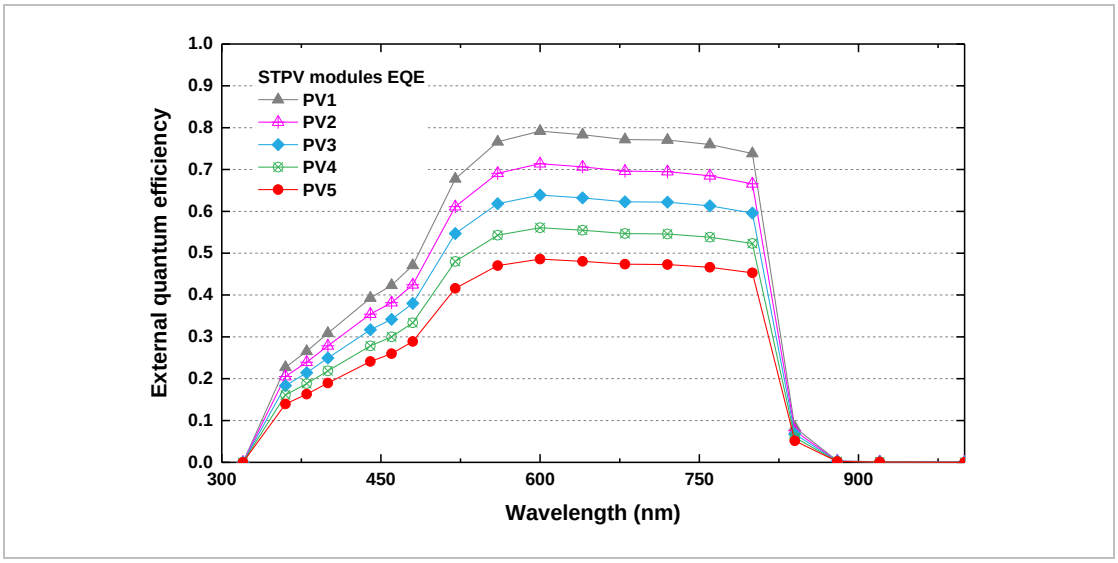

Figure 3-8: Measured external quantum efficiency of the selected STPV modules

Also, it is seen that the plateau region of the EQE remains between the wavelength range of 520nm and 800nm. After 800nm, the EQE started decreasing at a very fast rate and reached below 10% in a span of 40nm wavelength only. After 850nm the value of EQE further reduced and became zero.

3.4 Window system design and operation

The solar radiation reaches the earth surface in the form of electromagnetic wave. The energy of the radiation contains mostly in the wavelength range of 320 to 2500 nm. **Figure 3-9** shows the AM 1.5 spectrum of the solar radiation. The wavelength range (340 to 850 nm) in which the CdTe solar cell works are marked with color in the graph. It is seen that the considered STPV modules can't use the whole spectrum of the incident radiation to convert into electrical energy. The productive wavelength range contains only 628 W/m^2 out of the total 1000 W/m^2 incident energy.

The non-productive part of the incident radiation becomes the source of unwanted heat which adversely affects the working of the module by increasing in cell temperature. The increase in cell temperature reduces the power generation capacity of the STPV module due to a reduction in fill factor and efficiency **[27, 135].** The scenario demands to develop a configuration to reduce non-productive part of the solar spectrum and continuous heat removal from the STPV system.

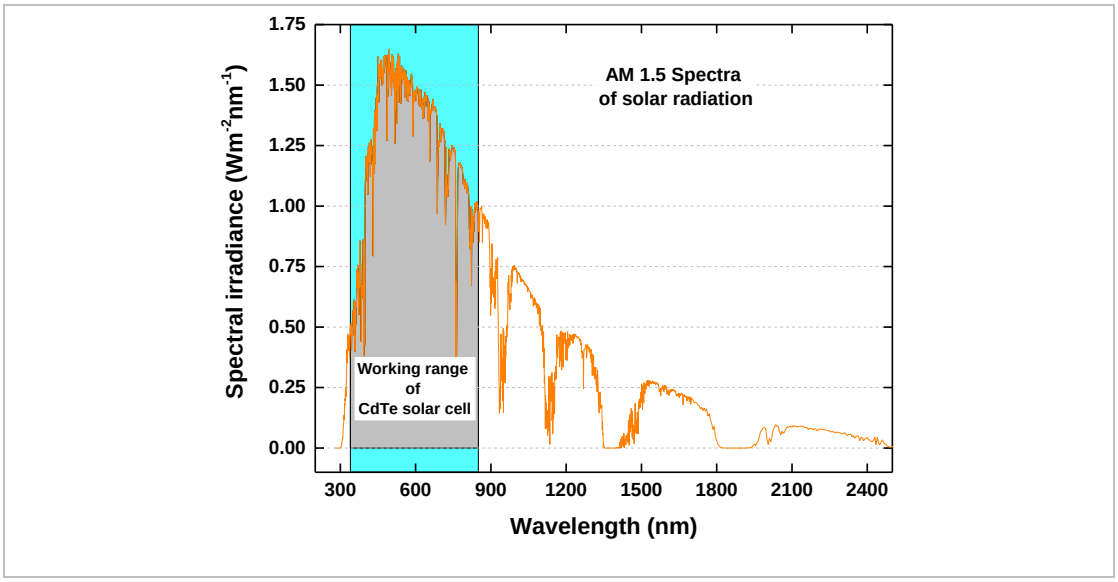

Figure 3-9: AM 1.5 spectra of solar radiation up to 2500 nm wavelength [NREL]

3.4.1 Window configurations

Blocking of the unproductive part of the incident solar spectrum from reaching the STPV module is one of the possible ways to manage STPV module temperature. **Figure**

3-10 and **Figure 3-11** present the optical characteristics of a conventional 4mm Clear Glass (CG) and a 3mm Low-e glass. The characteristics of the clear glass were measured using the spectrophotometer. While in the case of the Low-e glass, the characteristics were taken form Optics6 software database. The working wavelength range for the selected CdTe based STPV module is highlighted in the figures. The calculation shows that the selected Clear Glass and Low-e glass can block the unproductive part of the incoming spectrum by 17.3 % and 60.6 % respectively if used in front of the selected CdTe based STPV modules.

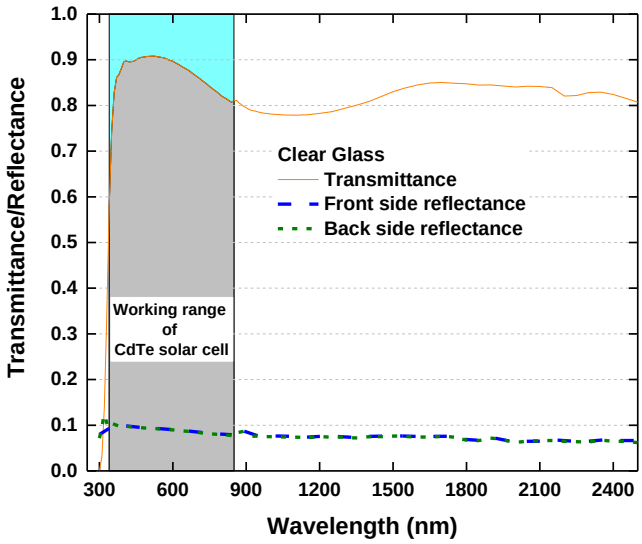

Figure 3-10: Measured optical characteristics of the selected clear glass (CG)

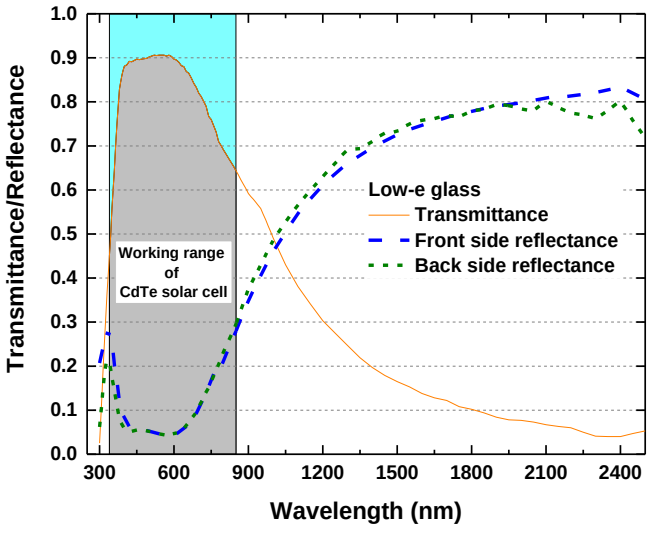

Figure 3-11: Optical characteristics of the selected Low-e glass [Source: Optics6 software]

In the present research, four double pane window configurations were constructed to investigate in terms of electrical and thermal performance. Layerwise, the construction of the four windows configurations were (CG/gap/PV3); (Low-e/gap/PV3); (PV3/gap/CG) and (PV3/gap/Low-e). For the analysis, the window configurations were labeled as W, X, Y, and Z respectively. Schematically, the window configurations are shown in **Figure 3-12.**

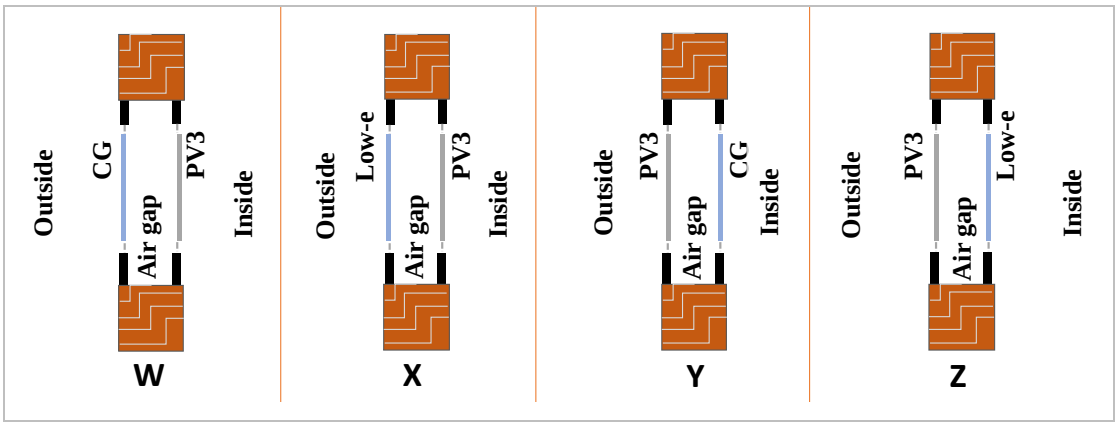

Figure 3-12: Schematic diagram of the proposed window configurations

Another set of five window systems were also considered in the present research. This set of window systems were constructed by using all the five STPV modules and the selected Low-e glass. Layerwise, the constructions of this set of window systems were (PV1/gap/Low-e); (PV2/gap/Low-e); (PV3/gap/Low-e); (PV4/gap/Low-e); and (PV5/gap/Low-e). In the analysis, these window systems were labeled as A, B, C, D, and E respectively.

3.4.2 Airflow strategies

Application of airflow through the cavity of a double pane window systems is one of the option to facilitate continuous heat removal from the system. The airflow cools the STPV module compared to no flow condition and thus helps in improving the photovoltaic conversion efficiency. The airflow also protects the system from overheating. Further, when the STPV module integrated windows are installed in an air conditioning building, the cooling and heating loads also become important. Therefore, the proposed window systems were investigated under different airflow strategies. **Figure 3-13** shows the schematic diagram of the considered airflow strategies. Four openable slits (J, L, M, N) were defined in the window system to release the hot air from the cavity. Three modes of airflow were attempted by selecting the appropriate slits as described below.

- In the first mode of operation, all window slits were kept closed, resulting in no airflow in the cavity. Two slits (O and P) in the opposite wall of the window systems were kept open for fresh air into the occupant area. This state of operation was deemed to be no airflow condition (F_0).
- In airflow type-1 (F_1), the front slits (J and K) were kept open. The hot air flows from the cavity to the outside environment without intervening with the occupant area
- In the airflow type-2 (F_2), two slits (J and L) were kept open. In this flow strategy, the hot air from the cavity flows into the occupant area.

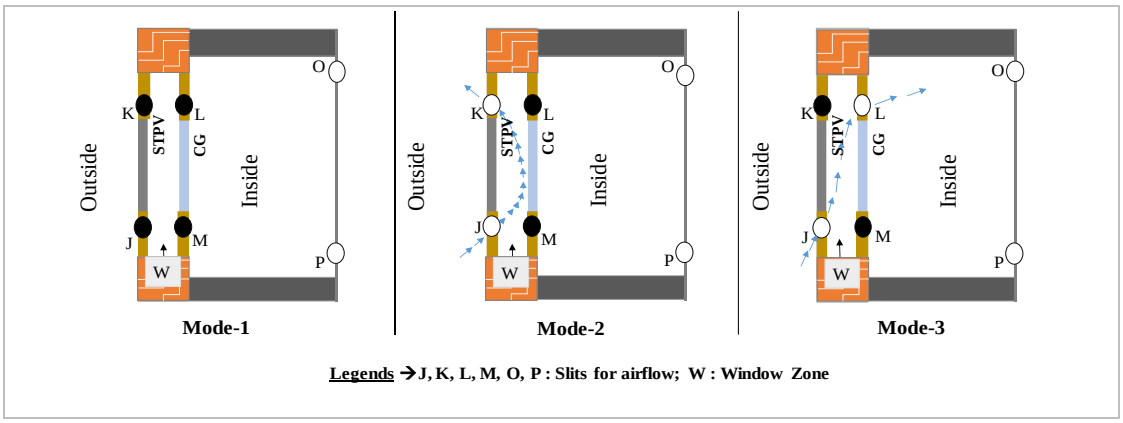

Figure 3-13: Schematic diagram of the proposed airflow strategies

3.5 Calculation method

The electrical and thermal energy along with daylighting performance of the proposed window systems have been the core parameters of the present research. These parameters were calculated in combination or individually in four different aspects. The four aspects are as follows.

1. Impact of different key factors on the energy generation in window integrated STPV module
2. Effect of angle of incidence on energy generation in window integrated STPV module
3. Effect of window configurations and airflow strategies on the performance of STPV module integrated window systems
4. Effect of STPV module integrated window systems on lighting and air conditioning loads

3.5.1 Software and applications

In order to investigate different aspects of the present research, the measured material characteristics were processed by using various software. The selected software and their application in the present research are briefly described below.

a) Optics software

Optics is an energy efficiency analysis tool, developed by Lawrence Berkeley National Laboratory (LBNL). In the database, it covers valuable glazing properties in the categories of applied film, coated, laminated and monolithic. It also contains the provisions to feed user's glazing characteristics. Glazing systems of different features can be a model and analyze as per the need. In the present research, the Optics6 software was used for the following purposes.

- ❖ To calculate the optical properties of the considered STPV modules in solar and visible bands from the measured spectral characteristics.
- ❖ To feed the STPV modules measured spectral characteristics into the WINDOW software.

b) WINDOW software

WINDOW is another useful tool of LBNL to study the energy efficiency of a window system. The user's glazing characteristics can be feed directly or using the Optics software. However, the import of glazing characteristics using Optics software facilitates the calculation of the angular optical properties. The WINDOW software can calculate the crucial parameters of a window like U-value, SHGC, and VLT. In the present research, the WINDOW7.3 software was used for the following purposes.

- ❖ To calculate the U-value, SHGC, and VLT of glazing center of the proposed window systems
- ❖ To calculate the angular optical characteristics of the considered STPV modules

i. Working procedures of Optics6 and WINDOW7.3 software

Both Optics6 and WINDOW7.3 calculate the normalized weighted average values of transmittance, reflectance, absorptance and hemispherical emissivity by using the following equations **[136].**

- Transmittance or reflectance in the solar range,

$$\xi_{solar} = \int_a^b \xi(\lambda)\Delta_x(\lambda)\Gamma(\lambda)d\lambda \,/\, \int_a^b \Delta_x(\lambda)\Gamma(\lambda)d\lambda;\ \text{a:320nm and b:2500nm} \quad (3)$$

- Transmittance or reflectance in the visible range,

$$\xi_{Visible} = \int_d^e \xi(\lambda)\Delta_x(\lambda)\Gamma(\lambda)d\lambda \,/\, \int_d^e \Delta_x(\lambda)\Gamma(\lambda)d\lambda;\ \text{d:380nm and e:780nm} \quad (4)$$

Where $\xi(\lambda)$ is the wavelength dependent value of transmittance or reflectance in the spectral characteristics; Δ_x, spectral weighting function; Γ, the response of the detector.

- Absorptance

After the transmittance and reflectance, the tools calculate the absorptance in iteration using the following equations **[136].**

$$A_j = \frac{T_{1,j-1}(\lambda)A_j^f(\lambda)}{1-R_j^f(\lambda)R_{j-1,1}^b(\lambda)} + \frac{T_{1,j}(\lambda)R_{j+1}^f(\lambda)A_j^b(\lambda)}{1-R_{j,1}^b(\lambda)R_{j+1,N}^f(\lambda)} \quad (5)$$

Where, $A_j^f(\lambda)=1-T_{j,j}(\lambda)- R_{j,j}^f(\lambda)$ (6)

And, $A_j^b(\lambda)=1-T_{j,j}(\lambda)- R_{j,j}^b(\lambda)$ (7)

In the above equation, the superscripts ‘b’ and ‘f’ represent the back and front surfaces respectively.

- Infrared emissivity

The infrared emissivity at normal incidence is calculated by using the reflectance as follows

$$\varepsilon = 1-R, \quad (8)$$

However, in calculating the hemispherical emissivity, the tools use the following polynomial equations **[136]**

$$\varepsilon_{\cap} = 1.3217\varepsilon - 1.8766\varepsilon^2 + 4.658\varepsilon^3 - 5.8349\varepsilon^4 + 2.7406\varepsilon^5;\ \text{when}\ \varepsilon \le 0.65, \quad (9)$$

in this case, the tools assume the glazing as a coated surface.

$$\varepsilon_{\cap} = 0.1569\varepsilon + 3.7669\varepsilon^2 - 5.4398\varepsilon^3 + 2.4733\varepsilon^4;\quad \text{when}\ \varepsilon > 0.65, \quad (10)$$

in this case, the tools assume the glazing as an uncoated surface.

- Angular optical properties

In calculating the angular optical behavior, the WINDOW software first deals with the refractive index and extinction coefficient. After that, the transmissivity and reflectivity are calculated from the wavelength-dependent transmittance and reflectance values using the following equations **[136]**

For uncoated glass,

$$T_\lambda(\Phi)=\frac{\tau_\lambda(\Phi)^2 e^{-\alpha_\lambda d/\cos(\Phi)}}{1-\rho_\lambda(\Phi)^2 e^{-2\alpha_\lambda d/\cos(\Phi)}} \quad (11)$$

$$R_\lambda(\Phi)= \rho_\lambda(\Phi)(1 + T_\lambda(\Phi)e^{-\alpha_\lambda d/\cos(\Phi)}) \quad (12)$$

Where, d, the thickness of the sample; Φ, the angle of incidence; τ_λ, transmissivity; ρ_λ, reflectivity ; α_λ, the absorption coefficient

For coated glass, the tool uses fourth order polynomial equations to calculate the angular transmissivity and reflectivity.

$$\bar{\tau}(\Phi)=\overline{\tau_0} + \overline{\tau_1}\cos(\Phi)\overline{\tau_2}\cos^2(\Phi)\overline{\tau_3}\cos^3(\Phi)\overline{\tau_4}\cos^4(\Phi) \quad (13)$$

$$\bar{\rho}(\Phi)=\overline{\rho_0} + \overline{\rho_1}\cos(\Phi)\overline{\rho_2}\cos^2(\Phi)\overline{\rho_3}\cos^3(\Phi)\overline{\rho_4}\cos^4(\Phi) \quad (14)$$

The value of the coefficients with respect to clear and bronze glass may be found in reference works **[136-137].** After the polynomial functions are found, the tool calculates the angular transmissivity and reflectivity as follows.

For, $\tau_\lambda > 0.645$;

$$\tau_\lambda(\Phi)= \tau_\lambda \times \overline{\tau_{clr}}(\Phi); \quad (15)$$

$$\rho_\lambda(\Phi)= \rho_\lambda \times (1-\overline{\rho_{clr}}(\Phi)) + \overline{\rho_{clr}}(\Phi) \quad (16)$$

For , $\tau_\lambda \leq 0.645$;

$$\tau_\lambda(\Phi)= \tau_\lambda \times \overline{\tau_{bnz}}(\Phi); \quad (17)$$

$$\rho_\lambda(\Phi)= \rho_\lambda \times (1-\overline{\rho_{bnz}}(\Phi)) + \overline{\rho_{bnz}}(\Phi) \quad (18)$$

The optical properties of the STPV modules calculated using Optics6 software are given in **Table 2.** The measured thermal conductivities of the STPV modules are also shown in the table. The table also contains the properties of the clear and Low-e glasses.

Figure 3-14 illustrates the angular transmissivity and front surface reflectivity of the selected STPV modules calculated using the WINDOW7.3 software. The change in absorptivity with the angle of incidence is presented in **Figure 3-15.** For clarity purpose,

the properties of three modules (PV1, PV3, PV5) have only been presented in the figures.

Table 2: Calculated optical and thermal properties of the STPV modules, Low-e and clear glass (CG)

Property	Band	Side	PV1	PV2	PV3	PV4	PV5	Low-e	CG
Transmittance at normal incidence	Solar		0.060	0.102	0.145	0.210	0.275	0.295	0.843
	Visible		0.070	0.123	0.177	0.252	0.327	0.902	0.902
Reflectance at normal incidence	Solar	Front	0.079	0.082	0.085	0.086	0.088	0.631	0.084
		Back	0.159	0.154	0.149	0.139	0.128	0.301	0.083
	Visible	Front	0.063	0.066	0.069	0.071	0.074	0.048	0.092
		Back	0.170	0.164	0.158	0.149	0.140	0.070	0.091
IR hemispherical emissivity		Front	0.837	0.837	0.837	0.837	0.837	0.037	0.840
		Back	0.840	0.840	0.840	0.840	0.840	0.837	0.840
Thermal conductivity			0.980	0.980	0.980	0.980	0.980	1.000	1.000

Figure 3-14 shows that both transmissivity and reflectivity changes rapidly after 70^0 AOI. The change in transmissivity with AOI is unequal among the considered STPV modules.

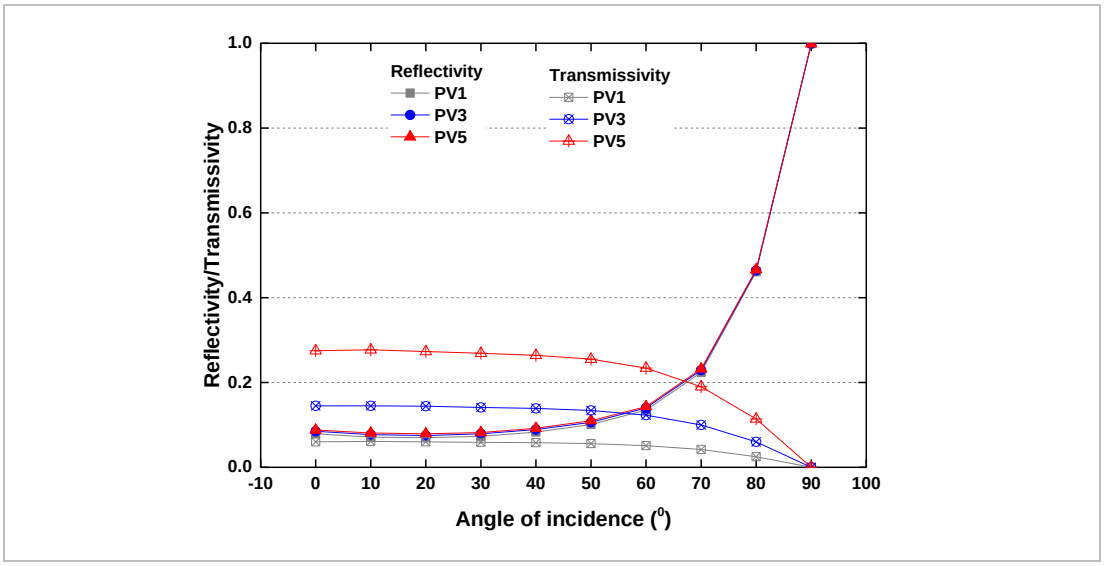

Figure 3-14: Calculated angular optical properties of the STPV modules (transmissivity and reflectivity)

On the other hand, the reflectivity changes at an equal rate. This difference in the change of transmissivity and reflectivity leads to an unequal change in absorptivity with AOI as shown in **Figure 3-15.** The difference becomes prominent in between 50^0 to 80^0 AOI.

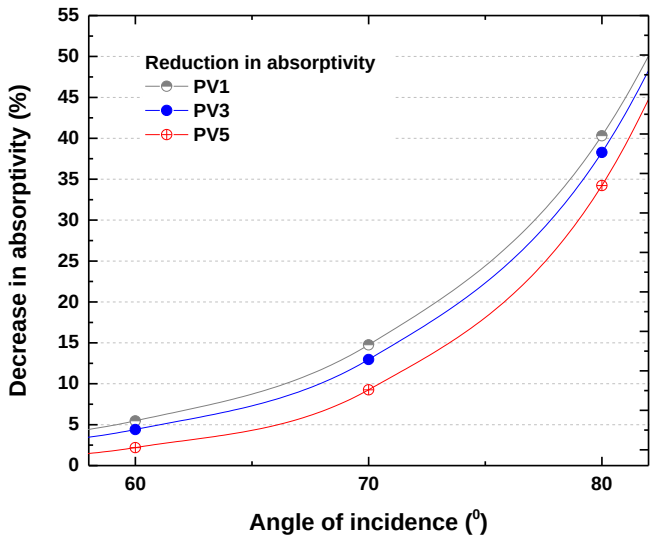

Figure 3-15: Calculated change in absorptivity of the STPV modules with AOI

- U-Value and SHGC

The WINDOW7.3 software calculates the thermal parameters like U-Value and SHGC, for the center of glazing as well as for a whole window assembly. In calculating the U-value of the glazing center, the tool uses the overall conductance (k_i) of thermal energy as follows **[136].**

$$U_C = 1/\sum_{j=1}^{N} k_i \quad (19)$$

Where N is the number of glazing layers

In calculating the SHGC, the tool uses the following equation.

$$SHGC_C = T_{1,N}^{sol} + \sum_{j=1}^{N} N_j A_j^{sol} \quad (20)$$

Where, $T_{1,N}^{sol}$, total transmittance through the glazing system ; N_j, inward flowing fraction of absorbed energy; A_j^{sol}, the absorptance of each layer of the window system.

The U-value, SHGC, and VLT of the glazing center in window systems A, B, C, D, and E, calculated using WINDOW7.3 are shown in **Table 3.** These U-values were calculated for 13mm, which is the most commonly used air gap between window pane.

The table also contains the same properties of a standard window (F) as per Energy Conservation Building Code (ECBC), India. The ECBC window was used to compare the building energy saving potential of the STPV integrated window systems (A, B, C, D, E). However, it is to be mentioned that WINDOW7.3 doesn't consider the energy generation by STPV module in calculating the SHGC values. Therefore, the SHGC will change slightly in the real operating conditions.

Table 3: Window systems and their properties calculated using WINDOW 7.3 software

Window systems	Construction	U-Value (W/m^2-K)	SHGC	VLT
A	PV1/gap/Low-e glass	1.812	0.129	0.064
B	PV2/gap/Low-e glass	1.812	0.158	0.112
C	PV3/gap/Low-e glass	1.812	0.186	0.160
D	PV4/gap/Low-e glass	1.812	0.228	0.229
E	PV5/gap/Low-e glass	1.812	0.271	0.297
F	Base case (ECBC window)	3.300	0.250	0.300

c) EnergyPlus software

The 'EnergyPlus' is a whole building energy simulation tool developed by the Department of Energy (DOE), the USA. The tool calculates the building energy load by simulating the building and associated energy systems through several interlinking programs. The core of the simulation is a model of the building that is based on fundamental heat balance principles **[137].** In the present research, EnergyPlus version 8.4 was used to calculate the following parameters for the considered window systems and airflow strategies.

- Incident solar radiation on the window surfaces
- Absorptivity of the window surface under the given working condition
- Surface temperature of the STPV module integrated window layers
- Heat transfer from window surface to the indoor environment

- Indoor air temperature
- Heating and cooling loads of the considered building
- Daylighting transmission through the STPV window and their influence on artificial lighting energy consumption

i. Window modeling in EnergyPlus software

In 'EnergyPlus' Version 8.4, the user's glazing characteristics can be feed in four different ways. They are a) full spectral data; b) spectral average data; c) data import from WINDOW software and; d) using U-Value, SHGC, and VLT. The window models developed by using the above data are known as a full spectral model (FSM), average spectral model (ASM), WINDOW 'EnergyPlus' model(W*M) and simple window model (SWM) respectively. The star (*) mark represents the version of the WINDOW software. In the present research, the ASM was used to model the window systems. Once the glazing characteristics are available in the simulation engine, different types of the window can be constructed as per the requirement. The window types are a simple window, equivalent layer, complex fenestration and airflow window. But none of these window constructions could model the airflow strategies proposed in the present study. Therefore, the airflow network model was used to analyze the window systems under different working conditions.

ii. Airflow Network

The Airflow Network (AFN) model can be used for multi-zone airflows driven by outdoor wind and forced air during HVAC system operation **[137].** For multi-zone natural airflow without distribution modeling, at least four objects are required to run the simulation. These objects are simulation control; multizone: zone; multizone: surface and multizone: components. The simulation control defines the parameters to be considered in the simulation. It also defines whether the wind coefficients are user input or auto-calculation. The multizone: zone object offers the option for selection of ventilation control mode. No-vent, temperature, enthalpy and constant are the available options to control the ventilation mode. The openable doors or window can be controlled as per the user need by importing the appropriate schedule into multizone: zone object. The schedule is defined in schedules: a compact object in the model. When the temperature is used to control the opening, the tool works based on the following

condition. The zone's openable doors/window is open if $T_{zone} > T_{out}$ and $T_{zone} > T_{set}$ and the ventilation schedule is on **[138].** Where, T_{zone}, $T_{out,}$ and T_{set} are respectively the temperatures of the considered thermal zone, ambient and set temperature for the slit opening and close.

In the modeling the airflows, the tool assumes an inlet and outlet nodes for each opening. The inlet and outlet nodes are linked by a relationship between mass airflow and pressure difference. The mass airflow is calculated by integrating the airflow velocity function in the relative gaps of airflow way. The pressure difference is calculated by assuming Bernoulli hypothesis that air density and pressure difference are linear functions of the height. Finally, the tool calculates the size and patterns of the flow depending upon the factors like wind pressure distribution, the state of the interior/exterior doors or windows, temperature between the zones and the outdoor environment **[138].**

iii. Incident radiation on window surfaces

In order to calculate the photovoltaic energy generation, the values of incident radiation are required in the form of total, direct and diffuse components. The weather file used in 'EnergyPlus' simulation contains solar radiation for horizontal surface only. Therefore, the values of radiation on the targeted surface were retrieved from the 'EnergyPlus' simulation results. The 'EnergyPlus' calculates the solar position and incident radiation for any time of the year using basic solar geometry as per the latitude, longitude, and elevation of the considered place. During the simulation, the 'EnergyPlus' engine considers these parameters from the weather file.

iv. Absorptivity of window surfaces

When simple window model (SWM) is used to model a window, the 'EnergyPlus' calculates the optical properties in ten different ways depending upon the types of glass selected **[137].** However, when FSM or ASM is used, the 'EnergyPlus' calculates the absorptivity after calculating the transmissivity and reflectivity similar to the WINDOW7.3 software as discussed earlier.

v. Surface temperature, indoor air temperature, and thermal load

The 'EnergyPlus' software calculates the surface and zone air temperature in the process of zone heat balance. Three segments of calculations are included in the zone

heat balance, namely, surface heat balances, internal gains, and air flows. The Conduction Transfer Function (CTF) algorithm was considered for the surface heat balance calculation. The CTF represents the thermal response as per material properties. In this algorithm, the current heat flux and temperature are determined concerning the weighted sum of the past (history) wall heat fluxes and surface temperatures **[139].** For the inside and outside surfaces, the program used the following equations **[137].**

$$q''_{ki}(t) = -Z_0 T_{i,t} - \sum_{j=1}^{nz} Z_j T_{i,t-j\delta} + Y_o T_{o,t} + \sum_{j=1}^{ny} Y_j T_{o,t} + \sum_{j=1}^{nq} \Phi_j q''_{ki,t-j\delta} \quad (21)$$

$$q''_{ko}(t) = -Y_0 T_{i,t} - \sum_{j=1}^{ny} Y T_{i,t-j\delta} + X_o T_{o,t} + \sum_{j=1}^{nx} X_j T_{o,t} + \sum_{j=1}^{nq} \Phi_j q''_{ko,t-j\delta} \quad (22)$$

Where; q''_{ki}, q''_{ko}, conduction heat flux on inside and outside surfaces; X_j, Y_j, and Z_j, are a surface to surface outside, cross and inside CTF coefficients respectively with j=0, 1……nz; T_i, $T_o$inside and outside face temperature; Φ_j, Flux CTF coefficient with j=1, 2……nz; nx, ny and nz, number of exteriors, cross and interior CTF terms; nq, number of flux history terms; t, current time; δ, time steps.

For zone air energy balance, the program provides three algorithms, third order backward difference, Euler method and analytical solution. The internal gains are dealt with respect to convective, radiation and latent heat energy. For calculation of zone thermal loads, 'EnergyPlus' directly uses the heat balance method of the American Society of Heating Refrigeration and Air-conditioning (ASHRAE). This method calculates the thermal loads in four steps, a) Outside face heat balance, b) Wall conduction process, c) Inside face heat balance, d) Air heat balance **[140].**

vi. Daylight transmission through the window systems

The 'EnergyPlus' simulation software was also used to calculate the available daylight and their contribution in saving the artificial lighting energy consumption. The software calculates daylighting and resultant effect in three steps. At first, it calculates the daylight factor, the ratio between the inside and outside illuminance. Secondly, it calculates the illuminance at the reference points. Finally, it calculates the lighting energy demand depending upon the difference between the available daylight and the design illuminance.

3.5.2 Climate features of considered locations

Out of the four aspects described in section **3.5,** aspect numbers 1,3 and 4 were investigated for the Jaipur city of India (Latitude:26.82^0N). On the other hand, four

different cities, including Jaipur, were considered in the investigation of aspect number 2. The climatic features of the consider locations are described below.

As per the National Building Code (NBC), the Jaipur city falls under the composite climatic zone of India **[141].** High solar insolation except for some typical months, the high temperature in summer, cold in winter, high humidity during monsoon are some of the prominent characteristics of this climatic zone **[142].** The temperature of this location reaches as high as 40^0C during the summer and as low as 4^0C in the winter **[143].** The maximum and minimum daily mean temperatures in different months of a year are shown in **Figure 3-16(a).** The figure shows that in the winter months the temperatures are below the comfort temperature. While in the summer months the temperatures are much above the comfort level. The heat wave during the summer months is another significant characteristic of this climatic condition. In a year, the location receives 5.68 kWh/m^2/day solar radiation on a horizontal surface. The monthly radiations incident on a horizontal surface is shown in **Figure 3-16(b).**

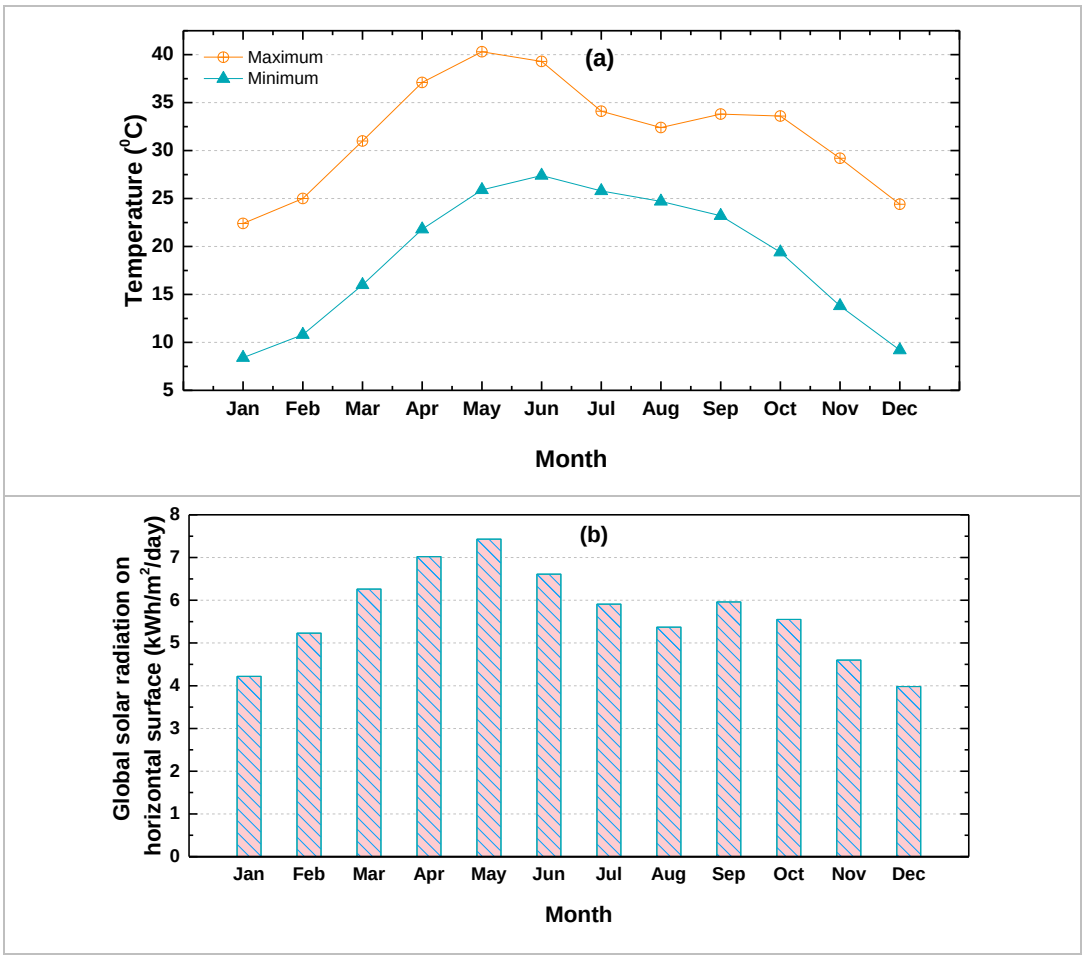

Figure 3-16: (a) Variation of maximum and minimum daily mean temperature of Jaipur [144] (b) Global solar radiation on horizontal surface at Jaipur [145]

It is seen that across the months, the incident radiation is above 4 kWh/m^2 per day which is a positive factor from the photovoltaic energy generation point of view.

To investigate the effect of angle of incidence on energy generation which was included in aspect-2, the selected locations are Thiruvananthapuram (Trivandrum), Akola, Jaipur, and Srinagar. The latitudes and longitudes of the cities are (8.48^0N, 76.9^0E); (20.70^0N, 77.0^0E); (26.82^0N, 75.7^0E) and (34.48^0N, 74.7^0E) respectively. Climate-wise, the southernmost city (Trivandrum) comes under the hot and humid climate while Akola falls in hot & dry climatic condition. As explained earlier, the city (Jaipur) which is just above the Tropic of Cancer experiences composite climate. On the other hand, the northernmost city (Srinagar) falls under the cold and cloudy climatic condition. The detail characteristics of these climatic conditions may be found in the standard documents like ECBC 2007 **[142].** From south to north, the considered locations receive 5.75, 5.70, 5.68 and 4.98 kWh/m^2/day, global solar radiation on a horizontal surface **[145].**

3.5.3 Building geometry and modeling

Two buildings geometries were used to investigate all the four aspects of the present research. The aspects number 1,2 and 3 were investigated with a naturally ventilated building. While the aspect number 4, was investigated with respect to an air conditioning building. The geometry and modeling of the buildings are described below.

In the naturally ventilated case, a building geometry of size 3×3×3m (H×W×B) was used to generate the basic inputs for the 'EnergyPlus' simulation. The detailed geometry of the building is shown in **Figure 3-17.** The openable slits in the figure represent the openings for airflow in the window cavity. In the 'EnrgyPlus' software, Input Data File (IDF) editor was used to change the construction materials in order to set the building envelope's thermal properties as per the ECBC standard. The thermos-physical properties of the construction materials were imported from the 'EnergyPlus' software database.

For the construction of the window systems, the required properties of the STPV layers and conventional glasses were fed from **Table 2.** The considered window configurations, orientations and airflow type in the investigation of different aspects were as flows.

- Aspect-1→ Window configuration: Y; Orientation: South; Airflow type: F_1
- Aspect-2→Window configuration: Y (window systems: A, B, C, D, F); Orientation: South, East, West, North; Airflow type: F_1
- Aspect-3→Window configurations: W, X, Y, Z; Orientation: South; Airflow type: F_0, F_1, and F_2

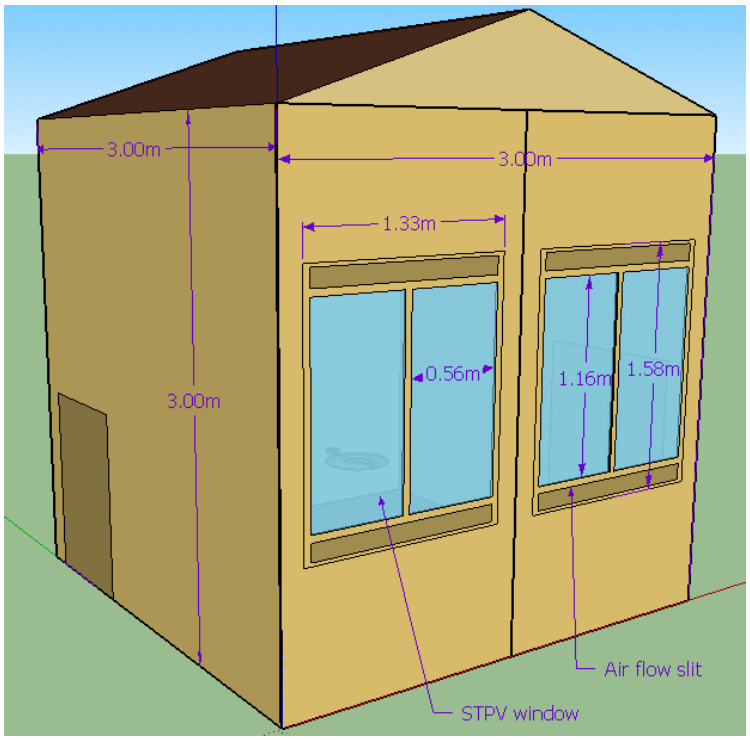

Figure 3-17: Building geometry used to investigated the aspect numbers 1, 2 and 3

In the simulation, two windows of one configuration were considered in the wall of one orientation. The size of each window was 1.33×1.85 m with glazing area 1.3 m^2. Therefore, for the given wall dimension, the glazing area of two windows create a window to wall ratio (WWR) of 28.8%.

In the investigation of aspect 4, a square building geometry having the ground floor only was used to create the basic input for the simulation. The length and width of the building were 15m with 3m floor to ceiling height. In this case, the thermos-physical properties of various materials were also imported from the software database. U-values of different parts of the building envelope were maintained as per the prescribed values in the ECBC guidelines for daytime used building in the composite climate of India. The resultant U-values of the exterior walls and roof were computed to be 0.493 W/m^2-

K and 0.352 W/m^2-K respectively. Window system wise, the aspect-4 was investigated with A(PV1/gap/Low-e), B(PV2/gap/Low-e), C(PV3/gap/Low-e), D(PV4/gap/Low-e), and E(PV5/gap/Low-e). A standard window system F was also considered in the investigation of this aspect. The properties of the STPV layer and Low-e glass were used from **Table 2,** in constructing the STPV integrated window systems in 'EnergyPlus' software. The detailed geometry of the building is shown in **Figure 3-18(a).** The thermal zone planning used in the study is shown in **Figure 3-18 (b).**

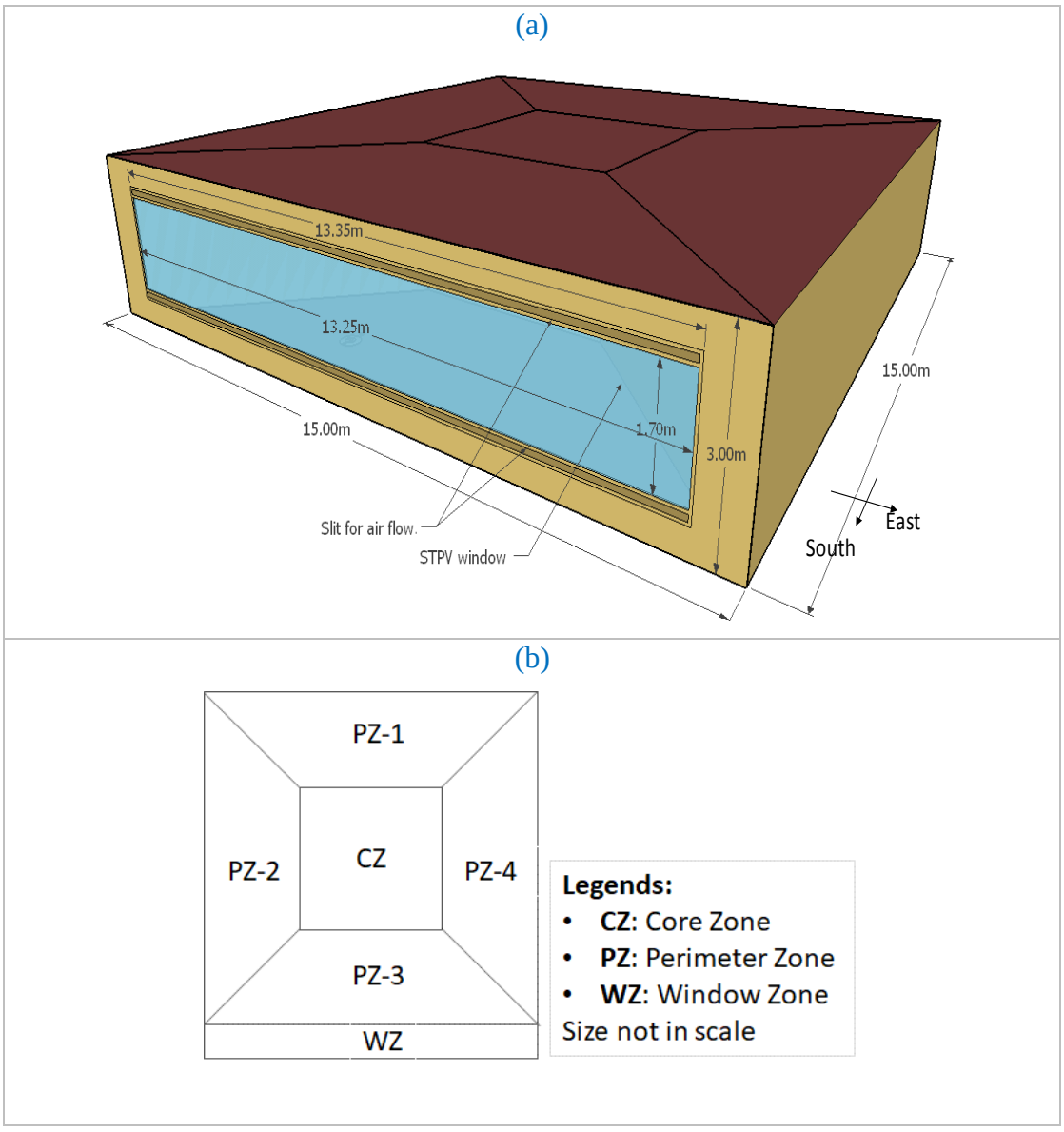

Figure 3-18: (a) Building geometry; (b) Thermal zone planning of the building used to investigate the aspect-4

Different building models were used to change the window to wall ratio from 20% to 50% in the step of 10%. Window position wise all four geographic orientations were

considered one after the other for each window systems. Among the proposed airflow types, detail study was carried out with F_1.

In the simulation the window slits and the natural ventilation were modeled by using the airflow network object in the natural ventilation and duct leakage component of the EnergyPlus. The complete process needed four objects. 1. Airflow Network: Simulation control, where the airflow control is defined as multizone without distribution or with distribution. 2. Airflow Network Multizone: Zone, where the control mode such as constant, temperature, enthalpy etc are defined. 3. Airflow Multizone: Surface, where targeted surface such as a plate of the slits, door etc are defines. 4. Airflow Network Multizone: Component: Detail opening, where the state of the opening such closed, quarterly open, half open or fully open are defined.

3.5.4 Electrical and thermal energy calculation

In the light of the involvement of several inter-depended parameters, such as temperature, AOI, energy generation, cooling, heating, and lighting loads, the 'EnergyPlus' simulation software was found to be the suitable platform. In the present study, EnergyPlus version 8.4 has been used for the thermal simulation. This version of the software can reasonably calculate the energy generation of building attached opaque type photovoltaic system. However, the tool cannot directly simulate the energy generation by building integrated semi-transparent solar photovoltaic modules. Therefore, in the present research, the energy generations by the STPV modules were calculated separately. Subsequently, the energy generation by photovoltaic conversion was incorporated in the thermal calculation through the reflection of the outermost surface of the window system. In this case, the reflection of the outermost surface was modified by adding an amount equivalent to the energy generation. Therefore, in the final step of the simulation, the modified reflection of the outermost window surface was feed in the 'EnergyPlus' software. The similar concept was also proposed by Didone E. et al. **[118].** The detail description of the calculation processes is presented below.

a) Calculation of electrical energy generation

The quantum efficiency and hence the short circuit current density of solar cell changes with the wavelength of the incident radiation. This fundamental concept was used to calculate the electrical energy generation in the present study. The detail discussion on

the relation between short-circuit current density and quantum efficiency of the solar cell may be found in standard literature, e.g., Chapter 3 of Solar Photovoltaics; fundamentals, technologies, and applications **[146].**

The electrical energy calculation involved many formulae. Some of the applied formulae are given below.

I. Photon flux

$$\phi_\lambda = \frac{E_\lambda \times \lambda}{hc} \quad (23)$$

II. Short circuit current density

a) $J_{sc,\lambda} = q\phi_\lambda \times EQE_\lambda$ (24)

b) $J_{sc,\lambda} = q\phi_\lambda \times \alpha_\lambda \times IQE_\lambda$ (25)

III. Open circuit voltage

$$V_{oc} = \frac{KT_{25}}{q} \times \ln\left(\frac{J_{sc}}{J_0} + 1\right) \quad (26)$$

IV. Conversion efficiency

$$\eta_{T_{25}} = \frac{J_{sc} \times V_{oc} \times FF}{E} \quad (27)$$

V. Operating cell temperature

$$T_c = T_m + \frac{E}{E_0} \times \Delta T \quad (28)$$

VI. Temperature dependent conversion efficiency

$$\eta_{T_c} = \eta_{T_{25}}\{1 + \theta_k(T_c - 25)\} \quad (29)$$

VII. Power generation at operating cell temperature

$$P = \eta_{T_c} \times E \quad (30)$$

VIII. Power generation with efficiency at STC condition

$$P_{STC} = \eta_{STC} \times E \quad (31)$$

IX. Spectral mismatch factor **[147]**

$$M = b_0 + b_1.AM_a + b_2.p_{wat} + b_3.\sqrt{AM_a} + b_4\sqrt{p_{wat}} + b_5\frac{AM_a}{\sqrt{p_{wat}}} \quad (32)$$

In Equation (V), ΔT is the temperature difference between the cell and the module back surface at an irradiance level of 1000 W/m^2. In the case of a plain glass-cell-glass module, the values changes from 1 to 3 **[19].** In Equation (VI), θ_k, is the temperature coefficient for maximum power output. For the considered CdTe modules, the value of $\theta_k$is -0.214 % per °C (provided by the manufacturer). In Equation IX, the values of the

coefficients for CdTe modules are, b_0:0.7946; b_1:-0.05423; b_2:-0.01319; b_3:0.1724; b_4:0.8372; b_5:-0.004376 **[147].**

The steps involved in the electrical energy calculation of the present research are described below.

i. Collection of the hourly total, beam and diffuse incident radiation on the STPV module integrated window surfaces from the 'EnergyPlus' simulation results. The radiations were collected for every hour of the year for the time duration 8:00 AM to 6:00 PM
ii. Conversion of the incident radiation into spectral characteristics considering AM 1.5 spectrum of NREL. In converting the radiation, the wavelength ranges were kept equal to the range of available EQE values
iii. Conversion of spectral characteristics into equivalent photon flux by using Equation I
iv. Calculation of short-circuit current densities for each wavelength range using Equation II(b). In this step, the experimentally computed values of absorptivity at normal AOI were used with total and diffuse incident radiation. The absorptivity values of STPV modules at actual AOI collected from 'EnergyPlus' simulation were used with the beam component of the incident radiation. In this step, it has been assumed that the reflectivity or transmissivity are equal for all wavelength for a particular AOI.
v. Conversion of short-circuit current density into hourly values by integrating all the individual data in different wavelength ranges.
vi. Calculation of perceptible water content in the atmosphere by applying a defined equation in ref. **[148] .** The required hourly air temperature and relative humidity were collected from the weather file of the considered location
vii. Calculation of effective air mass by using the concept of zenith angle and variation of pressure with height **[149]**
viii. Calculation of spectrum mismatch (M) factor for CdTe module by using Equation IX
ix. Calculation of hourly short-circuit current density, open circuit voltage and conversion efficiency with the actual incident radiation spectrum. Equation III was used to calculate the hourly open circuit voltage. The hourly conversion efficiency was calculated by using Equation IV. Experimentally measured

values of fill factor corresponding to a range of open circuit voltage were used in the calculation of conversion efficiency

x. Collection of STPV module's back surface temperature from 'EnergyPlus' simulation results.

xi. Calculation of operating cell temperature using Equation V

xii. Calculation of temperature dependent hourly conversion efficiency using Equation VI

xiii. Calculation of hourly power generation of the year using Equation VII

xiv. Calculation of hourly power generation throughout the year for all three types of incident radiation separately. The energy generations by diffused and beam radiation were combined to calculate the energy generation at actual AOI. In the present study, the energy generation at actual AOI was calculated in four different latitudes, orientations and five STPV module transmittance.

The optical properties of the STPV module are the basic inputs for the 'EnergyPlus' simulation. Thus, in calculating the absorptivity of the STPV modules at the different time of a day, the 'EnergyPlus' takes into account both optical characteristics and AOI. These indicate that the energy generation at actual AOI calculated in the present work included both cosine and optical effect. Here it was assumed that the AOI does not affect the energy generation by diffuse radiation. The similar observation was also drawn by Fanney et al. **[70]**

xv. Calculation of daily, monthly and yearly energy generation by using the hourly values

b) Thermal energy calculation

The thermal calculations involved in the present study were carried out using the 'EnergyPlus' software. For this purpose, the energy generations by the STPV modules were considered as an additional reflection from the outermost surface of the window systems as explained earlier. With the modified optical properties, the 'EnergyPlus' models were executed further to investigate the thermal performance in all the aspects of the research. The parameters for which the values were collected from the EnergyPlus simulation are mentioned below.

i. Temperature of the window surfaces

ii. Heat transfer through the window into the indoor environment
iii. Mass flow rate of hot air from window cavity
iv. Indoor air temperature

In the investigation of aspect-4, the effect of the STPV module integrated window on the lighting and air conditioning loads, the 'EnergyPlus' simulation was carried out under the following considerations. For the calculation of Heating Ventilation and Air Conditioning (HVAC) system, simple core-perimeter thermal zoning patterns were considered. A separate thermal zone was used to design the window system, which was subsequently merged into a thermal zone of the building. In this pattern, the building was divided into four perimeters and one core thermal zones as shown in **Figure 3-18(b).** Five working days in a week and office occupancy schedule were considered to calculate the heating and cooling demand of the building. The area allowed for each occupant was $7m^2$. As per the NBC of India, the range of comfort temperature in winter and summer seasons are 21-23^{0}C and 23-26^{0}C respectively **[141].** In the present work, the thermostat was set at 22^{0}C and 24^{0}C respectively for heating and cooling loads calculation. However, it is to be mentioned that since the design of the cooling or heating system is not the prime objective(s) of the study, the ideal loads were calculated and analyzed. Further, to evaluate the impact of the STPV integrated systems exclusively, the zone merged the window was only considered in the analysis of energy saving potential. The assumptions and schedules used in the HVAC calculation are summarized in **Table 4.**

Table 4: Assumptions and schedules considered in the HVAC calculation

Parameters	Values
Occupancy (m^2 per person)	7
Office schedule	09:00 AM to 06:00 PM
Operational days	Weekdays except for holidays
Type of HVAC	Ideal
Constant heating setpoint (^{0}C)	22
Constant cooling set point (^{0}C)	24
Office equipment (W/m^2)	11.4

3.5.5 Daylight transmission through window systems

The daylight transmission through the window systems and their influences on the Artificial Lighting Energy Consumption (ALEC) were also calculated using

'EnergyPlus' simulation. Among the different aspects of the research, this factor was studied in aspect-4 only. In the calculation of lighting energy demand, the working and occupancy schedule and area per person were similar to the HVAC calculation. The lighting power density of 10.8 W/m^2 was considered as per the recommendation of ECBC for an office building **[142].** The reference point for artificial lighting control concerning the available daylight was taken from the middle of the window system at a depth of 1m and height of 0.85m. The assumptions used in the daylighting calculation are summarized in **Table 5.**

Table 5: Assumptions considered in daylighting calculation

Parameters	Values
Depth of daylight control reference point (m)	1
Lighting power density (W/m^2)	10.8
Lumen levels (Lux)	500
Schedule	09:00 AM to 06:00 PM

3.6 Design of experimental investigation

Experimental investigations were carried for both electrical and thermal energy performances. In the electrical energy category, the investigated parameters were the short-circuit current density and open circuit voltage and the power generation. In the thermal performance category, the measured parameters are the temperature of different layers of the window system, heat flux through the window and room temperature. The incident radiation on the window surface was measured in the form of total and diffuse radiation. On the other hand, the global radiation on the horizontal surface was taken from the weather station at the Centre for Energy and Environment, MNIT Jaipur. The experimental setup and the applied instruments are explained below.

3.6.1 Experimental setup

The experimental setup was constructed on the campus of Malaviya National Institute of Technology Jaipur (MNITJ). It was a lightweight, portable 3×3-meter chamber. The floor to ceiling highest is also 3 meter. The outer and inner walls were made of Polyvinyl chloride (PVC) profile. In between two PVC profiles, extruded polystyrene (XPS) insulation of 50mm thickness was placed for thermal insulation. For enough mechanical strength, the skeleton of the chamber was made of mild steel (MS) hollow pipe. The gap between two consecutive pipes was 762 mm (2.5ft). The floor of the chamber was also made up of MS pipe, XPS insulation, and plywood.

The preliminary calculation showed that the window configuration contains STPV module in front of the conventional glass generates more photovoltaic energy than the other configurations. Further, the value of transmissivity of PV3 is middle among all the considered STPV modules with a reasonable VLT. Moreover, the selected clear glass is easily available in the local market. Therefore, the window configuration 'Y' (PV3/gap/clear glass) was considered in the experimental setup. Two windows of the selected configuration were installed in a designated wall of the chamber. Each window contained two STPV modules. The length and width of the modules are 1.2m and 0.6m respectively. Out of the given length and width, 2 mm of each side goes inside the window frame. Therefore, for the given wall dimension, the two windows create a WWR of 28.8 %. For airflow purposes, four slits were constructed in the wall opposite to the window systems. The dimensions of the slits were 20×138 cm (H×W). In cognizance with **Figure 3-17,** the slits in the opposite wall were constructed at 20 cm below and above the window level. The experimental setup is shown in **Figure 3-19.** Different stages of the construction process are given in the Appendix.

Figure 3-19: Photograph of the experimental setup

3.6.2 Details of the instruments used

In order to measure various parameters during the experiment, the required sensors were installed in the appropriate location of the test chamber. **Table 6** presents the specifications of the applied instruments in the experimental investigation.

Table 6: List of instruments used in the experiment and their specification

Sl. No	Name	Accuracy	Make	Application	Remark
1	U-value Kit-1 U-value Kit-2	8.49 [μV/(W/m^2)] 16.8 [μV/(W/m^2)]	greenTEG	Wall U-value Ceiling U-value	Different models have different sensitivity **[150]**
2	Conductive heat flux sensor Radiative heat flux sensor	2.8 [μV/(W/m^2)] 7 [μV/(W/m^2)]	Captec Enterprise	Conductive heat flux through the window Radiative heat flux through the window	Sensitivity calculated using extrapolation
3	L-19 data logger	1 [μV]	Leiderdorp Instruments	Heat flux sensor data logging	
4	Pyranometer	1 [mV/(W/m^2)]	DELTA-T devices Ltd	Incident radiation on the window	Measured both total and diffuse radiation
5	Thermocouple	0.5[^{0}C]	Radix Electrosystems Pvt Ltd	Temperature of window surfaces, cavity inlet/outlet, and room	
6	MPPT Charge controller	≤0.1%±50 [mV]	Morningstar	To charge and discharge of battery, record V_{max}, P_{max}	
7	Universal data logger	2% up to 50 [^{0}C]	Agilent Technology	Temperature logging	
8	Weather station	15 [mV/(W/m^2)] for radiation	Virtual Electronics	Radiation, ambient temperature, wind speed, precipitation	

Two U-value kits were installed in the wall and ceiling of the test changer to measure the U-value of the respective parts. One Pyranometer made by DELTA-T device limited was installed along the surface of the window to measure the incident solar radiation. The same pyranometer was used to measure both the global and diffuse radiation incident on the window surface. For the measurement of window surface temperature, the K-type thermocouples were carefully installed in the backside of the modules and the glass. In order to get the more reliable values of temperature, three thermocouples were installed on a single surface. One thermocouple was also installed in the middle of the room to measure the room air temperature. Two heat flux sensors were installed on the innermost surface of the window system. Out of the two heat flux sensors, one measures the conductive part, while the other measures the radiative part of the total heat flux from window to the room. However, in the results the combined values have been used. In order to draw the power from the STPV modules, a charge controller with maximum power point tracking (MPPT) was used in the experiment. The output power of the STPV modules was supplied to a battery through the charge controller. The same charge controller was used to record the voltage and maximum power of the STPV modules.

3.6.3 Measurement and model validation

The experiment was performed in June 2017. The hourly values of different parameters were measured by using the appropriate sensor. The measured parameters are mentioned below.

- Solar radiation on the horizontal and window surface
- Ambient air temperature
- Heat transfer through the window systems into the room
- Room air temperature
- STPV module back surface temperature
- Power generation by the STPV modules

After the experiment, the 'EnergyPlus' simulation and related calculations were performed for the similar constructions and working scenario. In order to calibrate the model, the simulation was performed with the measured ambient temperature and solar radiation on the horizontal surface. Finally, the reliability of the simulated values vis-a-vis experimental measurements was checked by using statistical parameters such as

Mean Bias Error (MBE) and Coefficient of Variation of the Root Mean Squared Error CV(RMSE). The formulae used to calculate the MBE and CV(RMSE) values are given below **[151].**

- Mean Bias Error (MBE)

$$\text{MBE}\ (\%) = \frac{\sum_{i=1}^{N}(M_i - S_i)}{\sum_{i=1}^{N} M_i} \times 100 \quad (33)$$

- Coefficient of Variation of Root Mean Square Error [CV(RMSE)]

$$\text{CV(RMSE)}(\%) = \frac{\sqrt{\frac{\sum_{i=1}^{N}(M_i - S_i)^2}{N}}}{\frac{\sum_{i=1}^{N} M_i}{N}} \times 100 \quad (34)$$

Where,

M_i, S_i, measured and predicted (simulated) values at the time 'i'; N, number of values used in the calculation.

3.7 Chapter summary

This chapter discussed various steps involved in the methodology of the present research. Five different sections have been used to explain the methodology. The chapter clearly described the following points.

- Materials and their characteristics used in the present study
- Different window configurations and their working
- The building geometry and climatic features considered in the study
- Working and applications of the considered software
- Calculation process of different parameters like energy generation by the STPV integrated window system.
- The experimental investigation conducted in the present research

CHAPTER 4
RESULTS AND DISCUSSIONS

4.1 Preamble

STPV window performs differently with the change in system design and operation strategy. The performance is also affected by module characteristics and local climatic conditions. This chapter presents the findings of the present research under all the considered variables. The basic science associated with STPV window system has been used to discuss the findings. The results have presented in the following four sections.

1. Impact of different key factors on the energy generation in window integrated STPV module
2. Effect of angle of incidence on energy generation in window integrated STPV module
3. Effect of window configurations and airflow strategies on the performance of STPV module integrated window systems
4. Effect of STPV module integrated window systems on lighting and air conditioning loads

4.2 Model validation

In the present study, all the investigations related to the non-air conditioning building have been carried out using an experimentally validated simulation model. The experiment was carried in Jaipur (Latitude 26.82^0N). The applied window configuration was 'Y' (PV3/gap/CG) with air flow type F_1, described in sections **3.4.1** & **3.4.2.** The experiment was carried in June. The parameters observed during the experiment are global radiation on horizontal and window surfaces; ambient, module, room air temperature; heat flux through the window system into the room; and the power generation by the STPV module.

The incident global radiation on a horizontal surface in June is shown in **Figure 4-1.** For clarity, the values have been presented in three sub-graphs of ten days. It is seen that except a few days, the solar radiation was not very stable in June. Therefore, detail analysis of the investigated parameters has been presented for some selected days having relatively stable solar radiation. The selected days are 14,15,16, and 17^{th} of June.

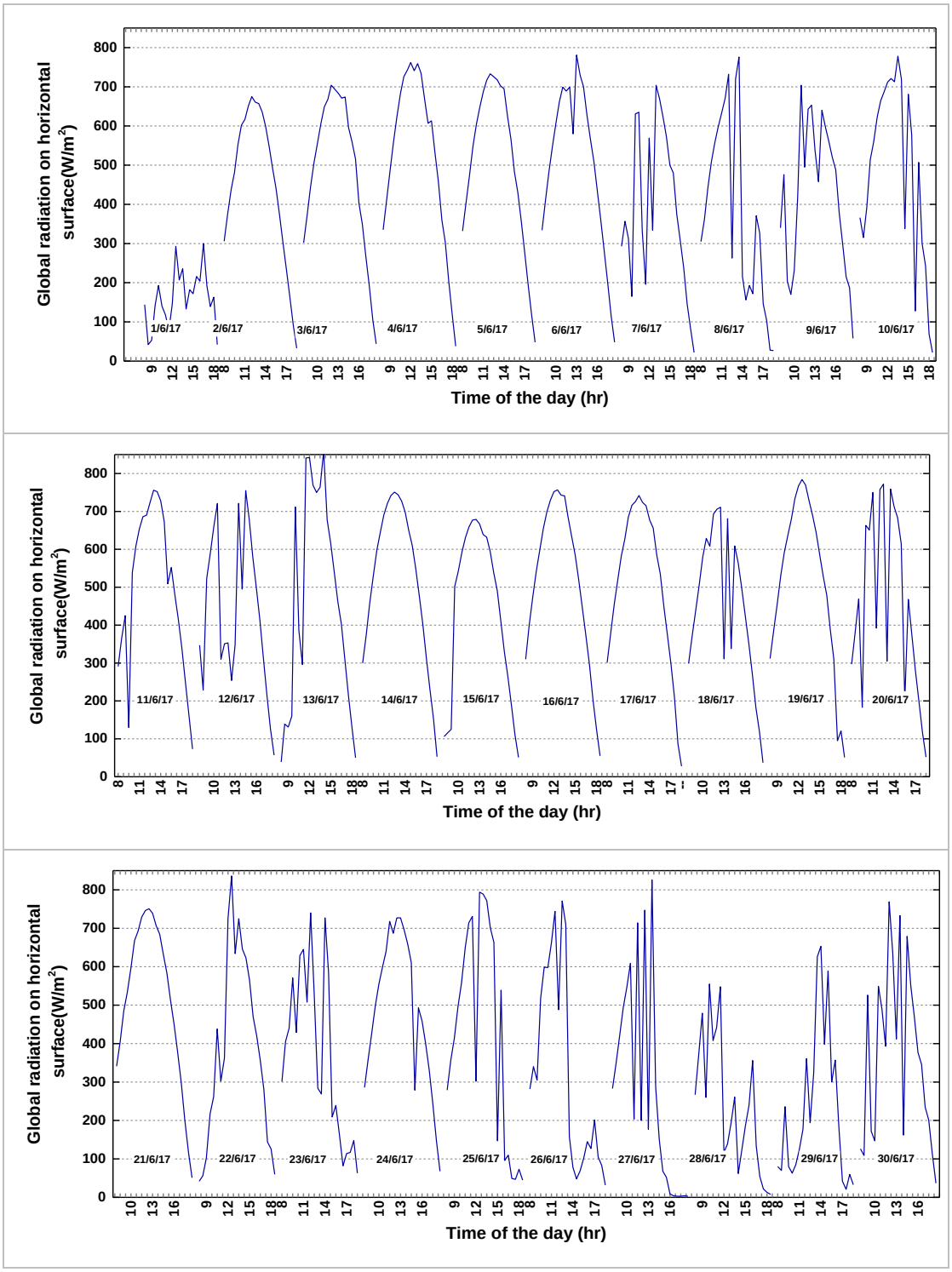

Figure 4-1: Measured global solar radiation on a horizontal surface on different days in the month of June

4.2.1 Validation of heat flux through STPV module integrated window

In the experiment, the heat fluxes were measured using the conductive and radiation heat fluxes meters, described in section **3.6.2.** On the other case, the software automatically calculated in the simulation. A comparison of the measured and simulated values of heat fluxes through the window is presented in **Figure 4-2.** It is observed that the simulated values are slightly lower than the measured values. The maximum MBE and Cv(RMSE) between the measured and simulated values are 4.15% and 9.63%.

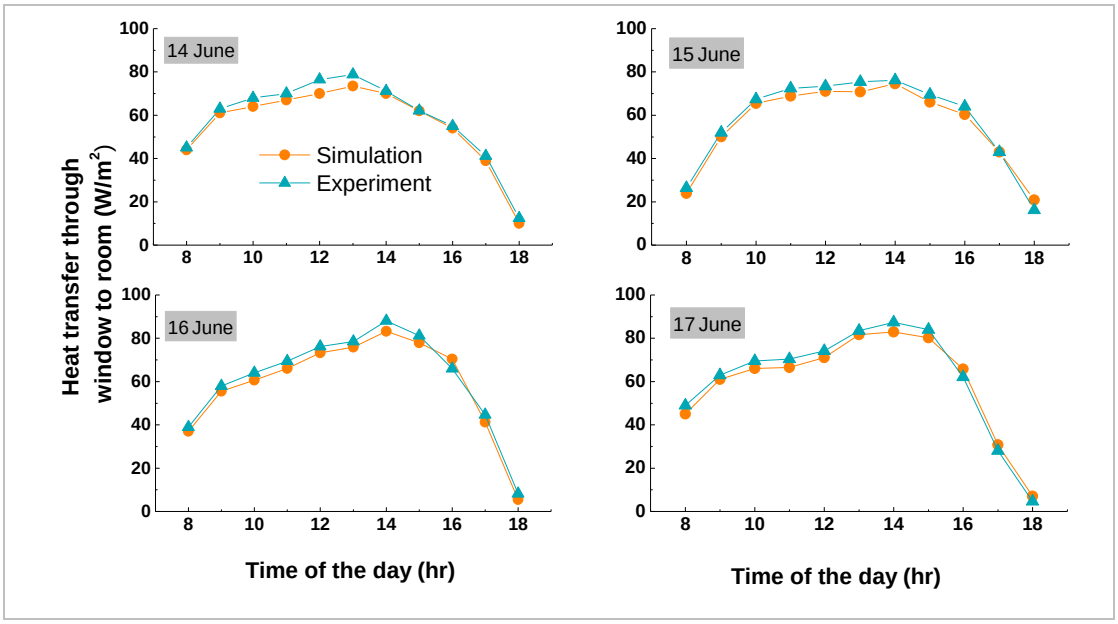

Figure 4-2: Measured and simulated values of heat flux through STPV window system into the occupant area

4.2.2 Validation of room air temperature

The U-value of the building envelope used in the simulation and the experiment are similar. Further, the solar radiation and ambient temperature in the weather file were replaced with the measured values during the simulation. This helped in creating a simulation model equivalent to the experimental setup.

A comparison of the measured and simulated room temperature is shown in Figure 4-3. It is seen that the simulated values of room temperature are quite matching with the measured values. The maximum difference between the predicted and observed values of room temperature is 0.67^0C. The maximum value of MBE and CV(RMSE) between the simulated and measured room air temperature are 1.04% and 0.49% respectively. These errors are very low. These indicate that the simulated model could predict the room temperature quite accurately.

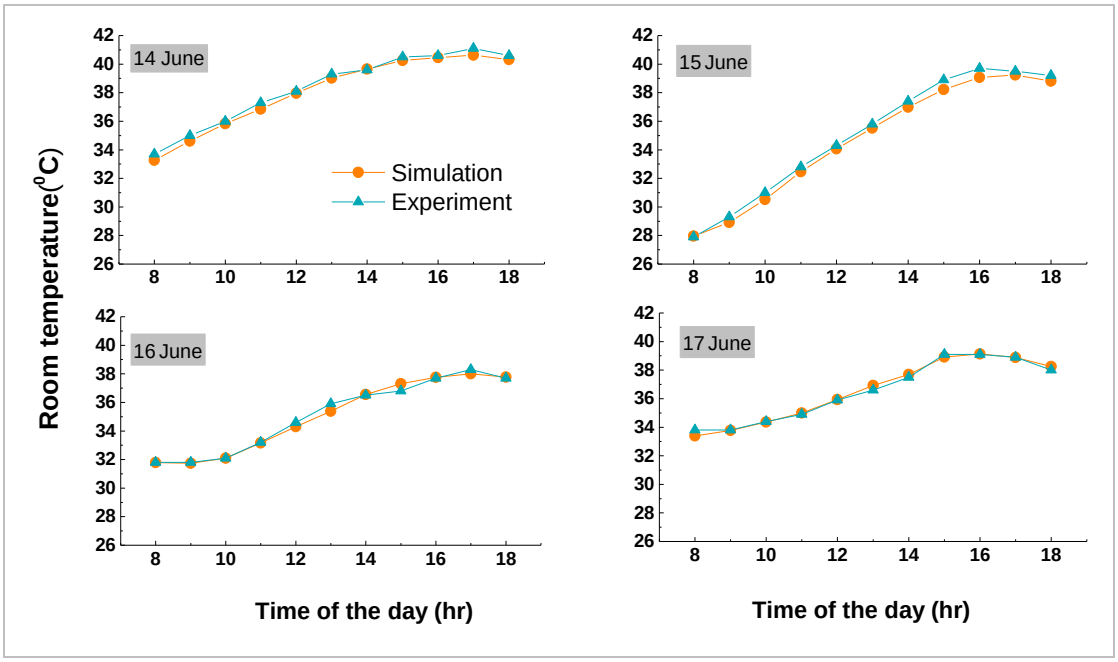

Figure 4-3: Measured and simulation values of room air temperature

4.2.3 Validation of STPV module temperature

In June, the incident radiation on the window panes is dominated by diffuse radiation in the early and later time of the day. However, at the noontime, the incident radiation on the window surface also contains some beam component. In the experiment, the temperature was collected from three different points. For this purpose, the thermocouples were fitted diagonally in the backside of the STPV modules. Finally, an average value was calculated for the analysis. A comparison between the simulated and experimentally measured module temperature is presented in **Figure 4-4.**

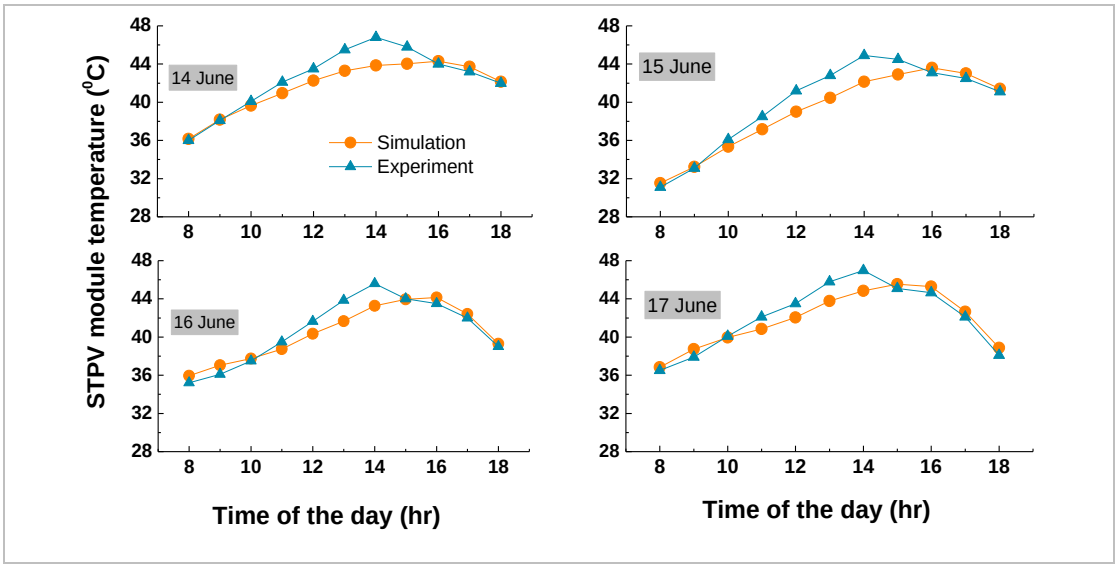

Figure 4-4: Measured and simulated values of STPV module back surface temperature

It is seen that at the noontime the experimentally measured temperature are little higher than the simulated values. The maximum difference between the experiment and simulation is found to be 2.9^0C. The maximum values of MBE and CV(RMSE) between the experimental and simulated module temperature are 2.1% and 5.4% respectively. These errors are still low. In other words, it can be stated that the simulation model predicts the module temperature with reasonable accuracy.

4.2.4 Validation of power generation by the STPV module

A comparison between the experimental and the calculated power generation is presented in **Figure 4-5.** Since the measured solar radiation was used in the simulation, the effect of variation in the radiation had also been seen in the simulation results. In the experiment, the power generations were measured and recorded using the solar charge controller. In the other case, the power generation was calculated using the steps described in section **3.5.4** after collecting the required parameters from the simulation. As explained earlier, the effect of four key parameters has been included in the calculation of power generation. However, in the actual scenario, some other factors such as soiling, interconnection among the module and so on also affect the power generation. For all these reasons, the power generation in the actual condition is slightly lower than the calculated values. The MBE and CV(RMSE) between the measured and simulated values of the power generation are -6.5% and 4.3% respectively.

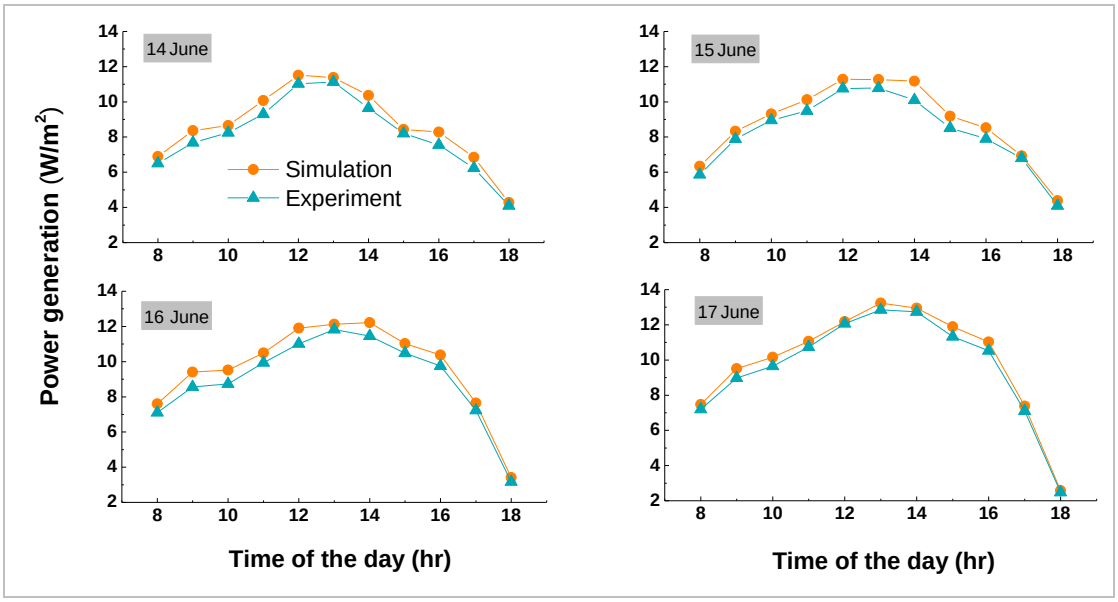

Figure 4-5: Measured and calculated values of power generation

From the above discussion, it is observed that the statistical errors in case of all the important parameters are very low. Therefore, it can be stated that the simulation model qualifies to use for the yearly simulation.

4.3 Impact of different key factors on the energy generation of window integrated STPV module

The energy generation of a photovoltaic module is affected by several factors in the actual field. Due to the influence of these factors, the photovoltaic module delivers less energy than specified by the manufacturers. Among various factors, four factors dominate the effect. These factors are the amount of incident radiation, type of incident spectrum, module temperature and angle of incident. In this section, the variation of these factors and their impact on the energy generation by window integrated STPV module has been presented in detailed.

4.3.1 Variation of the key factors

The variation of incident solar radiation and STPV module back side temperatures in the typical winter (21st January) and summer (21st May) days are shown in **Figure 4-6 (a) & (b).** The figure shows that the amount of incident radiation varies from morning to evening in both the days with a peak during the noon. At first, the radiation strikes the front photovoltaic module and get absorbed after reflection and transmission. Some part of the absorbed radiation converted into electrical energy. The leftover absorbed energy converted into heat and increased the photovoltaic module temperature. Due to more incident radiation, the photovoltaic module temperature is much higher in winter than that of the summer day.

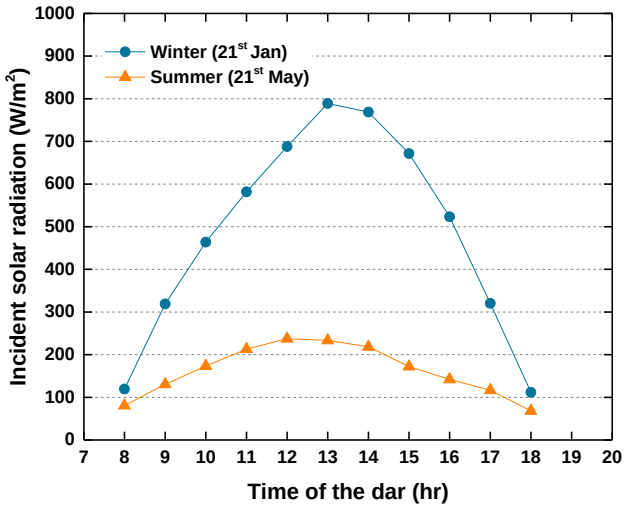

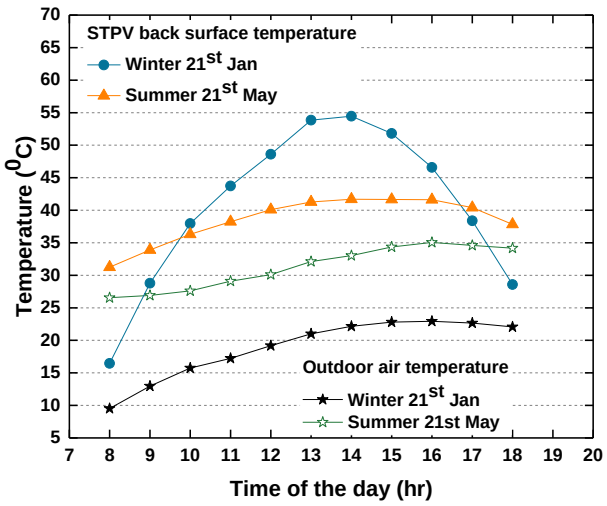

Figure 4-6: Variation for south facing vertical window at Jaipur during typical winter and summer days (a) Total incident solar radiation; (b) STPV module backside temperatures in comparison to outdoor air temperature

Further, for south facing vertical window in the considered location, the Sun remains at lower altitude in the winter season. For this reason, the solar radiation strikes the window surface relatively with smaller AOI. On the other hand, the reverse condition occurs during the summer season. The variation of AOI for the south-facing window on the typical winter and summer days are shown in **Figure 4-7.** It is observed that the in the typical summer day the AOI remain above 90^0 in most of the time. These values of AOI indicate that during the summer days the window systems receive very less amount of beam radiation. In the typical winter and summer days, the AOI vary in the range of 45.6^0 to 72.9^0 and 84.9^0 to104.1^0 respectively.

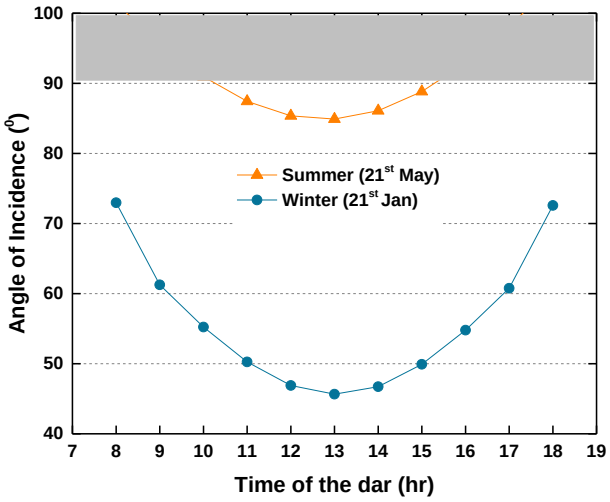

Figure 4-7: Variation of AOI for south-facing vertical window in the typical winter (21st Jan) and summer (21st May) days at Jaipur

4.3.2 Impact of the key factors and energy generation

The hourly, daily, monthly and yearly energy generation were calculated separately to investigate the effect of all the four key factors. The energy generated in the typical months of winter, summer, monsoon and post-monsoon periods are shown in **Figure4-8.** The conversion efficiency given by the manufacturer is measured with 1000 W/m^2 at the normal incidence and AM 1.5 spectrum. During the measurement, the cell temperature is maintained at 25°C. The energy generations with this efficiency are 13.9, 7.1, 4.3 and 11.4 kWh/m^2 respectively for January, April, July, and October. It is seen that the energy generation is maximum in the winter month (January). This occurs mainly due to more incident radiation on the window surface. On the other hand, due to less incident radiation, the energy generation is minimum in the monsoon period (July).

However, in the real operating condition, the window surface doesn't receive the radiation as used in the laboratory. The cell temperature also changes from 25°C. Therefore, the conversion efficiency changes in the real operating condition. Among the considered months, the incident radiation on the window surface is minimum during July. Therefore, the difference with the standard value of radiation (1000 W/m^2) is highest in this month. Consequently, the percentage change in energy generation due to the radiation factor is higher in the summer and monsoon seasons. With the consideration of the effect of incident radiation on conversion efficiency, the values of energy generations in the typical months changes to 13.7, 6.9, 4.1 and 11.1 kWh/m^2.

As far as the effect of AOI is considered, two parameters contribute to the energy loss. The parameters are the module surface characteristics and cosine effect. The amount of beam component in the total incident radiation and the corresponding incidence angle determine the final effect of AOI. The maximum effect of AOI has been observed during April. When the effect of AOI is included, the energy generations become 13.1, 6.3, 4.0 and 10.6 kWh/m^2 respectively for January, April, July, and October.

Water vapor is virtually transparent for the CdTe module's working wavelengths range **[55].** This resulted in the more efficient spectrum for CdTe module in the monsoon and post-monsoon seasons compared to the other periods. Therefore, when the effect of the incident spectrum is considered the energy generation slightly increases in the monsoon and post monsoon seasons. With the effect of the incident spectrum, the energy generation changes to 13.0, 6.2, 4.1 and 10.7 kWh/m^2 respectively.

The more incident radiation during winter leads to higher module temperature compared to the summer season. Further, due to high humidity in the post-monsoon season, the module temperature gets stagnant in that period. The higher module temperature leads to a drop in conversion efficiency and hence the power generation. With the effect of cell operating temperature the energy generations become 12.4, 6.0, 4.0 and 10.0 kWh/m^2 respectively for January, April, July, and October.

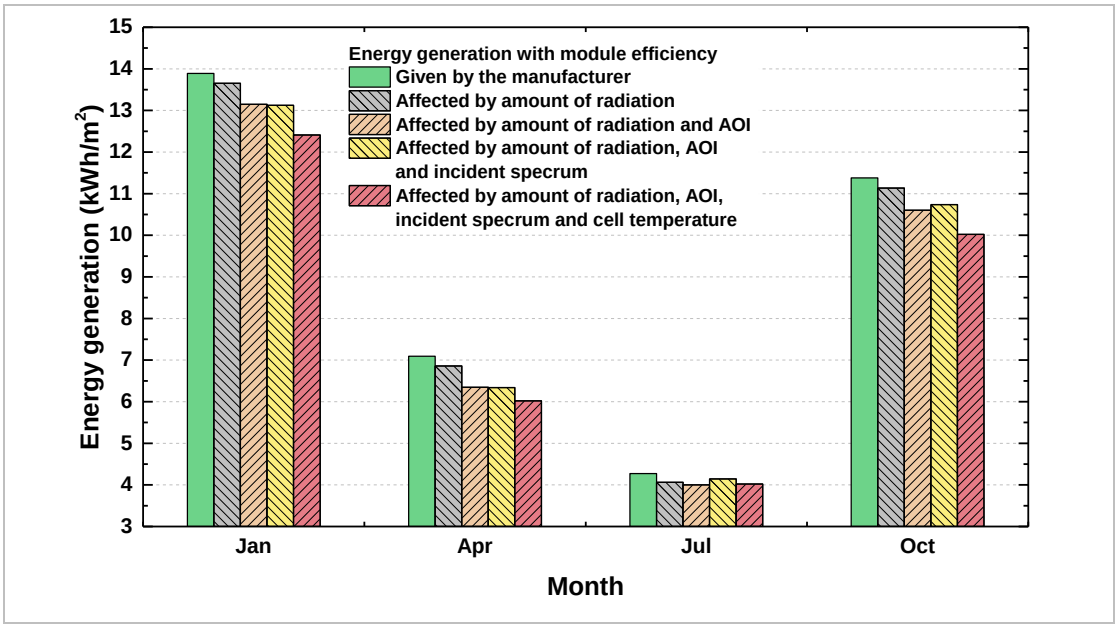

Figure4-8: Energy generation by STPV window system (PV3/gap/Low-e) at Jaipur in typical months

From the above discussion, it can be summarised that among the four key factors, the AOI, and cell temperature effect, the conversion efficiency and hence the power generation, the most. Further, due to the collective effect of all the four key factors, the annual energy generation has observed to be reduced by a maximum of 10.0% compared to the unaffected generation.

A comparison of energy generation in different months of a year, after considering the effect of all the four factors is shown in **Figure 4-9.** As mentioned earlier, the vertical south-facing window system at Jaipur receives maximum solar radiation during the winter season. The higher incident radiation resulted in more energy generation during the winter months. In January and December, the energy generations by the window system are 12.4 and 12.7 kWh/m^2 respectively. In the summer season, the window receives lower radiation with the mostly diffuse component. For this reason, the energy generations during the summer are lower than in the winter months. Among all the months, the energy generation (3.5 kWh/m^2) is lowest in June. Finally, for the

considered window system [PV3/gap/CG], the annual energy generation is found to be 95.3 kWh/m^2. Without considering the effect of all the four key factors, the calculated annual energy comes out to be 106.0 kWh/m^2.

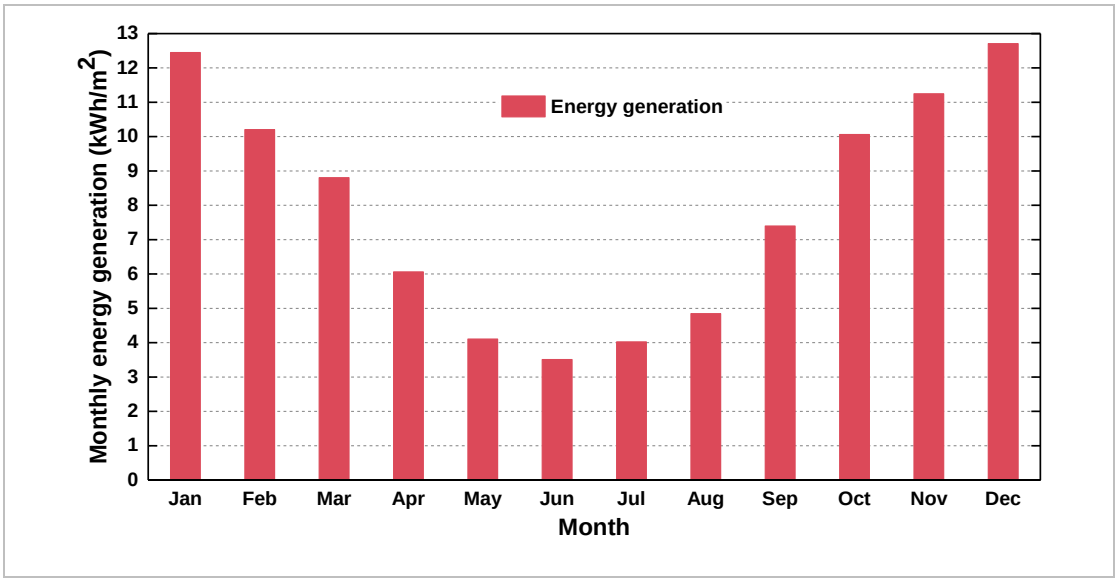

Figure 4-9: Monthly energy generation by STPV window system (PV3/gap/Low-e) at Jaipur

4.4 Effect of AOI on energy generation in window integrated STPV module

The conversion efficiency of photovoltaic modules is measured at normal incidence in the laboratory. However, in the real-life operating condition, the solar radiation is hardly incident normally in photovoltaic systems. Since the reflectivity of the STPV module increase with AOI, the energy generation decrease when the solar radiation deviated from the normal incidence. In case of vertical photovoltaic applications (window), the AOI remains higher for a longer time than the ground mounted system. Therefore, the effect of AOI become more prominent in the vertical systems. The effect also varies with other factors such as place of installation, orientation and surface property of the photovoltaic module.

In this section, the influence of AOI on the energy generation of window integrated STPV module has been investigated in four cities (latitudes) of India. The name and latitudes of the considered cities are Srinagar (34.08^{0}N), Jaipur (26.82^{0}N), Akola (20.07^{0}N) and Trivandrum (8.48^{0}N). These latitudes cover India from south to north. In choosing the latitudes, the climatic variations were also kept in mind. Besides the latitudes, the effect was also investigated for different orientation and module transmissivity.

4.4.1 Effect of AOI and energy generation by window integrated STPV module in different latitudes

In a year, the position of the Sun changes from Tropic of Cancer to the Tropic of Capricorn. On 21st June and 22nd December, the position of the Sun remains at the Tropic of Cancer and Capricorn respectively. Therefore, the extreme AOI for any location will be on these two days. Among the considered four latitudes, two are above the Tropic of Cancer. For south facing vertical window at the latitude(s) above this geographic line, the AOI remain below 90^0 in most of the time of a year. **Figure 4-10** presents the variation of AOI for the south-facing vertical window on the solar Solstices and Equinoxes days in the considered latitudes. The figure shows that for Srinagar (34.08^0N) which is the extreme northern considered city, the AOI varies under 90^0 for some time in the Summer Solstice (21st June) day. On this day, the AOIs remain below 90^0 for some time at Jaipur also. However, for the remaining two cities, the AOIs don't come below 90^0 for the south-facing window on 21st June. However, in the other representative days, the AOI remain below 90^0 for the south-facing window in all the selected cities.

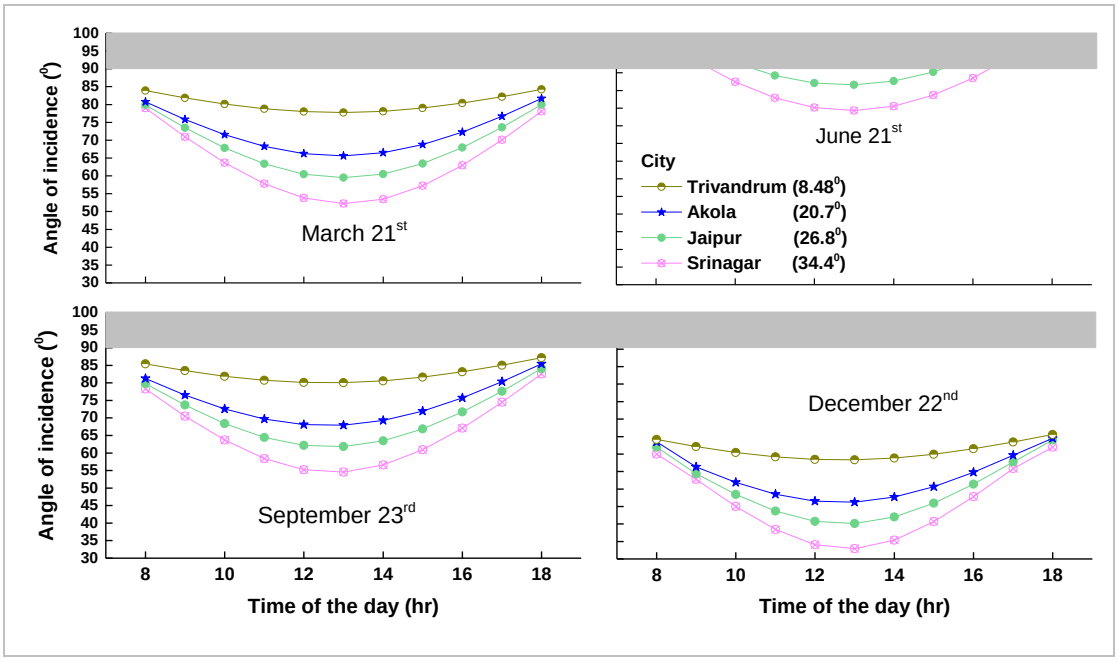

Figure 4-10: Angle of incidence for south facing vertical window in the considered latitudes during solar solstices and equinoxes

Theoretically, the surface for which the AOI is low receives more solar radiation. However, the amount of radiation in a particular location is also affected by the prevailing weather condition. **Figure 4-11** presents a comparison of the theoretically

calculated and simulated values of the incident solar radiation on 21st March. It is observed that the theoretical incident radiation on the south facing surface is more in the city where AOIs are small (higher latitudes).

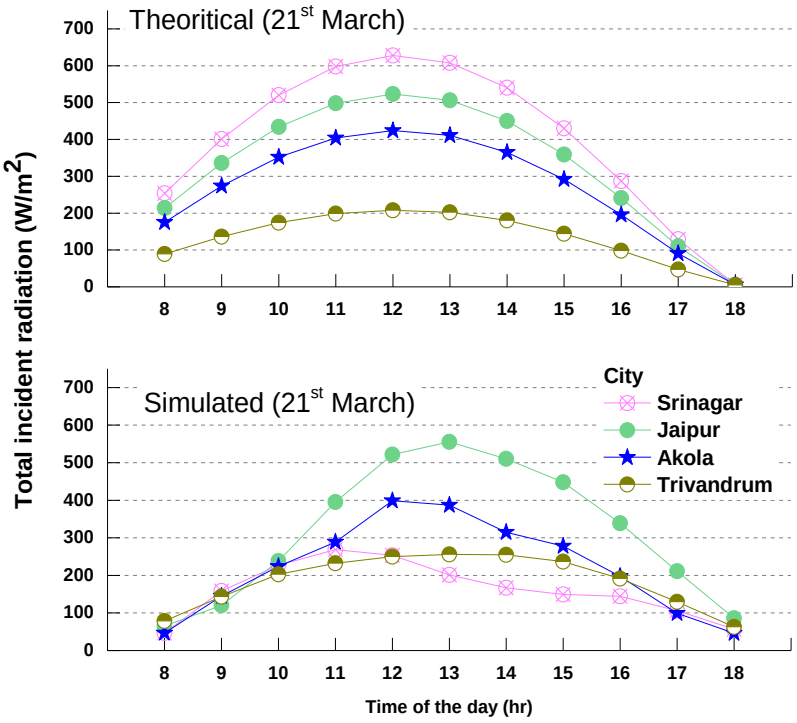

Figure 4-11: Theoretical and simulated values of incident radiation on 21st March at different latitudes in south-facing vertical surface

In other words, the theoretical value of incident radiation changes according to the AOI. However, due to the inclusion of local weather phenomena in the applied weather data, the simulated values of incident radiation don't follow the theoretical rule in the considered latitudes. Further, the northernmost city (Srinagar) experiences the cold and cloudy climatic condition. For this reason, the solar radiation differs widely from the theoretical values in this city. Due to the effect of local weather phenomena, the radiations in other latitudes also differ from the theoretical values.

The power generation on 21st March has been calculated for both the theoretical and simulated incident radiation at normal as well as actual AOI. In case of theoretical incident radiation, the maximum generation is found to be at the highest latitude (Srinagar). Latitude wise the maximum power generations are 58.5, 47.6, 38.4, and 18.5 W/m^2 respectively for Srinagar, Jaipur, Akola, and Trivandrum. These power generations are corresponding to the normal incident radiation. When the effect of AOI

is included, the power generations reduce to 55.5, 44.8, 35.2, and 16.3 W/m^2. These values indicate that compared to the normal incidence, the percentage reduction in power generation due to the effect AOI is maximum at the lowest latitude (Trivandrum). Further, the percentage reductions in energy generation decrease as moves towards the higher latitudes. Moreover, in all the latitudes, the effect of AOI increases significantly for AOI above 70^o.

The power generation with the simulated incident radiation is shown in **Figure 4-12.** It is observed that the highest power generation occurs at Jaipur instead of the highest latitude (Srinagar). This happens due to lower incidence radiation at Srinagar than that of the Jaipur. On the considered day, the maximum power generations at normal incidence are 25.3, 50.3,36.1 and 23.4 W/m^2 respectively for Srinagar, Jaipur, Akola, and Trivandrum. When the effect of AOI is considered, the generations reduced to 24.0, 47.4, 33.0 and 19.4W/m^2 respectively. These values indicate that compared to the normal incidence, the percentage reduction in power generations follow the trend similar to the theoretical case.

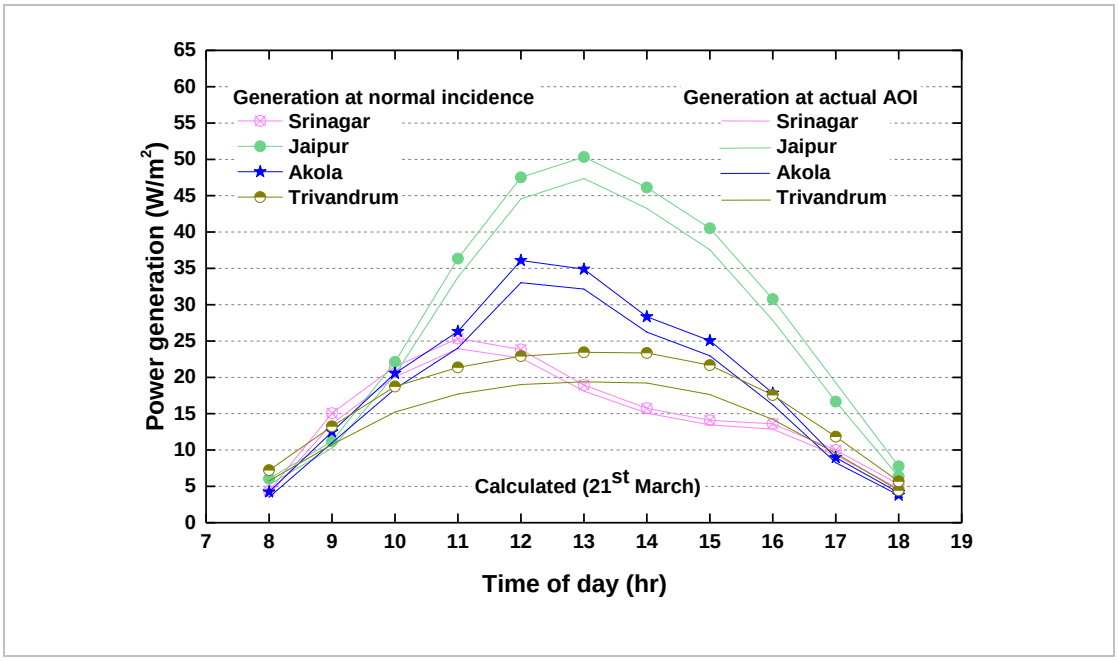

Figure 4-12: Photovoltaic power generation on 21st March at different latitudes by south facing vertical window for simulated incident radiation

In a particular location, the local weather drastically affects the solar radiation. For this reason, a location hardly receives solar radiation equal to the theoretical values. On the hand, the amount of energy generation by a photovoltaic module highly depends upon the available solar radiation. Therefore, a reliable source of radiation is very important

in predicting the energy generation of a photovoltaic system. Further, in the present study, the 'EnergyPlus' software has been used for the whole building simulation. In order to perform the 'EnergyPlus' simulation and subsequent analysis, many other weather parameters are required along with the solar radiation. Therefore, in the present study, the weather characteristics of the considered locations have been taken from ISHREA database. In this database, the files were created by utilizing weather data from various sources, including the Indian Meteorology Department (IMD), the US National Centre for Environmental Data, and satellite-derived solar radiation data developed by National Renewable Energy Laboratory (NREL), USA **[152].** Finally, the solar radiation retrieved from the 'EnergyPlus' simulation results have used to calculate the annual energy generation by the considered STPV window systems.

The annual incident radiation on the vertical south-facing window at Srinagar, Jaipur, Akola, and Trivandrum are 1310, 1383, 1095, and 947 kWh/m^2 respectively. It is observed that due to the influence of cloudy weather, the incident radiation is not maximum at the highest latitude (Srinagar). On the other hand, due to sunny weather and relatively lower AOI, the south facing window receives the highest solar radiation at Jaipur. In the other two locations, the south facing window receives relatively lower solar radiation mainly due to the higher AOI. The corresponding annual energy generations after considering the effect of AOI is shown in **Figure 4-13.**

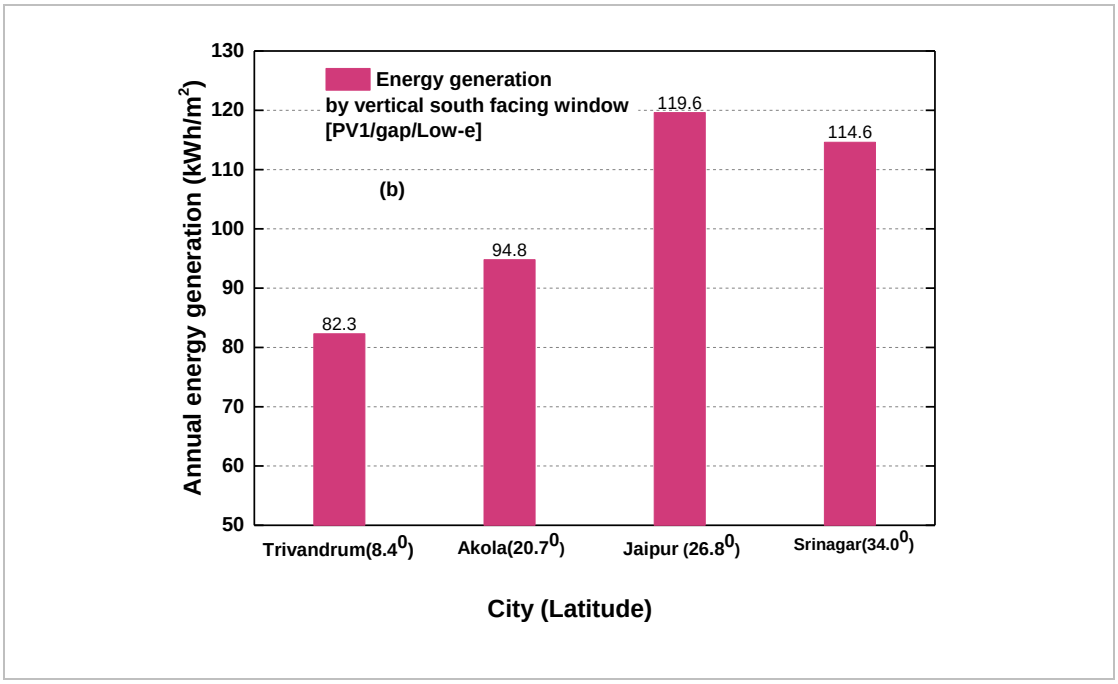

Figure 4-13: Annual incident energy generation by the vertical south-facing window at different latitudes

It is seen that the patter of the energy generations in different latitudes follows the incident solar radiation. The maximum energy generation of 119.6 kWh/m^2 is produced at Jaipur while it is minimum at Trivandrum.

4.4.2 Effect of AOI and energy generation by window integrated STPV module of different transmissivity

The measured values of solar transmittance of the considered STPV modules are 6.0%, 10.2%, 14.5%, 21.0% and 27.5% respectively for PV1, PV2, PV3, PV4, and PV5. It has been found that the absorptivity of the higher transparent module decreases at a slower rate with increase in AOI, as described in section **3.4.1.** The slower rate of decrease in absorptivity resulted in the fewer effect of AOI on the energy generation. Comparison of loss in energy generation due to AOI among the considered STPV modules at Jaipur is shown in **Figure 4-14.** It has been found that the annual energy loss for the lowest transparent STPV module (PV1, 6.0%), is 6.3kWh/m^2. On the other hand, the loss is only 3 kWh/m^2 for the highest transparent STPV module (PV5, 27.5%).

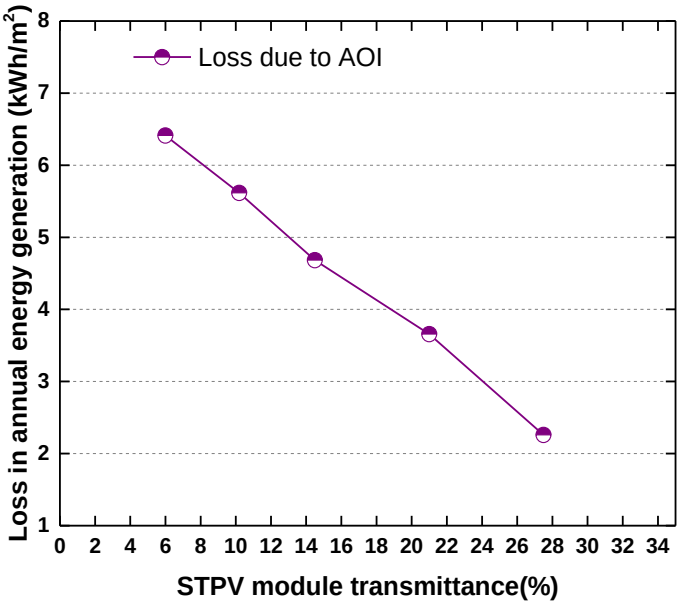

Figure 4-14: Annual energy loss due to AOI for different transparent STPV modules at Jaipur

Figure 4-15 presents the annual energy generation by different transparent STPV modules after considering the effect of AOI. The figure contains the energy generations for the south orientation at all the four latitudes. It is observed that the energy generation follows the trend of the incident radiation at the considered latitudes. Further, the lower transparent module convert a large portion of the incident radiation. For this reason, the

lowest transparent module (PV1) produced the highest annual energy at all the latitudes. The maximum energy of 119.6 kWh/m^2 is produced at Jaipur by PV1. On the other hand, the least transparent STPV module (PV5) produced 74.7 kWh/m^2 at the same latitude. Further, among the considered latitudes, the least incident radiation along with higher AOI lead to the minimum energy generation at Trivandrum. At this latitude, the annual energy generations are 82.3 kWh/m^2 and 51.5 kWh/m^2 for the lowest (PV1) and highest (PV5) transparent STPV modules respectively.

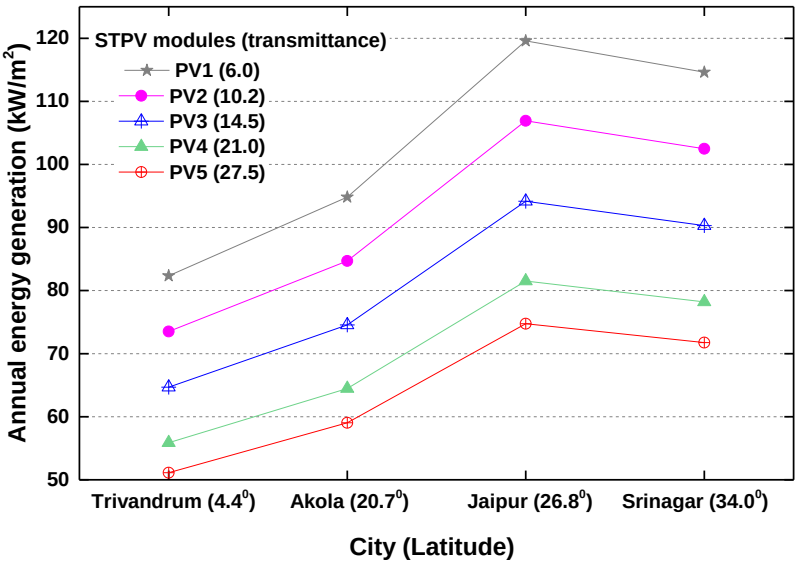

Figure 4-15: Annual energy generation by south facing window system with different transparent STPV modules and latitudes

4.4.3 Effect of AOI and energy generation by window integrated STPV module in different orientations

As far as orientations are considered, the AOI of the solar radiation changes for the south and north facing window when moves from one latitude to the other. In the northern hemisphere, the south facing window situated above the Tropic of Cancer receives direct solar radiation throughout the year. On the hand, the north facing window below this geographic line receives direct solar radiation during the summer months. Therefore the energy generations by the south and north facing windows are affected by AOI due to change in latitude and the diurnal variations of the Sun position.

On the other hand for the east and west facing windows, the AOI mainly changes due to the diurnal variation. Moreover, the direct solar radiation strikes the east and west facing window during the morning and afternoon half of the day respectively.

Therefore, the energy generations by east and west facing windows are affected by AOI during the morning and afternoon half. For this reason, the effect of AOI on energy generation is less in east and west compared to the south orientated window. For example, compared to the normal incidence, the energy generations are reduced by 5.1%, 3.9%, and 4.0% respectively for the south, east, and west-facing window at Jaipur.

The annual incident radiation on the window surface in different orientations and latitudes are shown in **Table 7.** It is observed that across the orientations and latitudes, the window surface receives the maximum solar radiation in the south direction at Jaipur. While due to its position above the Tropic of Cancer, the north facing surface at Srinagar receives the minimum solar radiation. Further, the north facing surface at the lowest latitude experiences the Sun for the longest time. This leads to highest solar radiation on the north-facing surface at Trivandrum. As far as the east and west facing surfaces are considered, they receive almost similar radiations at all the latitudes.

Table 7: Annual total incident solar radiation on the window surface in different orientations and latitudes (kWh/m^2)

Latitudes/ orientations	Trivandrum (4.4^0)	Akola (20.7^0)	Jaipur (26.8^0)	Srinagar (34.8^0)
South	947	1095	1383	1310
East	1082	1063	1101	1022
West	1104	1010	1089	1006
North	673	518	484	433

The annual energy generation in different orientations and latitudes after considering the effect of AOI are shown in **Figure 4-16.** The figure contains the energy generation for the window systems with lowest transparent STPV module (PV1). It is observed that similar to the incident radiation; the energy generation is maximum for the south-facing window at Jaipur. Due to lowest incident radiation, the energy generation is minimum for north facing window at Srinagar. Also, the widow systems produce almost similar energy in the east and west orientations.

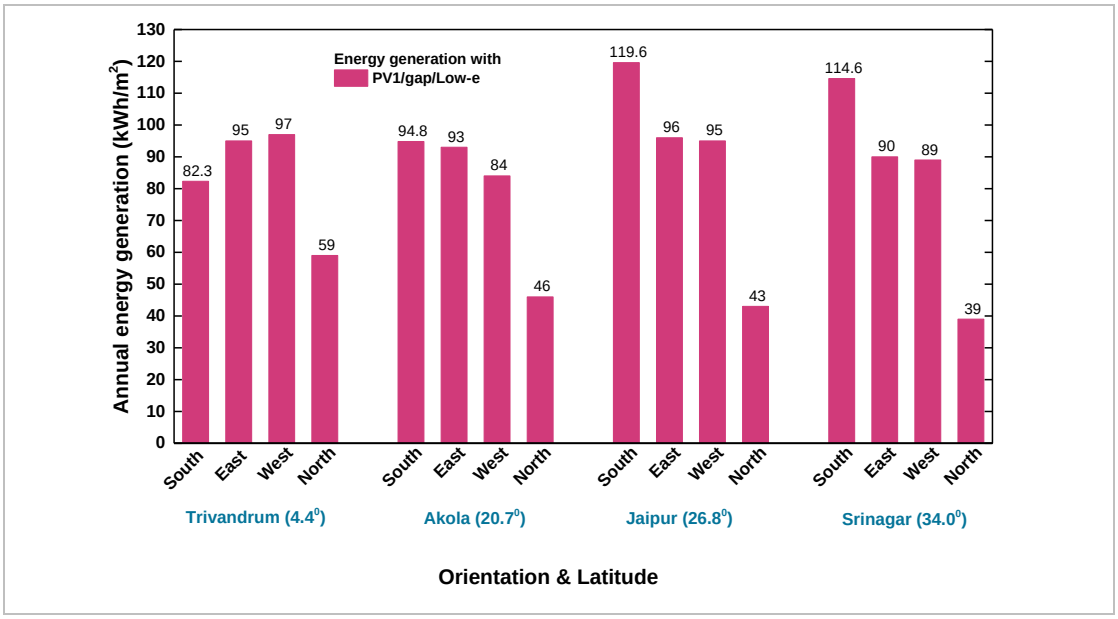

Figure 4-16: Annual energy generation in different orientations and latitudes by window system PV1/gap/Low-e

4.5 Summary

A summary of the energy generation after considering the effect of AOI in different latitudes and orientations are presented in **Table 8.** The table shows that across all the latitudes, orientations and STPV module transparencies, the south facing window with PV1 generated the maximum energy at Jaipur. As far as the orientations are considered, the window systems produce the highest energy in the south orientation in all latitudes except Trivandrum. The southernmost city, Trivandrum is situated far below the Tropic of Cancer and just above the equator. For this reason, the south facing window doesn't receive the maximum solar radiation at Trivandrum. At this latitude, the maximum energy is generated by the west-facing window. Further, the energy generation by the east and west facing windows are almost similar at all the latitudes. The table also shows that the energy generation by the north facing window is minimum across the latitudes. Moreover, for this orientation, the energy generation increases as moves towards the lower latitudes. Finally, the energy generations have found to decrease with increase in STPV module transmissivity. This trend is followed irrespective of the latitudes and orientations.

Table 8: Annual energy generation at different latitudes and orientations by the considered STPV window systems (kWh/m^2)

City (Latitude)	Orientation	Window system				
		PV1/gap/ Low-e	PV2/gap/ Low-e	PV3/gap/ Low-e	PV4/gap/ Low-e	PV5/gap/ Low-e
Srinagar (34.0^{0}N)	South	114.6	102.5	90.3	78.2	71.7
	East	90.0	81.2	71.5	61.8	56.6
	West	89.0	79.5	69.9	60.5	55.3
	North	39.0	35.5	31.2	26.8	24.4
Jaipur (26.8^{0}N)	South	119.6	106.9	94.7	81.5	74.7
	East	96.0	86.4	76.0	65.7	60.1
	West	95.0	84.9	74.7	64.6	59.0
	North	43.0	39.1	34.3	29.5	26.8
Akola (20.0^{0}N)	South	94.8	84.7	74.6	64.5	59.1
	East	93.0	83.1	73.1	63.2	57.8
	West	84.0	75.5	66.4	57.3	52.3
	North	46.0	41.3	36.3	31.2	28.4
Trivandrum (8.4^{0}N)	South	82.3	73.5	64.7	55.9	51.1
	East	95.0	85.3	75.0	64.7	59.2
	West	97.0	86.8	76.3	65.9	60.2
	North	59.0	53.1	46.9	40.2	36.7

4.6 Effect of window configurations and airflow strategies

Four window configurations described in section **3.4.1** have been investigated in this segment. Out of the four configurations, two have air cavity after the STPV module. In these two configurations, the solar radiation directly incident on the STPV module. On the other hand, the remaining two configurations contain the STPV module in the back of clear and Low-e glass. Therefore, in the latter two configurations, the solar radiation strikes the STPV modules after partially filtering by the front glasses.

In the airflow category, the effect of all three modes described in section **3.4.2** has been analyzed. As explained earlier, the first mode of airflow (F_0) represents a state without any opening for the hot cavity air. In the second mode of air flow (F_1), the hot cavity air release into the outdoor environment. The third mode of airflow (F_2) mixes the hot cavity air with the indoor air.

4.6.1 Effect of window configurations

The Sankey diagrams of the solar radiation incident on the window system in different configurations are shown in **Figure 4-17.** These values are for 11:00 AM on 21st January. At this point, the solar radiation strikes the window surface at 50^0 incident angle, as shown in **Figure 4-7.** The reflectivity of the STPV module and conventional glasses are AOI dependent. This feature leads to the different amount of reflections from the outermost surface of the window configurations. It has been observed that the amount of reflection is more for the configurations having the conventional glasses in front of the STPV module (W, X). In these configurations, the front glass also absorbs some part of the incident radiation. Therefore, the amount of radiation absorbs by the STPV module in these configurations are less compared to the remaining two (Y, Z). Thus, in the window configurations W and X, the STPV module receives 19% and 42.2% less radiation compared to Y and Z respectively. Finally, some radiation transmitted into the occupant area after absorbing in the window panes. It has been observed that the change in placing of the STPV module does not affect much on the amount of radiation transmitted into the occupant area.

Window configurations	Sankey diagram of incident radiation
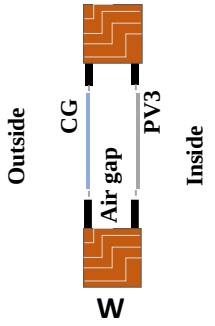	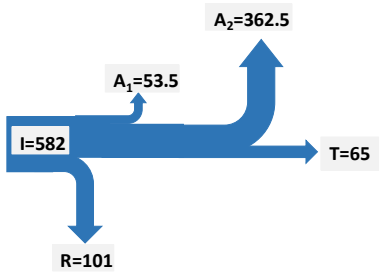
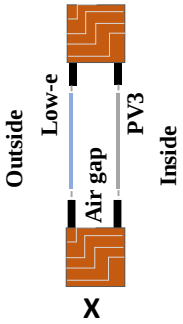	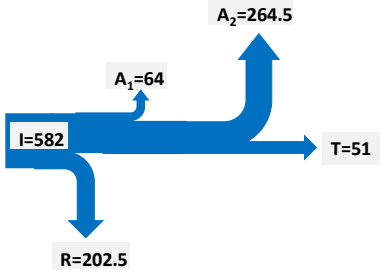
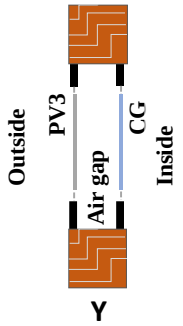	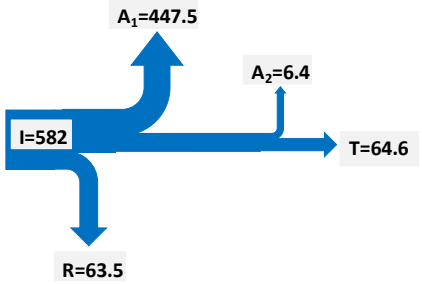
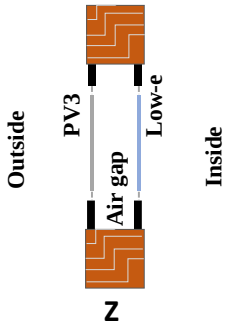	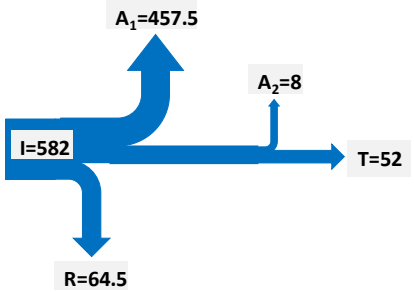

Legends:

- I →Total incident solar radiation on the window surface (W/m^2)
- R →Radiation reflected from the window system (W/m^2)
- A_1 → Radiation absorbed in the first window pane (W/m^2)
- A_2 → Radiation absorbed in the second window pane (W/m^2)
- T →Radiation transmitted through the window systems into the room (W/m^2)

Figure 4-17: Sankey diagram of the incident solar radiation for different window configurations on 21st January at 11:00 AM

a) Effect on STPV module and room temperature

A comparison of the STPV module back surface temperature on 21st January in different window configurations is presented in **Figure 4-18.** The figure also contains the ambient and room air temperatures of the same time. It is seen that by changing the window configurations, the module temperature can be managed. The module backside temperature in case of W and X is much lower than the Y and Z window configurations. This occurs mainly because of two reasons. First, in the window configurations W and X, the STPV absorbs less solar radiation. Secondly, the influence of the room air temperature. On the other hand, in Y and Z window configurations, the STPV modules are influenced by the hot cavity air along with more incident radiation.

The U-value dominates the heat transfer through a window system. The highest U-value (2.68W/m^2-K) has been calculated for window configuration Y. In this configuration, the simple, clear glass was placed behind the STPV module. Therefore, once the temperature of the front STPV module increases, the heat can easily transfer into the occupant area.

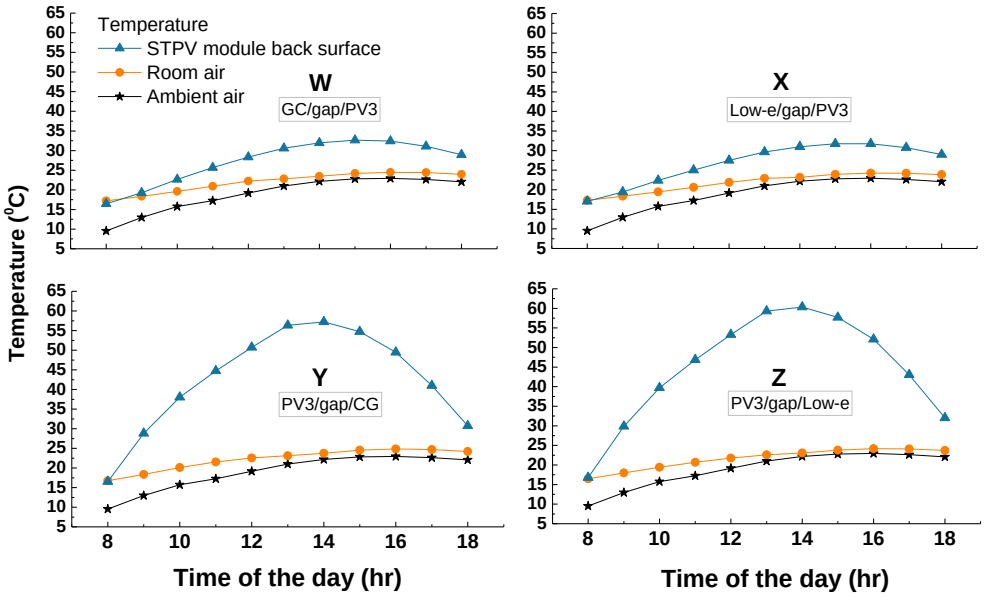

Figure 4-18: Ambient, room and STPV module back surface temperature in different window configurations on 21st January

This resulted in maximum room temperature with this window configuration. On the other hand, the lowest room temperature has been observed with window configuration Z. This configuration has the lowest U-value (1.658 W/m^2-K) due to the presence of the

Low-e glass at the back of the STPV module. At 14:00 PM on 21st January, the calculated room air temperature with window configurations W, X, Y, and Z are 23.5^{0}C, 23.2^{0}C, 23.7^{0}C and 23.1^{0}C respectively.

b) Effect on energy generation

The lower STPV module temperatures are beneficial for the conversion efficiency and power generation. Besides temperature, the conversion efficiency and hence the power generations are also affected by the spectrum of the incident radiation. For instance, the STPV module backside temperature at 11:00 AM on 21st January in different window configurations are as follows. W,25.7 ^{0}C; X,25.0^{0}C; Y,44.7^{0}C; Z,46.9^{0}C. The values indicate that there are temperature differences of 19.0^{0}C and 21.9^{0}C between the window configuration W vs. Y and X vs. Z respectively. For the applied STPV module, the temperature coefficient of maximum power is 0.214% per ^{0}C. Therefore, compared to window configurations Y and Z, there is a dividend of 4.07% and 4.67% in conversion efficiency in case of window configurations W and X respectively. In Y and Z configurations the STPV module produces 42.1 W/m^2 power at 11:00 AM on 21st January. With the improved conversion efficiency, and the given incident radiation the corresponding power generations for W and X configuration should have been 32.2 W/m^2 and 23.9 W/m^2 respectively. However, in these two configurations, the power generations have been calculated to 38.9 W/m^2 and 37.2 W/m^2 respectively. These indicate the availability of more effective spectrum after the conventional glasses. However, in absolute value, the power generation for W and X configurations are still low due to the blocking of some part of the effective wavelength of the incident radiation by the front glasses.

A comparison of energy performance of the considered window configurations is presented in **Table 9.** The table also contains the values of radiation absorbed by the STPV module in different window configurations. It is observed that the window configurations having the STPV module as the front layer produced more energy. However, the reduction in energy generation due to the presence of the front glasses are lower than the corresponding drop in incident radiation on the STPV module. When window configuration Y is altered to W, the energy generation is reduced by 8.7% corresponding to 14.9 % drop in incident radiation. The gap further increases in case of window configurations having the Low-e glass. The Low-e glass selectively reduced

the Infrared (IR) part of the incident radiation as shown in **Figure 3-11.** Therefore, in the radiation passing through the Low-e glass contains more effective spectrum for photovoltaic conversion. The energy generation is dropped by only 10.6% against 35.3% reduction in incident radiation when Z window configuration is altered to X.

Table 9: Annual incident radiation on the STPV module and energy generation by different window configurations at Jaipur in south orientation

Window configurations	**Y**	**W**	**Z**	**X**
Descriptions	PV3/gap/ CG	CG/gap/ PV3	PV3/gap/ Low-e	Low-e/gap/ PV3
Incident radiation on the STPV module (kWh/m^2)	1383	1177	1383	895
Annual energy generation (kWh/m^2)	94.9	86.7	94.7	84.8

4.6.2 Effect of the airflow strategies

The airflow strategies have been used to manage the hot cavity air. The module temperature, corresponding conversion efficiency, and indoor air temperature changes with the type of the selected air flow. A detailed analysis of these parameters in comparison to the no air flow condition has been presented in this section. These analyses have been carried for the naturally ventilated building with the window configuration Y(PV3/gap/CG).

a) Comparison of F_1 and F_0

The aim of air flow strategy-1 (F_1) is to release hot air from the window cavity to the outdoor environment. A comparison of the STPV module temperature with airflow types F_1 and F_0 in the typical winter and summer days is presented in **Figure 4-19.** The corresponding photovoltaic conversion efficiencies are also shown in the figure. It is seen that when the slits are open to release the hot cavity air, the module temperature decreases compared to F_0. The reduction of temperature is observed in both winter and summer days. However, due to high ambient temperature in the summer, the reductions are lower compared to the winter day. The maximum drop in STPV module temperatures is 3^0C and 1.1^0C in the typical winter and summer days respectively. Throughout the year, the maximum difference in STPV module temperature is found to be 3.8^0C at 3:00 PM on 15th December. The lower operating temperature of the STPV module is desirable for better photovoltaic conversion efficiency. Thus, the introduction

of airflow helps in improving the photovoltaic conversion efficiency of the STPV module. However, due to a small drop in STPV module temperature and a lower temperature coefficient of maximum power, the improvement in conversion efficiencies have not been significant in the present research. Corresponding to the maximum drop in STPV module temperature, the respective improvements in conversion efficiencies are 0.64% and 0.23% respectively in the typical winter and summer days.

From **Figure 4-19** it is also observed that in the morning and evening of a winter day, the conversion efficiencies are low even if the STPV module temperatures are comparatively low. It is due to the logarithmic dependence of the STPV module's open circuit voltage on incident solar radiation through short-circuiting current density as shown by Equation 26. The same reason can also be attributed to the maximum conversion efficiency in the summer day at noon though the temperature is relatively higher than that of the morning times.

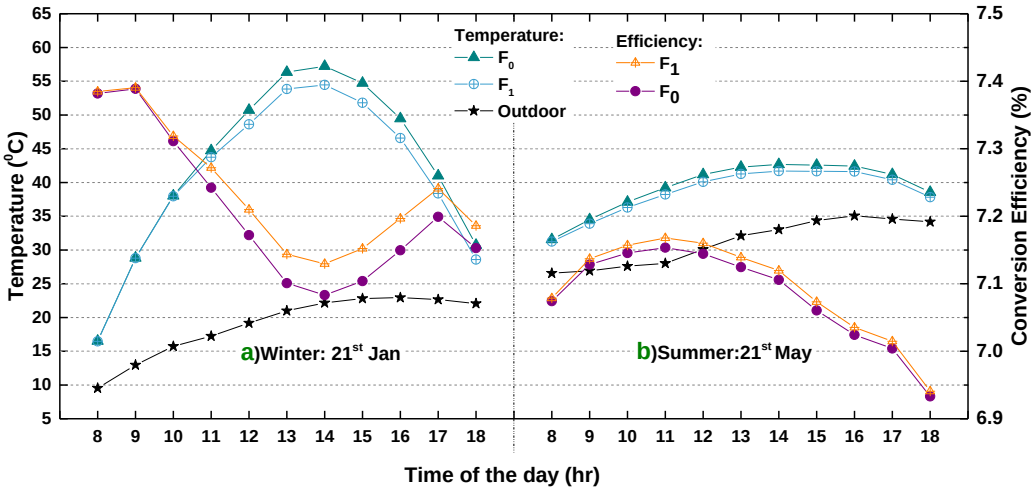

Figure 4-19: STPV module back surface temperature and conversion efficiency with F_1 compared to F_0

The temperature profiles of the innermost surface and occupant area with airflow strategies F_0 and F_1 are shown in **Figure 4-20.** In F_1, the slits J and K remain open. The hot air from the cavity keeps continuously going out of the system at varying mass flow rate through the top slit (K). The maximum mass flow rate of hot air going out of the window cavity is found to be 0.13 kg/sec for each window system. The temperature of the inner pane is highly influenced by the state of cavity air. The temperature is also affected by the amount of solar radiation transmitted through the front window pane.

Due to more incident solar radiation in the winter days, the diurnal variation of the inner window pane temperature is large compared to summer day as shown in **Figure 4-20(I).** It is found that the passing of fresh air through the cavity reduces the inner pane temperature also. The maximum drop in inner pane temperature with F_1 is 3.2^0C and 1.1^0Cin the typical days. The low surface temperature resulted in lower heat flux from the window pane to the indoor environment. In the typical winter day, the maximum heat gains and loss from the inner window pane with F_1 are 38.9 W/m^2 and 6.6 W/m^2 respectively. These heat transfers are lesser compared to F_0 condition.

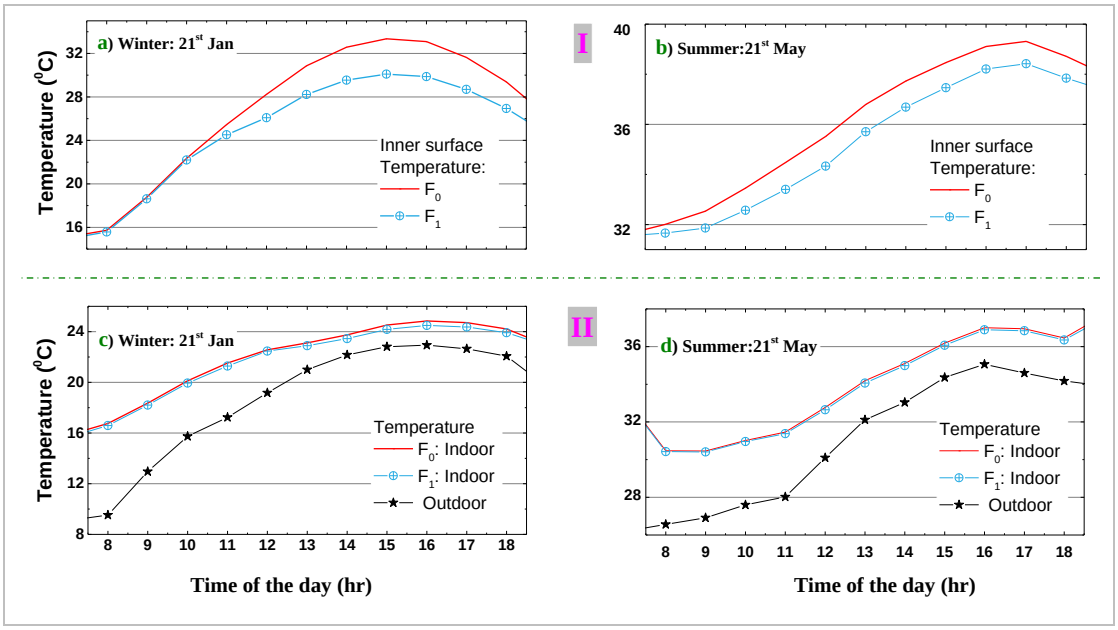

Figure 4-20: Comparison between F_1 and F_0 in the typical days I) window inner surface temperature II) Indoor and outdoor air temperature

Finally, the rate of heat gains or loss from the inner window pane along with the other part of the envelope determines the indoor air temperature. The indoor air temperature with F_1 has found to be slightly low compared to F_0 as shown in **Figure 4-20(II).** This occurs because of the release of hot cavity air into the outdoor environment and low inner surface temperature of the window system.

The drop in indoor air temperature can be expected to increase by releasing more hot air from the cavity. It will also reduce the STPV module temperature. A wide air gap between the two window panes which leads to the full development of the stack effect may improve the above benefits. An externally operated exhaust fan may also be helpful in these regards. These findings suggest that the STPV double pane operated with F_1 could be more useful during the summer season.

b) Comparison of F_2 and F_0

In airflow type-2 (F_2), fresh air entered into the window cavity through the front bottom slit (J). After collecting the heat, the air moves into the occupant area. Therefore, in this mode of operation, the level of air flow rate is also directly influenced by the indoor environment. The STPV module backside temperature profile and corresponding photovoltaic conversion efficiency with F_2 and F_0 are shown in **Figure 4-21.** It is seen that compared to F_0, the STPV module backside temperature decreases with F_2. The maximum drop in temperature in the typical winter and summer days are 3 ^{0}C and 0.9 ^{0}C respectively. Throughout the year, the maximum drop is found to be 3.6 ^{0}C. In the typical days, the maximum improvement in conversion efficiencies is 0.68% and 0.2% respectively.

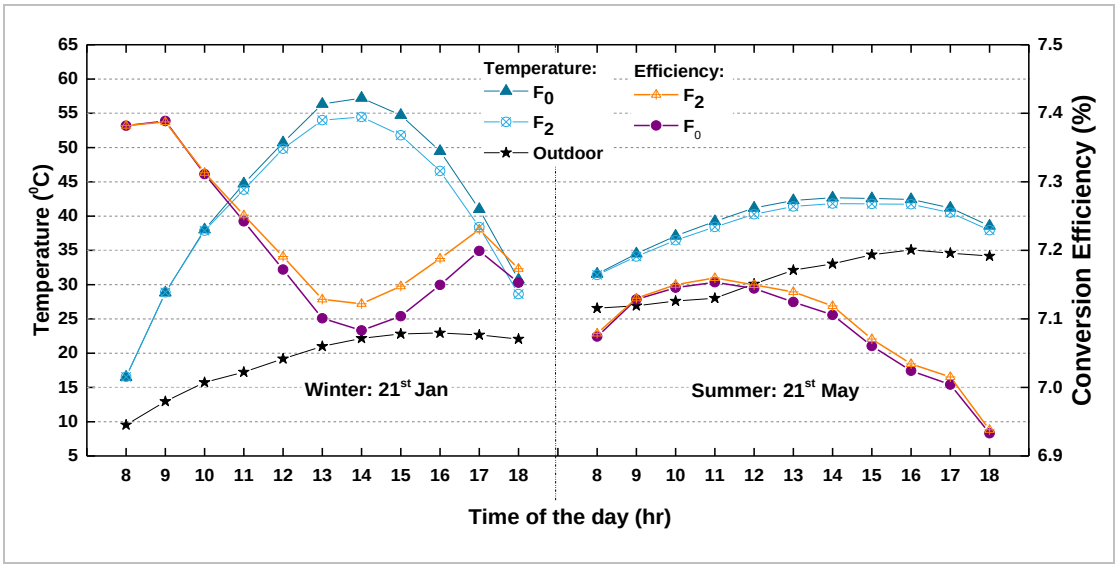

Figure 4-21: STPV module back surface temperature and conversion efficiency with F_2 compared to F_0

The diurnal variation of inner pane temperature, heat flux and indoor air temperature with F_2 in comparison to F_0 are shown in **Figure 4-22.** The inner pane temperature remains high almost throughout the day in F_0 as shown in **Figure 4-22(I).** In the typical winter and summer days, the respective maximum daytime temperature difference between F_0 and F_2 are 2.6 ^{0}C and 0.5 ^{0}C respectively. The high temperature resulted in high heat flux from the surface to the interior environment in case of F_0. At the peak, the difference in the rate of heat transfer between F_0 and F_2 is 33.2 W/m^2. However, the flow of hot air leads to an increase in indoor air temperature with F_2 as shown in **Figure 4-22(II).** On the other hand, the increase in indoor air temperature affects the hot air mass flow rate in negative ways. In the typical winter day, the maximum mass flow rate

is found to be 0.03 kg/sec. The increase in indoor air temperature is beneficial in the winter days. Compared to no air flow condition, the maximum increment in indoor air temperature in the typical winter day is found to be 2 ^{0}C.

The result indicates that the STPV window system working with F_2 air flow strategy can be helpful for thermal comfort in the winter season, especially in the heating demand locations. Besides increasing the indoor air temperature, F_2 maintains the benefit of airflow concerning STPV conversion efficiency. A wide air gap or externally operated exhaust fan installed at the opening (L) could increase the above benefits.

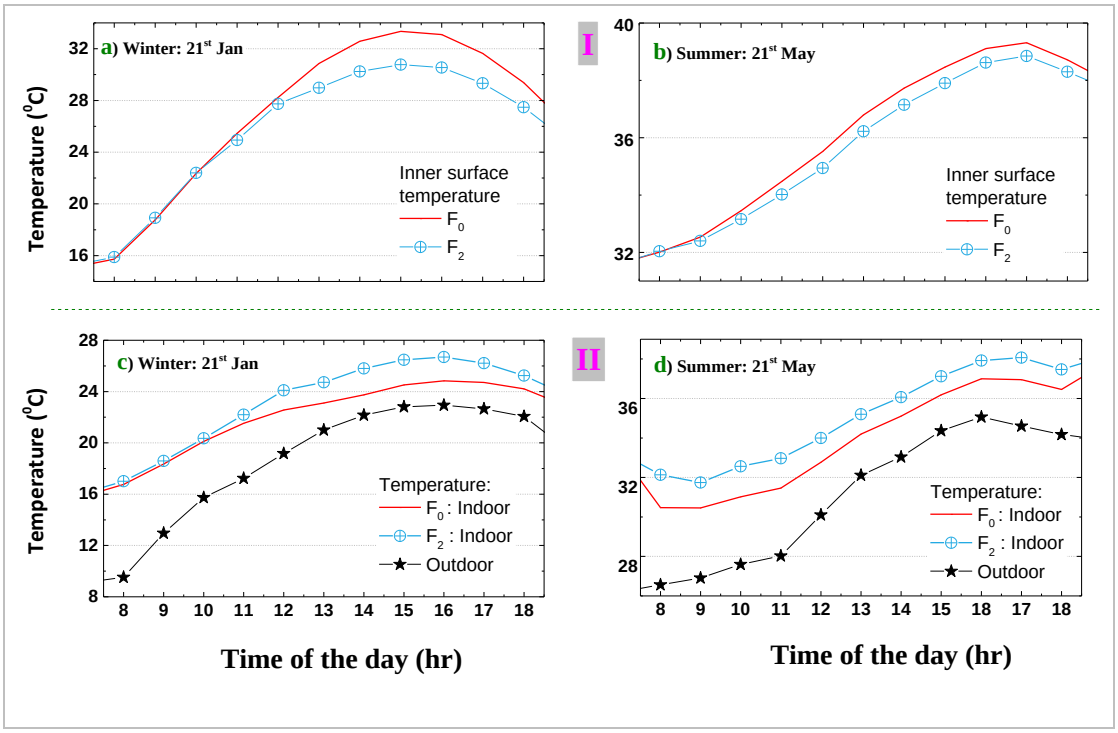

Figure 4-22: Comparison between F_2 and F_0 in the typical days I) window inner surface temperature II) Indoor and outdoor air temperature

4.7 Summary

The analysis shows that the application of conventional clear and selectively transparent (Low-e) glass in front of the STPV module block some part of the incident spectrum. The lesser amount of incident radiation along with the influence of the room air temperature resulted in lower STPV module temperature. However, with respect to energy generations, the application of clear and spectrally selective (Low-e) glasses in front of the STPV module have not found to be very encouraging. The energy generations dropped by 9% and 10% respectively when the clear and Low-e glasses were used as a front layer rather than behind the STPV module. The reductions in energy generations occurred due to the blocking of some part of the useful wavelengths of the

incident spectrum. Nevertheless, the reductions in energy generations have been lower than the corresponding decrease in the amount of incident radiation. The gap between the reduction in incident radiation and energy generation for window configuration X (Low-e/gap/PV3) is larger than W(CG/gap/PV3). These findings indicate the transmission of more effective wavelength for photovoltaic conversion through the selected Low-e glass compared to the clear glass.

Form the above discussion it is clear that the photovoltaic energy generation is higher for the window systems having STPV module in front of the conventional glasses. Further, the use of Low-e glass behind the STPV module helped in keeping the room temperature at a lower level in summer. Therefore, the window configurations with STPV module as the front layer have been selected in other investigations of the present research.

A summary of the considered airflow strategies is presented in **Table 10.** The table contains the values of the STPV module backside temperature, power generation, the temperature of the window innermost surface, heat gain through the window, air mass flow rate, and indoor air temperature. Values of both typical winter and summer days are presented in the table.

Table 10: Typical winter and summer day performance summary under different modes of air flow (time 14:00 PM)

Parameters	**Typical winter day**			**Typical summer day**		
	F_0	F_1	F_2	F_0	F_1	F_2
Module temperature (^{0}C)	59.4	56.6	57.0	43.2	42.3	43.0
Energy generation (W/m^2)	54.5	54.8	54.8	15.5	15.6	15.5
Window innermost surface temperature (^{0}C)	32.6	29.5	30.2	37.7	36.7	37.2
Heat gain (W/m^2)	41.4	27.1	23.8	6.8	2.4	1.2
Mass flow rate (kg/sec)	0	0.05	0.03	0	0.03	0.02
Indoor air temperature (^{0}C)	23.7	23.5	25.8	35.1	35.0	36.1

The results indicate that releasing of cavity air reduces the STPV module temperature. The heat transfer from the inner window pane and air mass flow rate are a function of indoor air, cavity air, and the surface temperature. Due to the high surface temperature,

the heat transfer is maximum in F_0. Since no slits are open, the mass flow rate is zero in this mode of operation. The results also indicate that when the slits are open, hot air gets ejected from the window cavity. If the removed hot air is passed through the occupant area, in the case of F_2, the indoor air temperature increases. Further, due to increased indoor air temperature, both surface heat transfer and air mass flow rate are less with F_2.

The annual energy generations of the STPV module under the considered airflow strategies are shown in **Figure 4-23.** The figure demonstrates that from the energy generation point of view, air flow type-1 (F_1) provides the best result. With this flow type, the annual energy generation per unit area of the selected STPV module is found to be 95.3 kWh/m^2. However, compared to F_0 the energy generation is increased by 0.41% only. Further due to the small difference in the module temperature, the energy generations are almost similar in all flow strategies.

Figure 4-23 also presents the variation of annual daytime heat gain through the window system. It is seen that the heat gain through the inner window pane is maximum in case of F_0. As shown in the figure, the least amount of heat is transferred from the window to the indoor environment in case of F_2. However, the discharge of hot air into the occupant area increases the indoor air temperature with this air flow type. With F_1, the heat transfer is lesser than F_0 and but higher than F_2. Further, the hot air from the window cavity is ejected into the outdoor environment. These conditions resulted slightly lower indoor air temperature with F_1 compared to the other cases.

Double pane window systems without any flow through the cavity provides the highest insulation **[94].** The high insulation property helps in lowering the heat loss from the occupant area in the winter season. With air flow the insulation of the window systems reduces. However, in the case of F_2, the hot cavity air enters into the occupant area. Moreover, the annual energy generation with F_2 is around 0.27% higher than F_0. Therefore, it can be stated that F_1 is the best airflow strategy for most of the time in a year. However, in the daytime of winter season, the F_2 air flow strategy can also be selected over F_1 and F_0.

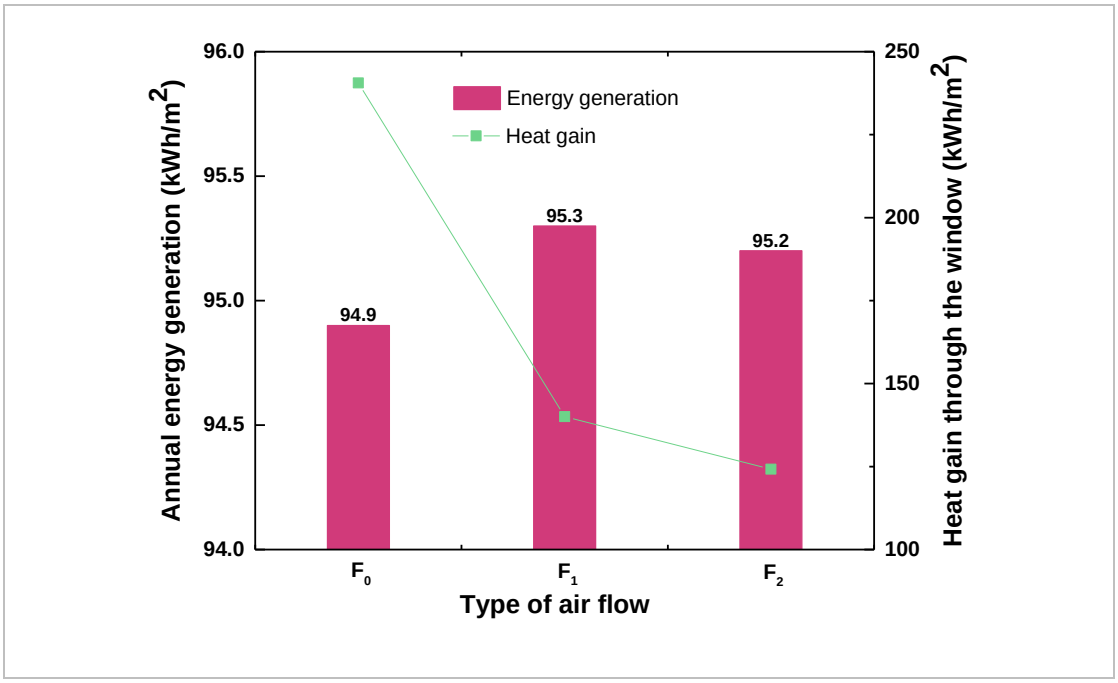

Figure 4-23: Annual energy generation and heat gain into the occupant area with different airflow strategies

4.8 Effect of STPV integrated window on lighting and air conditioning loads

This section presents an analysis of the effect of STPV module integrated window systems on the energy consumption of a daytime used office building in the composite climate of India. The analysis has been carried out for window configuration 'Z' with different transparent STPV modules. The building geometry used in this part has been described in section 3.4.3. To evaluate the effect of the window systems exclusively, the particular zone with which the window system was merged has only been considered during the analysis. The analysis has been carried out for energy generation, Artificial Lighting Energy Consumption (ALEC), heating/ cooling load and net energy performance. The above parameters have been investigated for varying module transmittance, orientation, and Window to Wall Ratio (WWR). Since the energy consumption by the equipment remains the same, it has not been included in the detail discussion. Finally, the energy performance characteristics of the STPV integrated windows have been compared with a standard system as per ECBC,2007 recommendations.

4.8.1 Influence of transmissivity, orientations, and WWR on energy generation

Solar PV module having same area and reflectance but lesser transmittance absorbs more radiation which is subsequently converted into electrical energy. Some results of this part have also been briefly discussed in section **4.5.** However, in the present section, the results have been discussed more detailed and their usefulness in terms of lighting and thermal demand. In this study, the window system 'A' has the lowest transparent module while 'E' has the highest one. These resulted in highest energy generation with window system 'A' and lowest with 'E.' The variation in energy generation among the STPV integrated window systems is presented in **Figure 4-24.** The figure shows that as the window transparency increases, the energy generation decreases. The lowest and highest transparent window systems (A, E), generated 119.6 kWh/m^2/yr and 74.7 kWh/m^2/yr energy respectively in the south orientation. These energy generations are equivalent to the finding in a previous research work **[21].** In that work, the researchers had considered a-Si STPV module of 6.2% conversion efficiency and found an energy generation of 65 kWh/m^2/yr. On the other hand, the conversion efficiency of the STPV module in the lowest transparent window system of our work is 9.91%, **Table 1.** Parallel to the referred work, this conversion efficiency should have delivered the energy of 103 kWh/m^2/yr. However, when the difference in incident solar radiation between the two places is also considered, the corresponding energy generation comes out to be equal to our results. In the referred work, the calculation was done based on a formula developed by Sandia National Laboratory (SNL), USA. The formula helped in including the effect of AOI, amount of incident radiation, type of incident spectrum in the energy generation. However, to use that particular formula, several parameters need to be calculated beforehand. In the present work, the effect of the above factors except the spectrum have been included by applying the wavelength based calculation using measured quantum efficiency. Therefore, this approach can be easily extended to new STPV module materials.

In the considered location (Jaipur), the vertical window received maximum solar radiation towards south direction. The annual average radiation receives by the window system in the south, east, west and north orientations are 1383, 1101, 1089, 484 kWh/m^2 respectively. The higher incident solar radiation in the southern direction resulted in higher energy generation compared to the other orientations. The variation in energy

generation with orientation are also presented in **Figure 4-24.** The figure illustrates that the energy generation changes with orientation according to the level of incident radiation. For instance, in the case of window system 'A,' the energy generation varies from 119.6 kWh/m^2 /yr to 43.8 kWh/m^2/yr if the orientation is changed from south to north direction. These resulted in 63.3% reduction in the energy generation. Corresponding to drop in incident solar radiation by 65%, the reduction in energy generation is lesser because of the effect of AOI. In the south direction, the total incident solar radiation is the combination of beam and diffuse radiation.

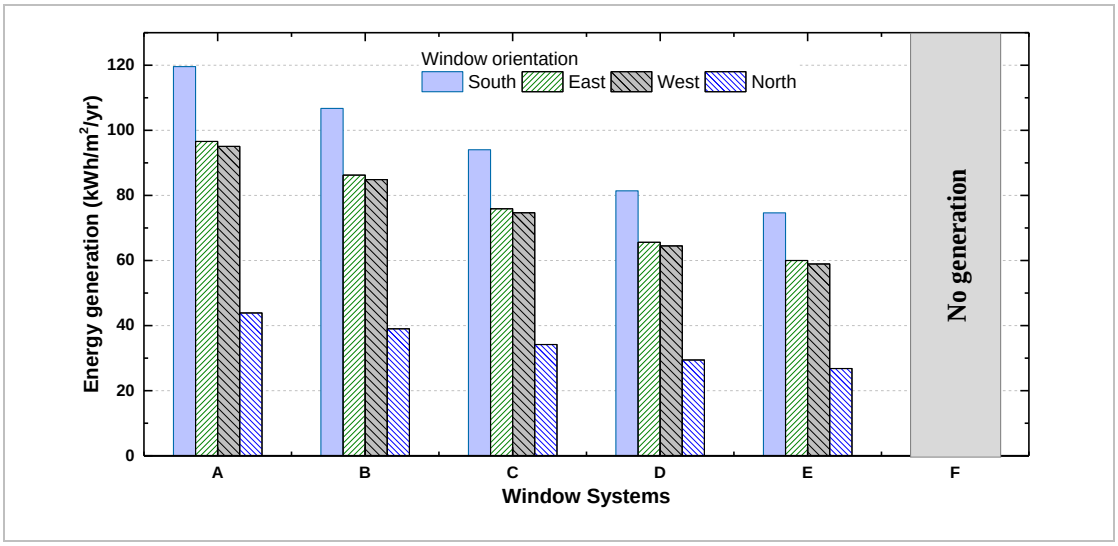

Figure 4-24: Annual energy generation by the window systems in different orientations [WWR 30%]

On the other hand, the north facing window receives mostly diffuse radiation. The beam radiation is a function of the AOI. Therefore, the energy generations are also affected by the AOI where beam radiation is a part of the total incident radiation.

Larger STPV module integrated window system facilitates a more active area for photovoltaic conversion. With the increase in the window area, the WWR rises. As mentioned earlier in the present research, the WWR has been changed from 20% to 50% in the step of 10%. The corresponding area of the STPV module increases from 9 to 22.5 m^2. More energy generation was found in the larger STPV module area. For example, the window system 'A' produces 1076.3 kWh/yr with WWR 20 % in the south direction. The same is found to be 2686.3 kWh/yr with WWR 50 % in the said direction. The 59.9% increment in energy generation is equivalent to the 60% rise in WWR. Finally, the rate of increase in energy generation was found to be linear with WWR. The per m^2 yields of the STPV window systems are comparatively lower than the

conventional photovoltaic power plant installed in the open field. The lower yield is mainly because of less amount of incident radiation on the vertical surface. Some part of the incident radiation also needs to transmit through the STPV window to provide daylight inside the occupant area. This requirement further reduces the energy generation in case of STPV window.

4.8.2 Effect on lighting energy consumption

The available daylight in conjunction with the appropriate controller can save ALEC of a daytime used building. Without daylight controller, the ALEC is 1169 kWh/yr. This ALEC is equivalent to 23.4 kWh/m^2/yr. Here, the sq. meter is representing the unit floor area of the considered thermal zone. However, when the daylight controller was considered, the ALEC get reduced. The amount of daylight entered through a window system depends upon Visible Light Transmittance (VLT) characteristics of the window system. As shown in, **Table 3** among all the STPV integrated window, the highest VLT is for the system 'E.' **Figure 4-25** shows the variation of ALEC among the window systems and orientations with 30 % WWR. The general trend is that the ALEC decreases with increase in window transparency. The ALEC also varies when the orientation changes from south to north. Among the STPV window systems, the minimum ALEC of 17.5 kWh/m^2 has been found for the highest transparent systems 'E'. On the other hand, the highest VLT of the ECBC window leads to the lowest ALEC among all the considered systems. Moreover, due to the highest daylight availability, the minimum ALEC occurs in the south orientation as shown in **Figure 4-25.**

Further, the analysis shows that for the southern zone, the energy generation by the STPV module crosses the lighting demand with all WWR except 20%. The same is found across all the window systems. For the window facing east and west, the energy generations are lower than that of south orientation. The energy generation also decreases with an increase in module transparency. The lower energy generation leads to the requirement of higher WWR in the east and west orientation for larger transparent window system to meet the lighting energy demand. For example, both 20% and 30% WWR are not sufficient to meet the lighting energy demand by STPV energy generation in case of window systems 'D' and 'E.' The energy generation for the window facing north is the lowest among all the orientations. Moreover, the available daylight is also minimum in the northern zone. The above two factors resulted that no STPV window system can meet the lighting energy demand in the northern zone.

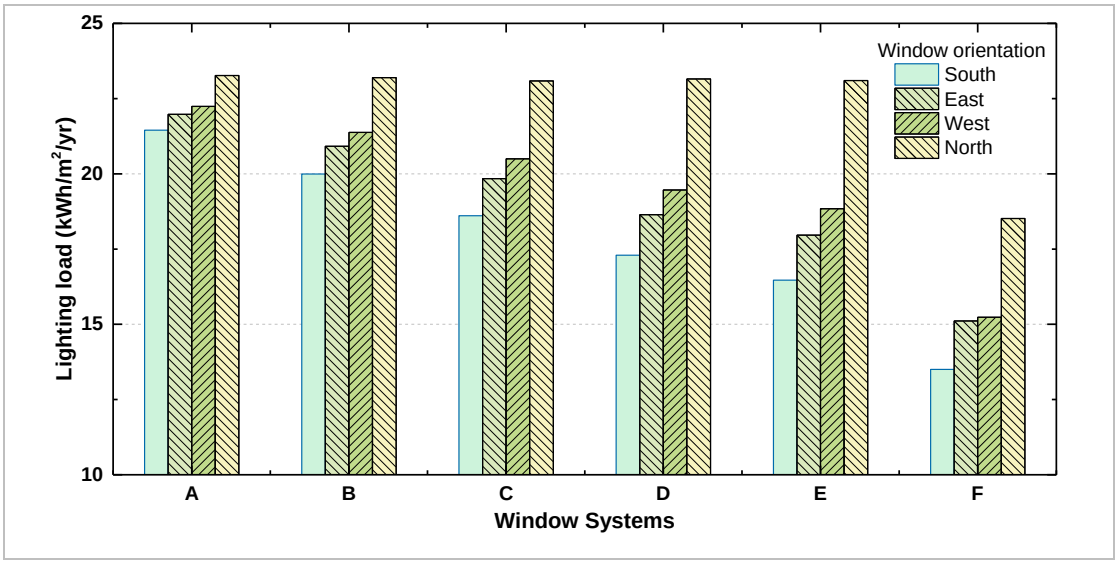

Figure 4-25: Annual artificial lighting energy consumption with the window systems in four orientations and WWR 30%

Finally, the evaluation of change in ALEC with module transparency shows that the rate of decrease in ALEC becomes faster as the transparency increase. On the other hand, with WWR, it remains almost linear at a slower rate. These findings indicate that window transparency is more effective than WWR in saving ALEC through daylight utilization.

4.8.3 Effect on thermal energy consumption

The thermal performances have been analyzed with respect to heating and cooling energies of the zone where the window systems were installed. Since the designing of heating or cooling systems are not the prime objectives, the ideal load conditions have been simulated and analyzed in this study. As mentioned earlier, the thermostat was set at 22^0C and 24^0C for heating and cooling respectively.

Due to uniform U-values, **Table 3,** the heating and cooling loads do not change considerably among the STPV integrated window systems. However, with transparency, the SHGC of the window systems increases slightly. The increase in SHGC causes a minor change in the heating and cooling demands. The general trend is that with transparency the heating load decreases while the cooling load rises at a slower rate as shown in **Figure 4-26** and **Figure 4-27.** The figures also demonstrate that the two thermal loads change with the orientation of the window system. As shown in the figures, the heating load is the minimum for the south direction while the same is maximum for the case when window systems are installed in the north orientation. The cooling loads show the reverse trend. Highest incident radiation in a south facing

window and lowest in the northern direction are the reason behind the reverses trends of heating and cooling loads. The east facing surface receives around 1.08% more solar radiation than the west facing one. Due to this reason, the heating load is slightly lesser with an east facing window than that of the west direction. The same reason produces a reverse condition in case of a cooling load. Both higher U-value and SHGC of the ECBC window helps in reducing the heating load in the direction having more solar radiation. On the other hand, the same parameters are responsible for a more cooling load with ECBC window compared to the STPV systems. Further, due to the prevalence of hot and humid climatic condition for the relatively long period, the annual cooling demand is much higher than the heating load.

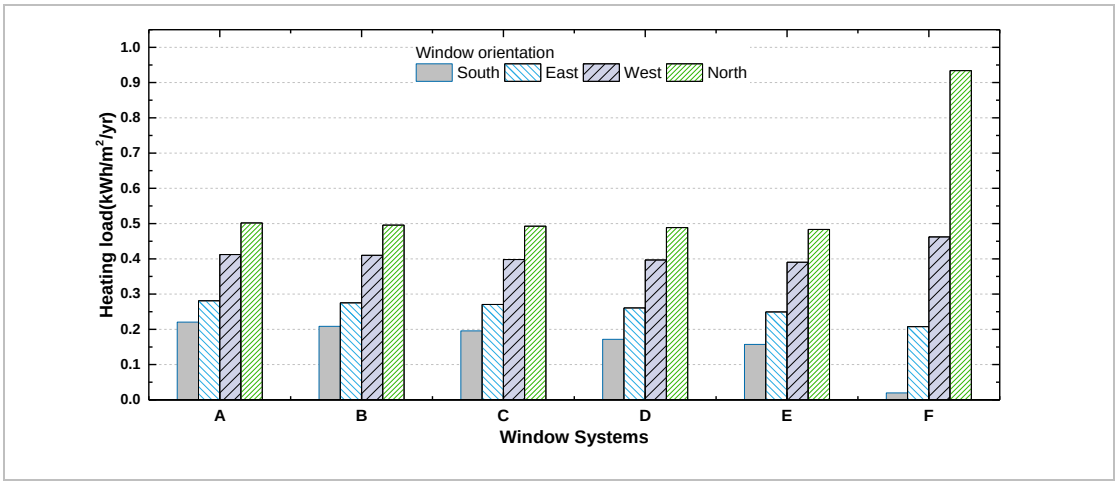

Figure 4-26: Annual heating energy consumption with window systems in four orientations and WWR 30%

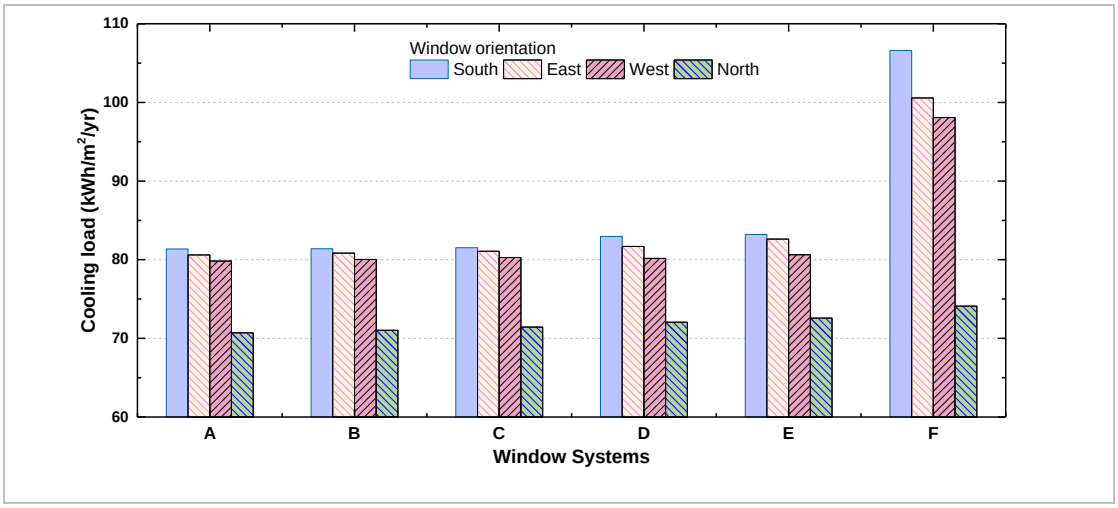

Figure 4-27: Annual cooling energy consumption with different window systems in four orientations and 30% WWR

The heating/cooling loads determining factors, U-value and SHGC, for window systems are higher than for the opaque wall. Therefore, as the WWR increases, the thermal load of the building rises. For instance, with 20 % WWR, the heating and cooling loads are 0.16 kWh/m^2 and 77.78 kWh/m^2 of floor area respectively with the window system 'A' facing south. However, when the WWR increase to 50%, the heating and cooling loads also increase to 0.35 kWh/m^2 and 88.05 kWh/m^2 of the floor area respectively. The changes resulted in 54.28% and 11.65% increment in heating and cooling loads per sq. meter of floor area respectively. Further, the analysis shows that the rate of heating and cooling loads rises almost linearly with increase in WWR. Moreover, SHGC of ventilated double pane window is lesser than the nonventilated system. This factor boosts the reduction in heat gain through the window and thus reduced the cooling load. The calculation shows that in the case of a window system 'A' and 20% WWR, the ventilated airflow reduces the cooling load by 14.2% compared to the non-ventilated case.

4.8.4 Net energy performance

The effect of the STPV window systems on the net energy performance has been analyzed by using the following relation.

Net energy performance= Artificial lighting energy consumption+ Energy consumption for cooling and heating -Photovoltaic energy generation

As indicated in the relation, the energy generation by the STPV module has been considered as outputs from the system in net energy demand calculation. Therefore, more the energy generation lesser is the net energy demand. **Figure 4-28** represents the net energy demand with all the considered window systems and orientations with 30% WWR. The figure shows that with window transparency, the net energy demand increases. The increment is mainly due to a drop in energy generation and a slight increase in cooling load. Orientation-wise, the net energy demand is the minimum for the south direction. The highest energy generation, availability of maximum daylight and minimum heating load are the reason for lowest net energy demand in that orientation. On the other hand, the lowest energy generation along with larger lighting and heating demands lead maximum net energy demand in the northern direction although the cooling load is relatively small. Energy generation, ALEC, and heating load decrease with increase in transparency while the cooling load shows the reverse

trend. For the higher transparent system, the rate of decrease in energy generation is faster than that of the LEC and heating load. It leads to a slightly faster rise in net energy consumption with window transparencies. On the other hand, with WWR the rate of change of energy generation, heating, cooling, and lighting loads varies almost linearly. While, energy generation along with heating and cooling loads increase, the lighting load shows the reverse trend. The slopes for both energy generation and heating load are steeper than the others. However, the overall demand for the heating load is minimal compared to the energy generation. Due to this steep rise in energy generation, the net energy demand decreases at a faster rate with increase in WWR of the building.

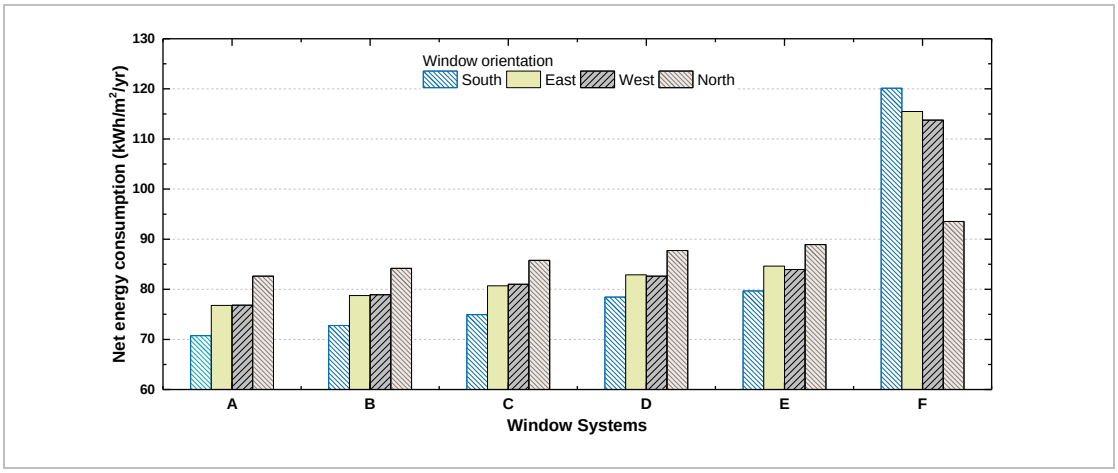

Figure 4-28: Annual net energy consumption with different window systems in four orientations and WWR 30%

Further, the electricity generation by the STPV window at the place of consumption nullified the losses incurred in the process of transmission and distribution besides saving fuel at the plant site. The primary energy corresponding to per kW STPV capacity has been calculated to 12330MJ/yr in the context of Indian coal thermal power plant.

4.8.5 Comparison of STPV window's performance with base case window (F)

The properties of the base case window system 'F' were considered as per the recommendation of ECBC for the composite climatic condition of India. The U-Value, SHGC, and VLT of this window system are given in **Table 3.** It is seen that all the three parameters of the base case window are higher than the STPV integrated systems. The higher VLT helps in reducing the LEC. On the other hand, the higher U-value and SHGC are responsible for intense heating and cooling loads. Since the cooling energy requirement is much larger than the lighting load, the net energy demand with window

system F is higher among all the window systems as shown in **Figure 4-28.** The absence of the STPV module in the window system F further enhanced the net energy consumption compared to the other systems.

Figure 4-29 presents the energy performance of the STPV integrated systems compared to base case window 'F' in south orientation and different WWR. In the figure, the sq. meter unit is representing the STPV area for the energy generation. In other energy cases, the sq. meter is the floor area of the thermal zone considered in the analysis. Here, different energies have been shown after subtracting the base case window part from the STPV systems. The energy higher than the base case system is shown as increased in energy while less one is shown as savings in energy. Further, the base case window system does not contain any STPV module. Therefore the energy generation is zero for this window.

Moreover, the energy generation increases with WWR due to the presence of more active area. However, for a unit area, the energy generation remains the same for a particular STPV window system. The figure indicates that compared to the base case window, the lighting energy demands are more with the STPV integrated system. The differences expand as the WWR increases across all the STPV window. However, as it moves towards the higher transparent window systems, the differences start decreasing.

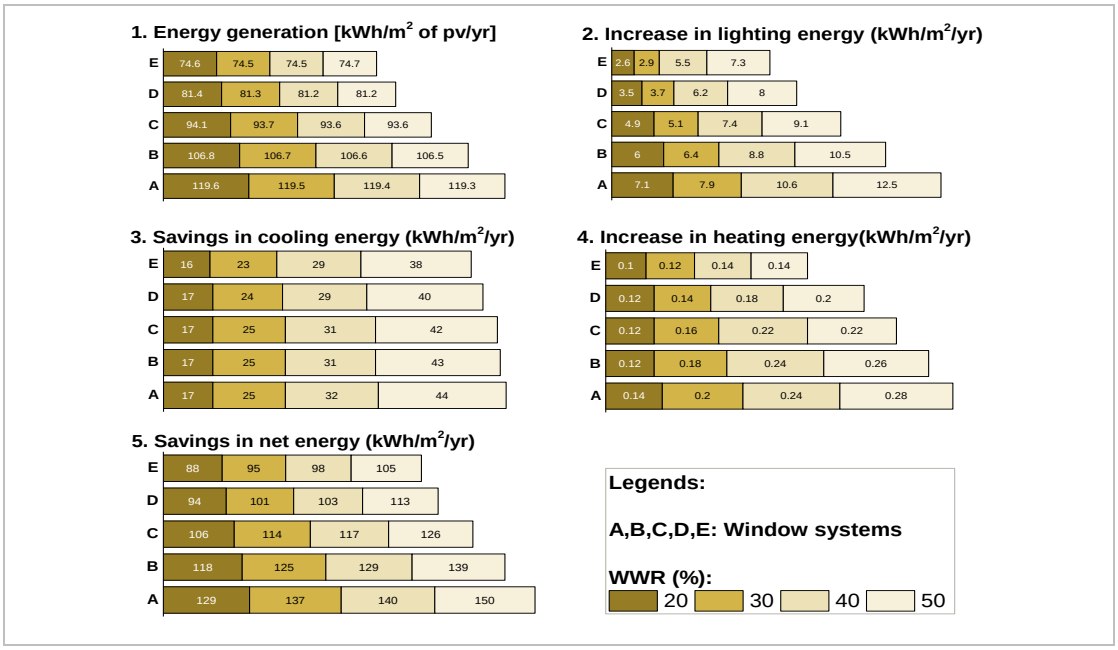

Figure 4-29: Annual energy performance of the STPV window systems compared to the base case window with different WWR (Window orientation: South)

Compared to the base case window, the heating energy requirements are more with the STPV systems. However, the cooling loads are less compared to the same. With WWR the cooling loads increase due to higher U-value of window compared to the opaque wall. Further, the U-value of the STPV systems are less than the ECBC window. The lower U-value helps in reducing the cooling loads with the STPV windows. Additionally, the least transparent STPV window has the lowest SHGC. These properties lead to a maximum saving in cooling load with the window system which is having the least transparent STPV module, as shown in **Figure 4-29.** Compared to window 'F,' a drop of 23.7% in cooling load has been found with the system having the least transparent STPV module. Finally, the net energy consumption with all the STPV systems has found to be lower compared to the ECBC window as shown in the figure. The difference in net energy consumption increases with WWR even though the gap between lighting energy consumption also rises with WWR. The absence of the STPV module in the base case window system further enhances the difference in net energy consumption. The maximum drop in net energy consumption is found for the window system having STPV module of least transparency.

4.9 Summary

The energy savings by the considered STPV systems compared to the base case window (ECBC) in different orientations and WWR are summarised in **Table 11.** The energy savings with the most commonly used WWR (30%) is also illustrated in **Figure 4-30.** Both the table and figure show that among all the systems, the maximum energy savings occurs for STPV window system A (PV1/gap/Low-e). As explained earlier, highest energy production and minimum cooling load are the reason behind this maximum savings with this window system. The level of energy generation from the STPV module also determines the nature of energy savings in different orientations and WWR. Since the energy generation is maximum in the southern orientation and 50% WWR, the reduction is maximum for the said direction and WWR. The maximum drop is account for 60.4% per annum with 50% WWR. However, the energy saving calculated in the present work is comparatively higher than the findings in some other previous research works **[21], [80].** More energy generation and lower U-value of the STPV integrated window systems are the main reasons for this higher energy saving in the present work.

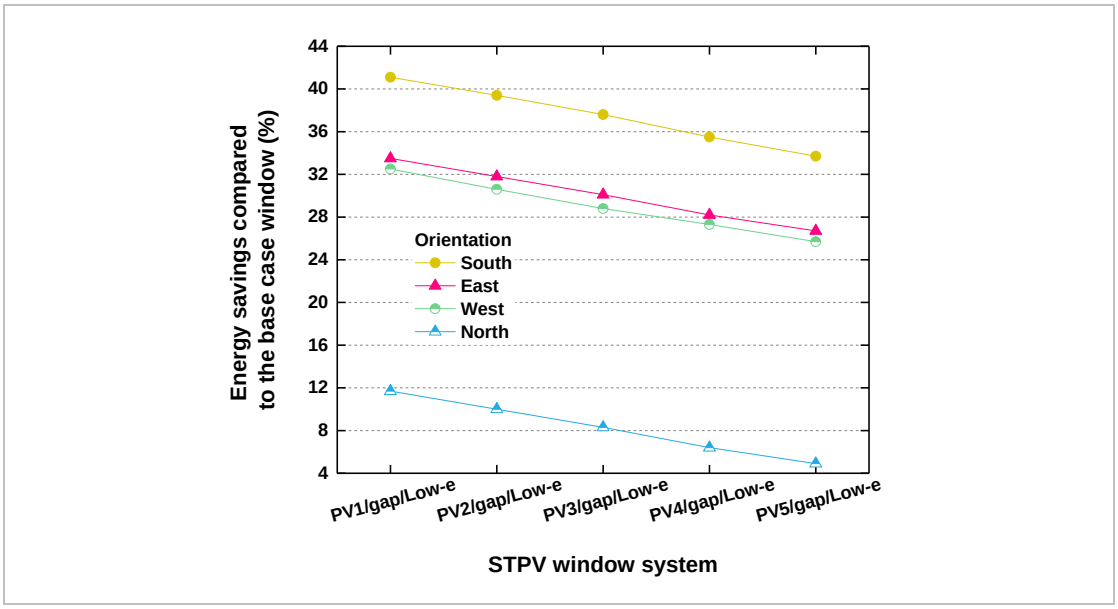

Figure 4-30: Energy savings by STPV window system compared to base case window with the most commonly used WWR (30%)

Nevertheless, it is to be mention that the VLT of the window systems, which provides maximum energy saving, is less than the prescribed value in ECBC. A good level of VLT provides visual comfort to the occupant besides facilitating daylight in the occupant area. Therefore, in choosing the STPV integrated window importance should also need be given on the level of VLT of the system. Experience shows that an STPV integrated double pane window system having VLT of 16 % provides decent visual access to the occupants. **Figure 4-31** presents the visuals through an STPV window system having 16% VLT. The maximum energy savings by the STPV window system with 16% VLT (system C) is found to be 53.5% with 50% WWR. With the commonly used WWR (30%) the energy saving comes to be 37.6%.

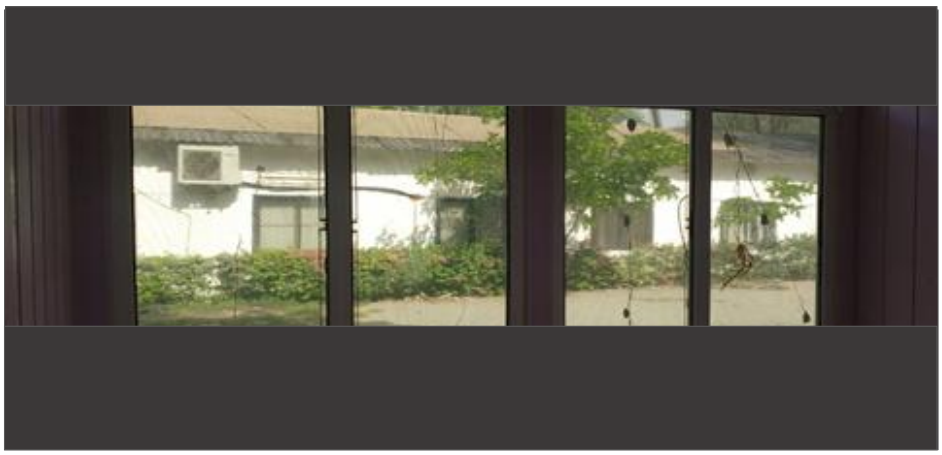

Figure 4-31: Outside view through window system Y (PV3/gap/CG) [STPV module's VLT: 17.7%]

Table 11: Energy savings with the STPV window systems compared to the base case window system in different orientations and WWR (all values are in %)

Orientation	WWR (%)	STPV window systems				
		PV1/gap/ Low-e (A)	PV2/gap/ Low-e (B)	PV3/gap/ Low-e (C)	PV4/gap/ Low-e (D)	PV5/gap/ Low-e (E)
South	20	28.4	27.3	26.2	25.3	24.8
	30	41.1	39.4	37.6	34.7	33.7
	40	50.2	47.8	44.7	40.5	39.5
	50	60.4	57.4	53.5	48.8	45.6
East	20	20.8	19.6	18.5	17.5	17.1
	30	33.5	31.8	30.1	28.2	26.7
	40	43.2	40.9	38.5	35.4	33.1
	50	52.2	49.8	46.3	42.2	39.1
West	20	19.1	17.7	16.3	15.7	15.5
	30	32.5	30.6	28.8	27.4	26.2
	40	42.0	39.5	37.4	34.6	31.3
	50	51.0	48.0	44.8	40.9	36.9
North	20	7.4	6.3	5.0	3.2	2.7
	30	11.7	10.0	8.3	6.2	4.9
	40	14.7	12.4	10.0	7.3	5.5
	50	17.1	14.3	11.2	7.8	4.9

4.10 Chapter Summary

This chapter described all results and related discussions of the present research. Some of the important results mentioned in this chapter are listed below.

- Effect of the amount of incident radiation, type of incident spectrum, and cell operating temperature on vertical STPV window system's energy generation
- Change in the effect of angle of incidence on vertical STPV window's energy generation with the place of installation (latitude), orientation and module's transmittance

- Energy generation by five transparent STPV window systems in four latitudes and orientations.
- Best window configurations from energy generation point of view
- Contribution of cavity airflow in the power generation of STPV integrated double pane window system
- Amount of heat transfer through STPV integrated window system into the occupant area
- Influence of STPV integrated window systems on ALEC, cooling, and heating energy consumption of a building. Variation of these parameters with WWR and window orientation
- Energy saving potential of STPV integrated double pane window system compared to the ECBC window in the composite climate of India. Variation of energy saving potential with WWR and window orientation

CHAPTER 5
CONCLUSIONS

5.1 Impact of different key factors on the energy generation of window integrated STPV module

In this section, the effect of four key factors on the energy generation of a CdTe module integrated double pane window system were analyzed by using a simplified approach in combination with 'EnergyPlus' software. The four key factors are module temperature, amount of incident radiation, characteristics of the incident spectrum and angle of incidence. This approach needs the basic opto-electrical properties of STPV module. Therefore, it bypasses the rigorous testing of many dynamic coefficients required to evaluate the energy performance of an STPV module based window/façade systems using the EnergyPlus software. Since the applied approach requires only the conventional opto-electrical properties, the same can be easily adapted to other material based STPV integrated window/façade systems. The findings of this part of work have been submitted to **Energy Strategy Reviews journal**. The major outcomes of this section are as follows.

- The STPV energy generations were found to be reduced due to increase in module temperature and Angle of Incidence (AOI). For instance, the energy generation was found to be reduced by 4.5% and 7.2% in April due to higher module temperature and deviation of radiation from the normal incidence respectively.
- Reduction in module efficiency and hence power generations was also observed due availability of lower incident radiation on the window system.
- The effect of incidence spectrums was observed to be positive during more precipitable water content in the atmosphere.
- Among all the parameters, the effect of cell operating temperature and AOI were dominant in the energy generation.
- Finally, the annual energy generation of 106 kWh/m^2 with conversion efficiency provided by the manufacturer dropped to 95.3 kWh/m^2 in the real operating condition. This reduction is accounted for 10.0 % per annum.

To summarise, the findings of this section indicate that the performance of the STPV module integrated double pane window systems are subjected to the weather conditions of the installed location.

5.2 Effect of angle of incidence on energy generation in window integrated STPV module

In this section, the effect of angle of incidence on energy generation of STPV module in vertical window systems was analyzed in four cities of India. The effect is also known as angular loss of energy generation. Reflection of beam radiation is subjected to the angle of incidence. Therefore, the amount of beam radiation available in the total incident radiation also played a significant role. The findings of this part of work have been submitted to **Sustainable Energy Technologies and Assessments journal**. The major conclusions of this sections are as follows.

- The effect of angle of incidence on the energy generation in window integrated STPV module increase significantly for AOI above 70^0.
- Orientation wise, the maximum effect of angle of incidence was observed for the south facing window system. For south-facing window system A (PV1/gap/Low-e), the annual energy reduced by 5.1% compared to the normal incidence at Jaipur (latitude: 26.82^0N).
- The effect of angle of incidence was found to be decreased with an increase in module transmissivity across all the latitudes and orientations. When the module transmittance was changed from 6.0% to 27.5%, the annual energy loss changed from 6.4 to 2.3 kWh/m^2 for the south-facing vertical window at Jaipur (latitude: 26.82^0N).

To summarize, the analysis suggests that the effect of angle of incidence is sensitive to the place of installation, orientation, and the STPV module characteristics. Therefore, this parameter needs special importance in design and optimization of STPV vertical systems for high-rise buildings in the cities.

5.3 Effect of window configurations and airflow strategies on the performance of STPV module integrated window systems

This section analyzed the effect of different window configurations and airflow strategies on the electrical and thermal performances of STPV module integrated window systems in the composite climate of India. The effect of the change in air cavity

position with respect to the STPV module is one of the focus of this section. Another focus of this section is the application of spectrally selective glass in front of the STPV module. The findings of this part of work have been published in **Solaris 2017, a national conference on Renewable Energy Sources for Sustainable Climate**. The major findings of this sections are as follows.

- Among all the investigated window configurations, the minimum module temperature was observed for the configuration having spectrally selective glass in front of the STPV module.
- When the STPV module was used behind clear or Low-e glass, some part of the effective wavelength also blocks from reaching the module. The reduction in effective wavelength eventually leads to a decrease in energy generation. However, the decrease in energy generation was lower compared to the reduction in incident radiation. When the clear and Low-e glasses were used in front of the STPV module the energy generations were decreased by 9% and 10% corresponding to 15% and 35% reduction in the amount of incident radiation respectively.
- With the introduction of air flow through the window cavity, the module temperature decreases. The maximum drop of 3.8^0C was found with F_1 on 15^{th} December. Therefore, F_1 facilitated the best photovoltaic conversion efficiency and delivered the maximum energy of 95.3 kWh/m^2 per annum.
- The analysis showed that the modes of airflow also affect the indoor air temperature. Compared to no flow condition, the indoor temperature was found to increase with F_2 while the reverse was observed with F_1. In the typical winter day, the maximum increase in indoor air temperature was 2^0C.

To summarize, the results indict that placing of clear or Low-e glasses in front of the STPV modules modify the spectrum of the incident radiation for better photovoltaic conversion. The results also imply that the indoor air temperature can be altered by meticulously maneuvering the window cavity air.

5.4 Effect of STPV module integrated window systems on lighting and air conditioning loads

Performance of STPV integrated window changes with the type of module's material and optical characteristics, place of installation, WWR, and orientation. In this section, the performance of five double pane window systems was analyzed with respect to the

energy generation, cooling, heating and lighting loads. The relevant findings of the previous sections were used in this section. Finally, a comparison with the ECBC recommended window was discussed. The major findings of this section are as follows. These findings have been published in the **Sustainable Cities and Society journal** (Ref. Vol 37, pp. 250-262, 2018)

- In the analysis, the photovoltaic energy generation was found to be changed with module transparency, orientation, and WWR. The maximum energy generation of 119.6 kWh/m^2/yr was achieved with the least transparent STPV module in south orientation.
- Due to change in energy generation and available daylighting, the combination of the STPV module's transparency and WWR changes with an orientation to meet or overcome the artificial lighting energy consumption (ALEC). While in the south direction all STPV window systems above 20% WWR were capable of meeting the ALEC, larger areas were required in east and west orientation for the same. Further, STPV module transparency was found to be more sensitive than WWR in reducing the ALEC by using daylighting.
- The analysis showed the opposite pattern of cooling and heating loads with STPV module transparency and WWR.
- The net energy consumption with the STPV window was found to be lowest for the system having the highest conversion efficient module. This occurred due to consideration of energy generation by the STPV module as an output of the window systems
- Compared to the reference window which was considered as per the ECBC recommendations, energy saving as high as 60.4% was achieved with the highest efficient STPV module integrated system.

To summarize, it can be stated that there is high energy saving potential in the daytime used buildings of composite climate by applying CdTe based STPV module integrated window system. The high-rise buildings are suitable establishments for STPV integrated window systems. Implementation of these systems will help in converting the buildings into low or net-zero energy buildings.

5.5 Major contributions of the thesis

- The present research proposed a simplified approach for the performance evaluation of semi-transparent photovoltaic module integrated window systems. The method can be easily adaptable to other types semi-transparent photovoltaic module for BIPV application. It is also applicable to any weather conditions.
- The thesis presents a critical analysis of the potential effect of four key factors on the performance of the STPV integrated window system in actual operating conditions
- The thesis includes a detailed analysis of the effectiveness of selective glass in curtailing the non-productive part of the incident solar spectrum for the photovoltaic conversions
- The thesis presents an estimation of energy generation by STPV window system. It also presents the energy saving potential by the STPV integrated window systems compared to a standard window. Effect of various design and operating conditions have been considered using experimentally validated models. Therefore, the thesis shall work as a valuable reference for the engineers, architectures and BIPV systems integrators.
- The STPV integrated window system has numerous benefits. The thesis presents a clear picture to end users about the energy-saving potential of this emerging technology.

5.6 Future prospects

Based on the findings of the present research, some future scopes of research are suggested below.

- Use of available spectrally selective glass as a front layer in a double pane window system significantly reduces the STPV module temperature. However, the energy generation also decreases due to the reduction of incident radiation in the useful wavelength range. Further research can be considered for the development of spectrally selective layer with significantly high transparency in the working wavelength range by solar module.
- The present research was carried out with the STPV module available in the market. In the applied module the back side glass is a simple glass. The emissivity of the back surface is high. The high emissivity increases the heat

ingress into the occupant area. Simulation study can be carried for the development of a transparent surface with lower emissivity. If proven beneficial from the building overall energy point of view, the experimental work and STPV module can be manufactured accordingly.

- For STPV integrated window system, the angle of incidence remains high in most of the time of a year. On the other hand, due to the high angle of incidence, a considerable amount of incident radiation reflected into the atmosphere. Research can be carried out to reduce the reflected radiation for useful application.
- A comprehensive study including the techno-economic and environmental factors can be carried for achieving the net zero or low energy building by applying the STPV window/façade. The outcome of this kind of study should constructively contribute to the development of green building policy of the country

REFERENCES

[1] "BP Statistical Review of World Energy," [Online] BP P.L.C., 2017. [Cited: 30 09 2017.] https://www.bp.com/content/dam/bp/en/corporate/pdf/energy-economics/statistical-review-2017/bp-statistical-review-of-world-energy-2017-fullreport.pdf.

[2] "Solar photovoltaic electricity empowering the world," [Online] Greenpeace, 2011. [Cited: 12 5 2016.] http://www.greenpeace.org/international/Global /international /publications/climate/2011/Final%20SolarGeneration%20VI%20full% 20report% 20lr.pdf.

[3] P. Moriarty, D. Honnery, "What is the global potential for renewable energy?," Renewable and Sustainable Energy Reviews, vol. 16, pp. 244-252, 2012.

[4] United Nations Environment Programme. [Online] [Cited: 30 04 2016.] http://www .unep.org/sbci/AboutSBCI/Background.asp.

[5] U.S. and India Building Energy Use. [Online] CBERD | "Building Technology & Urban Systems," 2016. [Cited: 10 01 2017.] http://cberd.org/building%20energy %20use/.

[6] R. Rawal, Y. Shukla. "Residential Buildings in India: Energy Use Projections and Savings Potentials," [Online] Global Buildings Performance Network (GBPN), 2014. [Cited: 29 04 2016.] http://www.gbpn.org/sites/default/ files/08.%20INDIA %20Baseline_ TR_ low.pdf.

[7] Climatic Works Foundation, "Reducing GHG Emissions in the Building Sector in India: A Strategy Paper," 2010.

[8] J. Yao, N. Zhu, "Evaluation of indoor thermal environmental, energy and daylighting performance of thermotropic windows," Building and Environment, vol. 49, pp. 283-290, 2012.

[9] R. Charron, A. Athienitis, "Design and Optimization of Net Zero Energy Solar Homes," ASHRAE Transactions, vol. 112, pp. 283-295, 2006.

[10] D. Kolokotsa, D. Rovas, E. Kosmatopoulos, K. Kalaitzakis, "A roadmap towards intelligent net zero- and positive-energy buildings," Solar Energy, vol. 85, pp. 3067-3084, 2011.

[11] R. Baetens, R. De Coninck J. Van Roy, B. Verbruggen, J. Driesen, L. Helsen, D. Saelens, "Assessing electrical bottlenecks at feeder level for residential net-zero-energy buildings by integrated system simulation," Applied Energy, vol. 96, pp. 74-83, 2012.

[12] ECBC: Energy Conservation Building Code. New Delhi, India: Bureau of Energy Efficiency, 2017.

[13] J. H. Yoon, S.R. Shim, Y. S. An, K. H. Lee, "An experimental study on the annual surface temperature characteristics of amorphous silicon BIPV window," Energy and Buildings, vol. 62, pp. 166-175, 2013.

[14] J. W. Lim, M. Shin, D. J. Lee, S. H. Lee, S. J. Yun, "Highly transparent amorphous silicon solar cells fabricated using thin absorber and high-bandgap energy n/i-interface layers," Solar Energy Materials & Solar Cells, vol. 128, pp. 301-306, 2014.

[15] P. W. Wong, Y. Shimoda, M. Nonaka, M. Inoue, M. Mizuno, "Semi-transparent PV: thermal performance, power generation, daylight modeling and energy saving potential in a residential application," Renewable Energy, Vol. 33, pp. 1024-36, 2008.

[16] Y. T. Chae, J. Kim, H. Park, B. Shin, "Building energy performance evaluation of building integrated photovoltaic (BIPV) window with semi-transparent solar cells," Applied Energy, vol. 129, pp. 217-227, 2014.

[17] J. Peng, L. Lu, H. Yang, "Review of life cycle assessment of energy payback and greenhouse gas emission of solar photovoltaic systems," Renewable and Sustainable Energy Reviews, vol. 19, pp. 255-274, 2013.

[18] F. Chen, S.K. Wittkopf, P. Khai Ng, H. Du, "Solar heat gain coefficient measurement of semi-transparent photovoltaic modules with indoor calorimetric hot box and solar simulator," Energy and Buildings, vol. 53, pp. 74-84, 2012.

[19] D.L. King, W.E. Boyson, J.A. Kratochvill. "Photovoltaic Array Performance Model," California: Sandia National Laboratories, SAND2004-3535, 2004.

[20] C. Peng, Y. Huang, Z. Wu, "Building-integrated photovoltaics (BIPV) in architectural design in China," Energy and Buildings, vol. 12, pp. 3592-3598, 2011.

[21] J. Peng, D. C. Crucijia, L. Lu, S. E. Selkowitz, H. Yang, W. Zhang, "Numerical investigation of the energy saving potential of a semi-transparent photovoltaic double-skin facade in a cool-summer Mediterranean climate," Applied Energy, vol. 165, pp. 345-356, 2016.

[22] P. W. Wong, Y. Shimoda, M. Nonaka, M. Inoue, M. Mizuno, "Semi-transparent PV: thermal performance, power generation, daylight modelling and energy saving potential in a residential application," Renewable Energy, vol. 33, pp. 1024-36, 2008.

[23] S. Yoo, H. Manz, "Available remodeling simulation for a BIPV as a shading device," Solar Energy Materials & Solar Cells, vol. 1, pp. 394-397, 2011.

[24] M. Mandalaki, K. Zervas, T. Tsoutsos, A. Vazakas, "Assessment of fixed shading devices with integrated PV for efficient energy use," Solar Energy, vol. 9, pp. 2561-2575, 2012.

[25] T.T. Chow, K.F. Fong, W. He, Z. Lin, A.L.S. Chan, "Performance evaluation of a PV ventilated window applying to office building of Hong Kong," Energy and Buildings, vol. 39, pp. 643-650, 2007.

[26] A. De Miguel, J. Bilbao, J.R.S. Cazorro, C. Martín. Cologne, "Performance analysis of a grid-connected PV system in a rural site in the Northwest of Spain," World Renewable Energy Congress VII, Germany, 2002.

[27] P. Singh, N.M. Ravindra, "Temperature dependence of solar cell performance—an analysis," Solar Energy Materials & Solar Cells, vol. 101, pp. 36-45, 2012.

[28] M. George, Z. Bastian, P. Alexander, S. Markus, G. E. Goerge, "Temperature and thermal annealing effects on different photovoltaic technologies," Renewable Energy, vol. 43, pp. 407-417, 2012.

[29] T. Yamawaki, S. Mizukami, T. Masui, H. Takahashi, "Experimental Investigation on generated power of amorphous PV module for roof azimuth," Solar Energy Materials and Solar Cells, vol. 67, pp. 369-377, 2001.

[30] K. Nagano, T. Mochida, K. Shimakura, K. Murashita, S. Takeda, "Development of thermal-photovoltaic hybrid exterior wallboards incorporating PV cells in and

their winter performances," Solar Energy Materials and Solar Cells, vol. 77, pp. 265-282, 2003.

[31] T.T. Chow, "Performance analysis of photovoltaic-thermal collector by explicit dynamic model," Solar Energy, vol. 75, pp. 143-152, 2003.

[32] H. A. Zondaga, D.W.de Vriesa, W. G. J. van Heldenb, R. J. C. van Zolingenc, A. A. van Steenhoven, "The yield of different combined PVthermal collector designs," Solar Energy, vol. 74, pp. 253-269, 2003.

[33] E. Radziemska, "The effect of temperature on the power drop in crystalline silicon solar cells," Renewable Energy, vol. 28, pp. 1-12, 2003.

[34] M. Bakker, H. A. Zondag, J. M. Elswijk, K. J. Strootman, M. J. M. Jong, "Performance and costs of roof-sized PV/thermal array combined with a ground coupled heat pump," Solar Energy, vol. 78, pp. 331-339, 2005.

[35] A. Tiwari, M. S. Sodha, "Performance evaluation of a solar PV/T system: a parametric study," Renewable Energy, vol. 31, pp. 2460-2474, 2006.

[36] A. Tiwari, M. S. Sodha, "Parametric study of various configurations of hybrid PV/thermal air collector: experimental validation of theoretical model," Solar Energy Materials and Solar Cells, vol. 91, pp. 17-28, 2007.

[37] Y. B. Assoa, C, Menezo, G. Fraisse, R. Yezou, J. Brau, "Study of a new concept of photovoltaic-thermal hybrid collector," Solar Energy, vol. 81, pp. 1132-1143, 2007.

[38] T. Hove, "A method for predicting long-term average performance of photovoltaic systems," Renewable Energy, vol. 21, pp. 207-229, 2000.

[39] M. D. Bazilian D, Prasad, "Modelling of a photovoltaic heat recovery system and its role in a design decision support tool for building professionals," Renewable Energy, vol. 27, pp. 57-68, 2002.

[40] T. Yamaguchi, Y. Okamoto, M. Taberi, "Investigation on abundant photovoltaic power generated by 40 kW PV system in Wakayama National College of Technology," Solar Energy Materials and Solar Cells, vol. 75, pp. 597-601, 2003.

[41] Z. Zhu, H. Yang, R. Jiang, Q. Wu, "Investigation of conjugate heat transfer in a photovoltaic wall," Heat Transfer-Asian Research, vol. 33, pp. 117-128, 2004.

[42] G. Notton, C. Cristofari, M. Mattei, P. Poggi, "Modelling of a double-glass photovoltaic module using finite differences," Applied Thermal Engineering, vol. 25, pp. 2854-2877, 2005.

[43] T. T. Chow, W. He, J. Ji, "Hybrid photovoltaic-thermosyphon water heating system for residential application," Solar Energy, vol. 80, pp. 298-306, 2006.

[44] N. Aste, G. Chiesa, F. Verri, "Design, development and performance monitoring of a photovoltaic-thermal (PVT) air collector," Renewable Energy, vol. 33, pp. 914-927, 2008.

[45] K.E. Park, G.H. Kang, H.I. Kim, G.J. Yu, J.T. Kim, "Analysis of thermal and electrical performance of semi-transparent photovoltaic (PV) module," Energy, vol. 35, pp. 35:2681-2687, 2010.

[46] S. Armstrong, W.G. Hurley, "A thermal model for photovoltaic panels under varying atmospheric conditions," Applied Thermal Engineering, vol. 30, pp. 1488-1495, 2010.

[47] D. Jones and C.P. Underwood, "A thermal model for photovoltaic systems," Solar Energy, vol. 70, pp. 349-359, 2001.

[48] K. Vats, V. Tomar, G.N. Tiwari, "Effect of packing factor on the performance of a building integrated semi-transparent photovoltaic thermal (BISPVT) system with air duct," Energy and Buildings, vol. 53, pp. 159-165, 2012.

[49] D. Kamthania, S. Nayak, G.N. Tiwari, "Performance evaluation of a hybrid photovoltaic thermal double pass facade for space heating," Energy and Buildings, vol. 43, pp. 2274-2281, 2011.

[50] S. Nayak, G.N. Tiwari, "Energy and exergy analysis of photovoltaic/thermal integrated with a solar greenhouse," Energy and Buildings, vol. 40, pp. 2015-2021, 2008.

[51] M. D'Orazio, C. Di Perna, E. Di Giuseppe, "Experimental operating cell temperature assessment of BIPV with different installation configurations on roofs under Mediterranean climate," Renewable Energy, vol. 68, pp. 378-396, 2014.

[52] Å. Skaaland, M. Ricke, K. Wallevik, R. Strandberg, A. G. Imenes. "Potential and Challenges for Building Integrated Photovoltaics in the Agder region," [Online] Report 2011. [Cited: 30 03 2016.] http://citeseerx.ist.psu.edu/viewdoc/ download?doi=10.1.1.704.2965&rep=rep1&type=pdf

[53] T. Minemoto, M. Toda, S. Nagae, M. Gotoh, A. Nakajima, K. Yamamoto, H. Takakura, Y. Hamakawa, "Effect of spectral irradiance distribution on the outdoor performance of amorphous Si//thin-film crystalline Si stacked photovoltaic modules," Solar Energy Materials & Solar Cells, vol. 91, pp. 120-122, 2007.

[54] A. Virtuani, D. Strepparava, G. Friesen, "A simple approach to model the performance of photovoltaic solar modules in operation," Solar Energy, vol. 120, pp. 439-449, 2015.

[55] L. Nelson, M. Frichtl, A. Panchula, "Changes in Cadmium Telluride Photovoltaic System Performance due to Spectrum," IEEE Journal of Photovoltaics, vol. 1, pp. 488-493, 2013.

[56] D. H.W. Li, J. C. Lam, "Predicting solar irradiance on inclined surfaces using sky radiance data," Energy Conversion and Management, vol. 45, pp. 1771-1783, 2004.

[57] G. Aaditya, R. Pillai, M. Mani, "An insight into real-time performance assessment of a building integrated photovoltaic (BIPV) installation in Bangalore (India)," Energy for Sustainable Development, vol. 17, pp. 431-437, 2013.

[58] D. H.W. Li, G. H.W. Cheung, J. C. Lam, "Analysis of the operational performance and efficiency characteristic for photovoltaic system in Hong Kong," Energy Conversion and Management, vol. 46, pp. 1107-1118, 2005.

[59] T. J. Silverman, U. Jahn, G. Friesen, M. Pravettoni, M. Apolloni, A. Louwen, WGJHM van Sark, M. Schweiger, G. Belluardo, J. Wagner, A. Tetzlaff, P. Ingenhoven, D. Moser, "Characterisation of Performance of Thin-film Photovoltaic Technologies," International Energy Agency (IEA), ISBN 978-3-906042-17-6, 2014.

[60] A. Kumar, O.S. Sastry, S.S. Chandel, V. Sharma, "Performance assessment of different solar photovoltaic technologies under similar outdoor conditions," Energy, vol. 58, pp. 511-518, 2013.

[61] S. V. Janakeeraman, "Angle of Incidence and Power Degradation Analysis of Photovoltaic Modules," Thesis; Master of Science in Technology, Arizona State University. [Online] May 2013. [Cited: 20 4 2016.]https://repositoryasu. edu/attachments/110481/content/VasanthaJanakeeraman_asu_0010N_12882.pdf.

[62] N. Martin, J.M. Ruiz, "Calculation of the PV modules angular losses under field conditions by means of an analytical model," Solar Energy Materials & Solar Cells, vol. 70, pp. 25-38, 2001.

[63] N. Martin, J. M. Ruiz, "A new model for PV modules angular losses under field conditions," International Journal of Solar Energy, vol. 1, pp. 19-31, 2002.

[64] N. Martin, J. M. Ruiz, "Annual angular reflection losses in PV modules," Progress in Photovoltaic: Research and Applications, vol. 13, pp. 75-84, 2005.

[65] P. Schaub, A. Mermoud, O. Guisan, "Evaluation of the different losses involved in two photovoltaic systems," Proceedings of 12th European PV Solar Energy Conference, Amsterdam, 1994.

[66] R. Preu, G. Kleiss, K. Reiche, K. Bucher, "PV-module reflection losses: measurement, simulation and influence on energy yield and performance ratio," 13th European PV Solar Energy Conference, Nice, France, 1995.

[67]. J. H. Wohlgemuth, "Standards for PV Modules and Components – Recent Developments and Challenges," 27th European Photovoltaic Solar Energy Conference and Exhibition, Frankfurt, Germany, 2012.

[68] B. Knisely, " Angle of Incidence and Non-Intrusive Cell Quantum Efficiency Measurements of Commercial Photovoltaic Modules," [Online] Arizona State University, December 2013. [Cited: 15 03 2017.] https://pdfs.semanticscholar. org/ 519f/ f04da3d679ab592982 2a1e6 46067bafc78b7.pdf.

[69] B. Knisely, S. V. Janakeeraman, J. Kuitche, G. TamizhMani, "Validation of IEC 61853-2 Standard (Draft): Angle of Incidence Effect on Photovoltaic Modules," IEEE 39th Photovoltaic Specialists Conference (PVSC), Tampa, FL, USA, 2013.

[70] A. H. Fanney, B. P. Dougherty, M. W. Davis, "Short-Term Characterization of Building Integrated Photovoltaic Panels," Journal of Solar Energy Engineering, vol. 135, pp. 13-20, 2003.

[71] A. H. Fanney, M. W. Davis, B. P. Dougherty, "Measured Performance of Building Integrated Photovoltaic Panels—Round 2," Journal of Solar Energy Engineering, vol. 3, pp. 314-323, 2005.

[72] L. Fanni, A. Virtuani, D. Chianese, "A detailed analysis of gains and losses of a fully-integrated flat roof amorphous silicon photovoltaic plant," Solar Energy, vol. 85, pp. 2360-2373, 2011.

[73] F. Chen, S. K. Wittkopf, P. K. Ng, H. Du, "Solar heat gain coefficient measurement of semi-transparent photovoltaic modules with indoor calorimetric hot box and solar simulator," Energy and Buildings, vol. 53, pp. 74-84, 2012.

[74] J. H. Song, Y. S. An, S. G. Kim, S. J. Lee, J. H. Yoon, Y. K. Choung, "Power output analysis of transparent thin-film module in building integrated photovoltaic system (BIPV)," Energy and Buildings, vol. 40, pp. 2067-2075, 2008.

[75] H. K. Elminir, V. Benda, J. Tousek, "Effects of solar irradiation conditions and other factors on the outdoor performance of photovoltaic modules," Journal of electrical engineering, vol. 52, pp. 125-133, 2001.

[76] P. K. Ng, N. Mithraratne, H. W. Kua, "Energy analysis of semi-transparent BIPV in Singapore buildings," Energy and Buildings, vol. 66, pp. 274-281, 2013.

[77] J. H. Yoon, J. Song, S. J. Lee, "Practical application of building integrated photovoltaic (BIPV) system using transparent amorphous silicon thin-film PV module," Solar Energy, vol. 85, pp. 723-733, 2011.

[78] G. Y. Yun, M. McEvoy, K. Steemers, "Design and overall energy performance of a ventilated photovoltaic facade," Solar Energy, vol. 81, pp. 383-394, 2007.

[79] S. Xu, W. Liao, J. Huang, J. Kang, "Optimal PV cell coverage ratio for semi-transparent photovoltaics on office building facades in central China," Energy and Buildings, vol. 77, pp. 130-138, 2014.

[80] T. Miyazaki, A. Akisawa, T. Kashiwagi, "Energy savings of office buildings by the use of semi-transparent solar cells for windows," Renewable Energy, vol. 30, pp. 281-304, 2005.

[81] F.J. Moralejo-Vázquez, N. Martín-Chivelet, L. Olivieri, E. C. Martín, "Luminous and solar characterization of PV modules for building integration," Energy and Buildings, vol. 103, pp. 326-337, 2015.

[82] J. W. Lim, S. H. Lee, D. J. Lee, Y. J. Lee, S. J. Yun, "Performances of amorphous silicon and silicon germanium semi-transparent solar cells," Thin Solid Films, vol. 54, pp. 212-215, 2013.

[83] L. Olivieri, E. Caamano-Martin, F. Olivieri, J. Neila, "Integral energy performance characterization of semi-transparent photovoltaic elements for building integration under real operation conditions," Energy and Buildings, vol. 68, pp. 280-291, 2014.

[84] K. Kapsis, A. K. Athienitis, "A study of the potential benefits of semi-transparent photovoltaics in commercial buildings," Solar Energy, vol. 115, pp. 120-132, 2015.

[85] J.H. Selj, T.T. Mongstad, R. Søndena, E.S. Marstein, "Reduction of optical losses in colored solar cells with multilayer antireflection coatings," Solar Energy Materials & Solar Cells, vol. 95, pp. 2576-2582, 2011.

[86] N. Lynn, L. Mohanty, S. Wittkopf, "Color rendering properties of semi-transparent thin-film PV modules," Building and Environment, vol. 54, pp. 148-158, 2012.

[87] Y. Y. Tady, Y. H. Fung, "Study on thermal performance of semi-transparent building-integrated photovoltaic glazing's," Energy and Buildings, vol. 40, pp. 341-350, 2008.

[88] T. E. Kuhn, "Calorimetric determination of the solar heat gain coefficient g with steady-state laboratory measurements," Energy and Buildings, vol. 84, pp. 388-402, 2014.

[89] L. Olivieri, F. Frontini, C. Polo-López, D. Pahud, E. C. Martín, "G-value indoor characterization of semi-transparent photovoltaic elements for building integration: New equipment and methodology," Energy and Buildings, vol. 101, pp. 84-94, 2015.

[90] I. David, E. Ursula, F. Volker, M Li, S. Jurgen, "A simplified approach to thermal performance calculation for building integrated mechanically ventilated PV facades," Building and Environment, vol. 41, pp. 893-901, 2006.

[91] F. Chen, S. K. Wittkopf, "Summer condition thermal transmittance measurement of fenestration systems using calorimetric hot box," Energy and Buildings, vol. 53, pp. 47-56, 2012.

[92] S. Cristina. L. Polo, S. Marco, "Comparison assessment of BIPV façade semi-transparent modules: further insights on human comfort conditions," Energy Procedia, vol. 48, pp. 1419-1428, 2014.

[93] M. Wang, J. Peng, N. Li, L. Lu, T. Ma, H. Yang, "Assessment of energy performance of semi-transparent PV insulating glass units using a validated simulation model," Energy, vol. 112, pp. 538-548, 2016.

[94] J. Peng, L. Lu, H. Yang, "An experimental study of the thermal performance of a novel photovoltaic double-skin facade in Hong Kong," Solar Energy, vol. 97, pp. 293-304, 2013.

[95] A.S. Kaiser, B. Zamora, R. Mazón, J.R. García, F. Vera, "Experimental study of cooling BIPV modules by forced convection in the air channel," Applied Energy, vol. 135, pp. 88-97, 2014.

[96] J. Peng, L. Lu, H. Yang, T. Ma, "Comparative study of the thermal and power performances of a semi-transparent photovoltaic façade under different ventilation modes," Applied Energy, vol. 138, pp. 572-583, 2015.

[97] J. Peng, L. Lu, H. Yang, "Review on life cycle assessment of energy payback and greenhouse gas emission of solar photovoltaic systems," Renewable and Sustainable Energy Reviews, vol. 19, pp. 255-274, 2013.

[98] M. Fossa, C. Menezo, E. Leonardi, "Experimental natural convection on vertical surfaces for building integrated photovoltaic (BIPV) applications," Experimental Thermal and Fluid Science, vol. 32, pp. 980-990, 2008.

[99] J. Han, L. Lu, H. Yang, "Numerical evaluation of the mixed convective heat transfer in a double-pane window integrated with see-through a-Si PV cells with low-e coatings," Applied Energy, vol. 87, pp. 3431-3437, 2010.

[100] W. He, Y.X. Zhang, W. Sun, J.X. Hou, Q.Y. Jiang, J. Ji, "Experimental and numerical investigation on the performance of amorphous silicon photovoltaics window in East China," Building and Environment, vol. 46, pp. 363-369, 2011.

[101] J. Han, L. Lu, J. Peng, H. Yang, "Performance of ventilated double-sided PV facade compared with conventional clear glass façade," Energy and Buildings, vol. 56, pp. 204-209, 2013.

[102] B. Agrawal, G.N. Tiwari, "Life cycle cost assessment of building integrated photovoltaic thermal (BIPVT) systems," Energy and Buildings, vol. 42, pp. 1472-1481, 2010.

[103] K. Vats, G.N. Tiwari, "Performance evaluation of a building integrated semi-transparent photovoltaic thermal system for roof and façade," Energy and Buildings, vol. 45, pp. 211-218, 2012.

[104] K. Vats, G. N. Tiwari, "Energy and exergy analysis of a building integrated semi-transparent photovoltaic thermal (BISPVT) system," Applied Energy, vol. 96, pp. 409-416, 2012.

[105] N. Aste, L.C. Tagliabue, C. Del Pero, D. Testa, R. Fusco, "Performance analysis of a large area luminescent solar concentrator module," Renewable Energy, vol. 76, pp. 330-337, 2015.

]106] J. Han, L. Lu, H. Yang, "Thermal behavior of a novel type see-through glazing system with integrated PV cells," Building and Environment, vol. 44, pp. 2129-2136, 2009

[107] G. Gan, "Numerical determination of adequate air gaps for building-integrated photovoltaics," Solar Energy, Vol 83, pp. 1253-1273, 2009.

[108] T.T. Chow, G. Pei, L.S. Chan, Z. Lin, K.F. Fong, "A Comparative Study of PV Glazing Performance in Warm Climate," Indoor and Built Environment, vol. 18, pp. 32-40, 2009.

[109] O. Zogou, H. Stapountzis, "Energy analysis of an improved concept of integrated PV panels in an office building in central Greece," Applied Energy, vol. 3, pp. 853-866, 2011.

[110] Y. Chen, A. K. Athienitis, K. Galal, "Modeling, design and thermal performance of a BIPV/T system thermally coupled with a ventilated concrete slab in a low energy solar house: part 1, BIPV/T system and house energy concept," Solar Energy, vol. 11, pp. 1892-1907, 2010.

[111] T. T. Chow, Z. Qiu, C. Li, Q. Zhongzhu, C. Li, "Potential application of ‘‘see-through’’ solar cells in ventilated glazing in Hong Kong," Solar Energy Materials & Solar Cells, vol. 93, pp. 230-238, 2009.

[112] G. Gan, S. B. Riffat, "CFD modelling of air flow and thermal performance of an atrium integrated with photovoltaics," Building and Environment, vol. 39, pp. 735-748, 2004.

[113] S. Dubey, G.S. Sandhu, G.N. Tiwari, "Analytical expression for electrical efficiency of PV/T hybrid air collector," Applied Energy, vol. 86, pp. 697-705, 2009.

[114] A. Gaur, G.N. Tiwari, "Performance of a-Si thin film PV modules with and without water flow: An experimental validation," Applied Energy, vol. 128, pp. 184-191, 2014.

[115] R. Charron, A. K. Athienitis, "Optimization of the performance of double-facades," Solar Energy, vol. 80, pp. 481-491, 2006.

[116] A. Sayyah, M. N. Horenstein, M. K. Mazumder, "Energy yield loss caused by dust deposition on photovoltaic panels," Solar Energy, vol. 107, pp. 576-604, 2014.

[117] L. Lu, K. M. Law, "Overall energy performance of semi-transparent single-glazed photovoltaic (PV) window for a typical office in Hong Kong," Renewable Energy, vol. 49, pp. 250-254, 2013.

[118] E. L. Didone, A. Wagner, "Semi-transparent PV windows: A study for office buildings in Brazil," Energy and Buildings, vol. 67, pp. 136–142, 2013.

[119] M. Ordenes, D. LMarinoski, P. Braun, R. Ruther, "The impact of building integrated Photovoltaics on the energy demand of multi-family dwellings in Brazil," Energy and Building, vol. 39, pp. 629–42, 2007

[120] S. A. Bahaj, P. A.B. James, M. F. Jentsch, "Potential of emerging glazing technologies for highly glazed buildings in hot arid climates," Energy and Buildings, vol 40, pp. 720-731, 2008.

[121] P. R. Defaix, WGJHM van Sark, E. Worrell, E. de Visser, "Technical potential for photovoltaics on buildings in the EU-27," Solar Energy, vol. 9, pp. 2644-2653, 2012.

[122] L. Olivieri, E. Caamano-Martín, F.J. Moralejo-Vazquez, N. Martín-Chivelet, F. Olivieri, F.J. Neila-Gonzalez, "Energy saving potential of semi-transparent photovoltaic elements for building integration," Energy, vol. 76, pp. 572-583, 2014

[123] P. Lotfabadi, "Solar considerations in high-rise buildings," Energy and Buildings, vol. 89, pp. 183-195, 2015.

[124] A. F. Infantes, J. Contreras, J. J. B. Agustín, "Design of grid connected PV systems considering electrical, economical and environmental aspects: a practical case," Renewable Energy, vol. 13, pp. 2042-62, 2006

[125] P. Eiffert, L. L. C, ImaginIt, "Guidelines for the Economic Evaluation of Building Integrated Photovoltaic Power Systems," International Energy Agency PVPS Task 7-05:2002, Task No. PVP28201.

[126] P. K. Ng, N. Mithraratne, "Lifetime performance of semi-transparent building-integrated photovoltaic (BIPV) glazing systems in the tropics," Renewable and Sustainable Energy Reviews, vol. 31, pp. 736-745, 2014.

[127] V.M. Fthenakis, H.C. Kim, "Photovoltaics: Life-cycle analyses," Solar Energy, vol. 85, pp. 1609-1628, 2011.

[128] A. Chel, G.N. Tiwari, A. Chandra, "Simplified method of sizing and life cycle cost assessment of building integrated photovoltaic system," Energy and Buildings, vol. 41, pp. 1172-1180, 2009.

[129] D. H.W. Li, T. N.T. Lam, W. W.H. Chan, A. H.L. Mak, "Energy and cost analysis of semi-transparent photovoltaic in office buildings," Applied Energy, vol. 86, pp. 722-729, 2009.

[130] P.A.B. James, M.F. Jentsch, A.S. Bahaj, "Quantifying the added value of BiPV as a shading solution in atria," Solar Energy, vol. 83, pp. 220-231, 2009.

[131] D. Kamthania, G.N. Tiwari, "Energy metrics analysis of semi-transparent hybrid PVT double pass facade considering various silicon and non-silicon based PV module Hyphen is accepted," Solar Energy, vol. 100, pp. 124-140, 2014.

[132] H. Radhi, "Energy analysis of facade-integrated photovoltaic systems applied to UAE commercial buildings," Solar Energy, vol. 84, pp. 2009-2021, 2010.

[133] M. S. Buker, B. Mempouo, S. B. Riffat, "Performance evaluation and techno economic analysis of a novel building integrated PV/T roof collector: An experimental validation," Energy and Buildings, vol. 76, pp. 164-175, 2014.

[134] "Applications and Use of Integrating Spheres," [Online] PerkinElmer. [Cited: 15 3 2016.] https://www. perkinelmer.com/CMSResources/Images/4474191APP _LAMBDA 650IntegratingSpheres.pdf.

[135] E. Skoplaki, J.A. Palyvos, "On the temperature dependence of photovoltaic module electrical performance: A review of efficiency/power correlations," Solar Energy, vol. 83, pp. 614-624, 2009.

[136] E.U.Finlayson, D.K. Arastech, C. Huizenga, M.D.Rubin. "WINDOW 4.0: Documentation of calculation procedure," Berkeley, The USA, Energy and Environment Division, Lawrence Berkeley Laboratory, 1993.

[137] Engineering Reference. "The Reference to EnergyPlus Calculations," Washington DC, USA: US Department of Energy, 2014.

[138] Input Output Reference: "The Encyclopedic Reference to EnergyPlus Input and Output," Washington DC, USA: U S Department of Energy, 2014.

[139] Caprioli, Tiziano, "Simulation models for Cooling load reduction by ventilation strategies," [Online] [Cited: 15 01 2017.] http://www.eurac.edu/en/research /technologies/renewableenergy/publications/Documents/Tesi_Caprioli_Tiziano.p df.

[140] "Non-residential cooling and heating load calculation procedures," [Online] ASHRAE. [Cited: 15 2 2017.]http://www.gordonprill.net/documents-online/ HGST%20CO2%20Skid%20A100%20Linde%20Installation/IFB%2092915/HG ST%20Specs/Z%20Ashrae/ I p/ 200 1/4 VOL_FpCh29.pdf.

[141] Bureau of Indian Standards (BIS), National Building Code of India, 2016.

[142] ECBC, "Energy Conservation Building Code," New Delh, India: Bureau of Energy Efficiency, 2007.

[143] S. Kumar, J. Mathur, S. Mathur, M.K. Singh, V. Loftness, "An adaptive approach to define thermal comfort zones on psychrometric chart for naturally ventilated

buildings in composite climate of India," Building and Environment, vol. 109, pp. 135-153, 2016.

[144] India Meteorological Department (IMD) Meteorological Centre Jaipur. [Online] [Cited: 15 03 2017.] http://amssdelhi.gov.in/Nigam/JAIPUR30/jaipur2.htm.

[145] "Solar Irradiance," [Online] Synergy Enviro Engineers. [Cited: 15 03 2017.] http://www.synergyenviron.com/tools/solar-irradiance/Jaipur%252CRajasthan %252CIndia.

[146] S. C. Singh, [Book] "Solar Photovoltaics, Fundamental, Technology and Applications," New Delhi: PHI Learning Pvt. Ltd., 2011.

[147] M. Lee and A. Panchula, "Spectral correction for photovoltaic module performance based on air mass and perceptible water," IEEE 43rd Photovoltaic Specialists Conference (PVSC), Portland, USA, 2016.

[148] W. M. Keogh, A. W. Blakers, "Accurate Measurement, Using Natural Sunlight of Silicon Solar Cells," Progress in Photovoltaic: Research and Applications, vol. 12, pp. 1-19, 2004.

[149] D. L. King, J. A. Kratochvil, W. E. Boyson, "Measuring solar spectral and angle-of-incidence Effects on Photovoltaic modules and solar irradiance sensors," 26th IEEE Photovoltaic Specialists Conference, CA, USA, 29 Sep - 3 Oct, 1997.

[150] Instruction Manual for gSKIN® U-Value Kit. [Online] 19 04 2016. [Cited: 15 09 2016.]https://www.greenteg.com/template/userfiles/files/gSKIN_UValue%20KIT_Manual_SW_ Version1.02.04.pdf.

[151] W. Lia, B. James, S. Dale, S. John, A. Erica, D. Steve, F. David, F. Ellen, J. David, S. Steve, S. Mark, S. Bob, "M&V Guidelines: Measurement and Verification for Performance-Based Contracts Version 4.0," [Online] 2015. [Cited: 14 3 2017.] https://energy.gov/ sites/prod/files/2016/01/f28/ mv_guide_4_0.pdf.

[152] "White Box Technologies Weather Data," [Online] 2014. [Cited: 25 02 2015.] http://weather. whiteboxtechnologies.com/ISHRAE.

1. Module datasheet [STPV module PV3]

SOLARFIRST

Solar First
S1 Series

CdTe Thin-Film
Photovoltaic Module

Warranty:

- 10 years materials and workmanship.
- 25 years power output guarantee for 90% of nominal output during first 10 years and 80% over 25 years.
- Modules are life cycle managed with a collection and recycling program, providing module owners with no cost， end-of-life take back, and recycling of the modules.

Electrical Specifications

(performance at STC: 1000W/m ², 25° C, AM1.5)

Specification	SF-ST1-56
Nominal Power(Pm)	56W
Open Circuit Voltage(Voc)	116V
Shot Circuit Current (Isc)	0.68A
Voltage at max. Power(Vm)	87V
Current at max. Power(Im)	0.64A
Transparency	30%

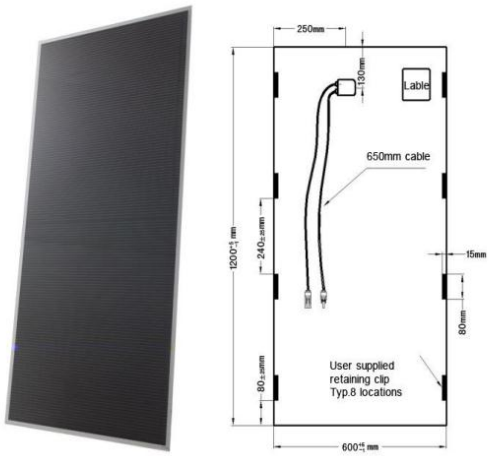

System Properties (at STC)

Maximum System Voltag	V_{SYS}(V)	1000(600UL)
Limiting Reverse Current	I_R(A)	2
Maximum Series Fuse	I_{CF}(A)	2

Temperature Coefficients (at STC)

Temperature Coefficients of Isc	α=0.060%/°C
Temperature Coefficients of Voc	β=-0.321%/°C
Temperature Coefficients of Pm	γ=-0.214%/°C

Mechanical Specifications

Length	1200mm
Width	600mm
Thickness	6.8mm
Area	0.72m ²
Weight	11.8kg
Frame	None
Lead Cable	2.5mm² 700mm
Connectors	MC4
Bypass Diode	10A
Cell Type	Cadmium Telluride (CdTe)
Cover Type	3.2+0.76EVA/PVB+3.2mm
Back Glass	Tempered/Tinted/UV
Encapsulation	EVA / PVB

Figure A-1: Data sheet of PV3 STPV module provided by the manufacturer

2. Drawing on the window system

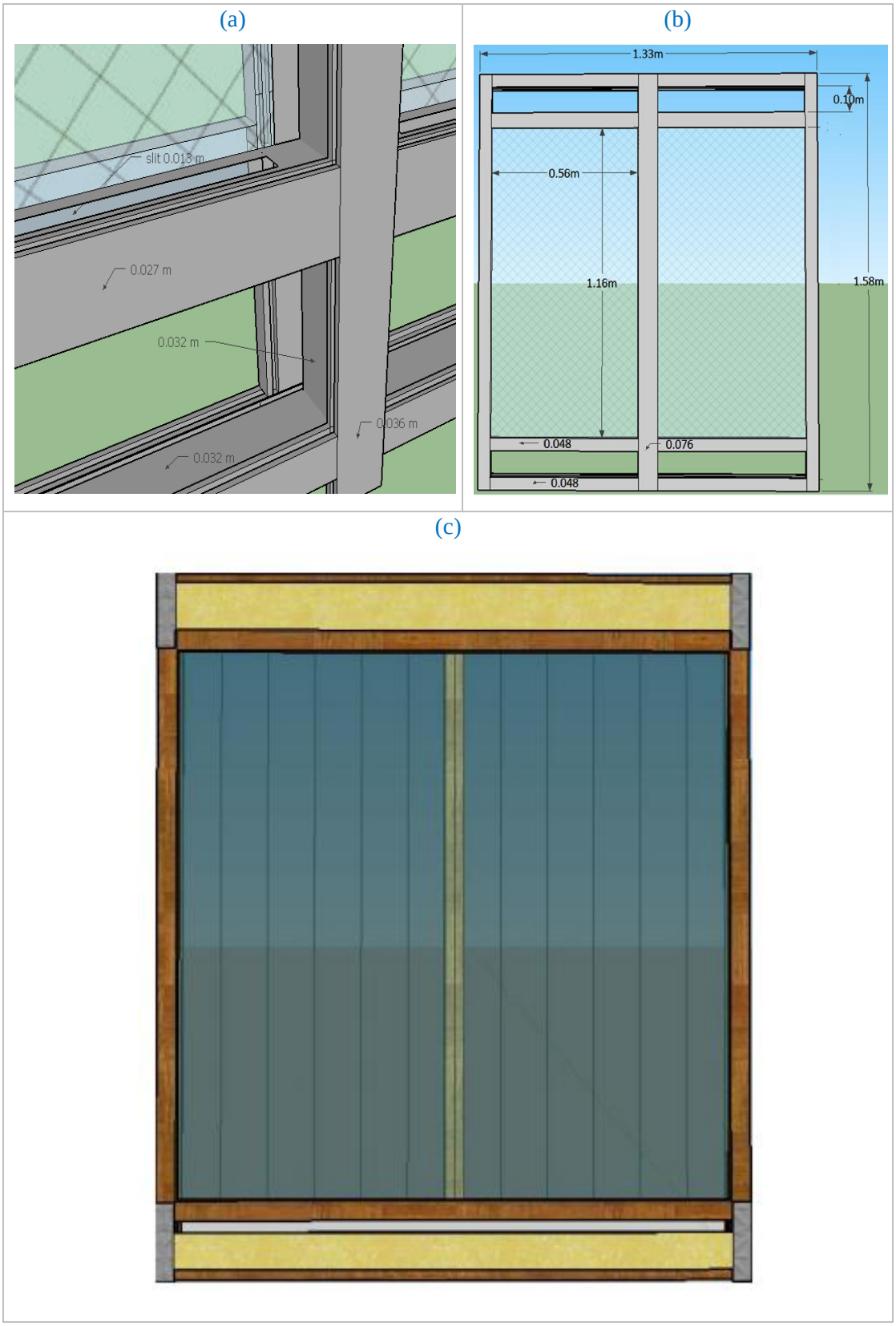

Figure A-2: Stages of the window systems development in software (a) dimension of the frame (b) Total and glazing dimension (c) Rendered image of the window systems

3. Drawing of the test chamber

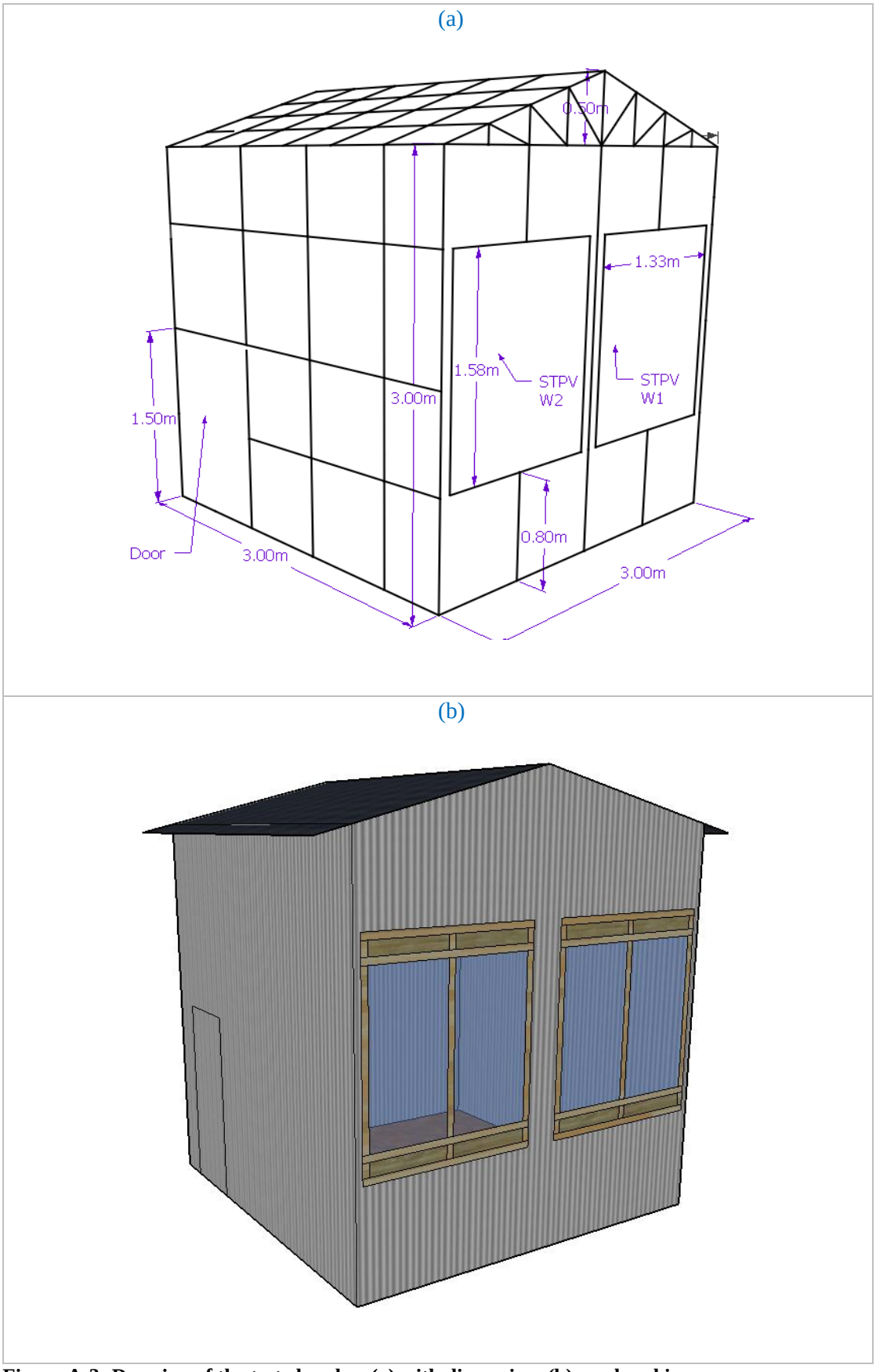

Figure A-3: Drawing of the test chamber (a) with dimension, (b) rendered image

4. Construction of the test chamber

(a) (b)

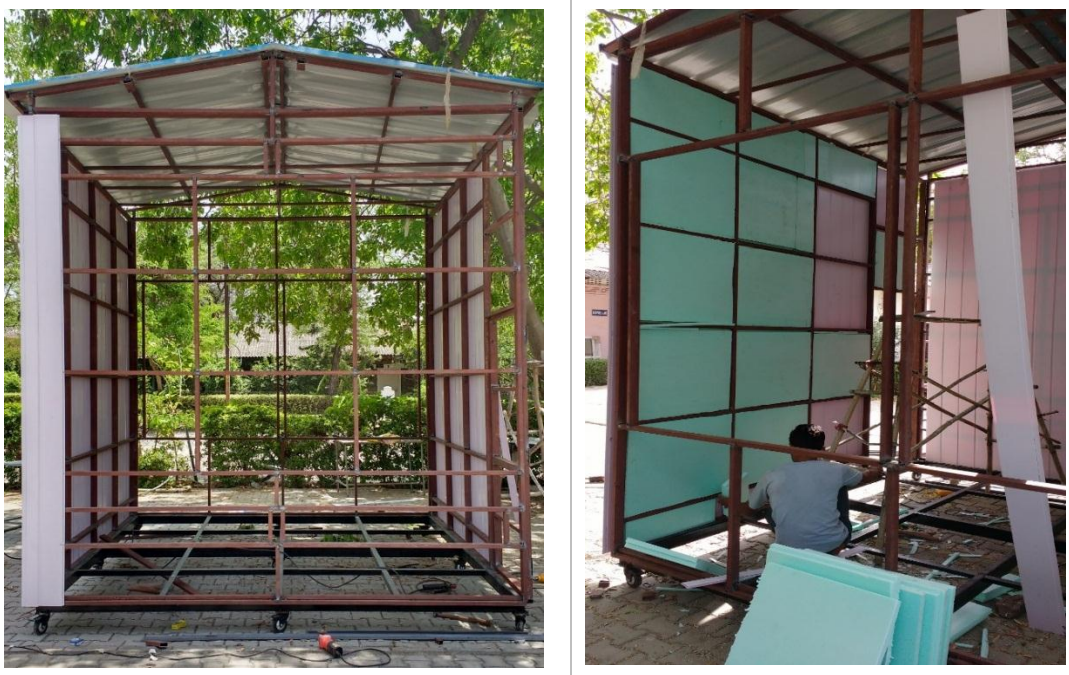

Figure A-4: Different stages of the test chamber development (a) M.S. skeleton, (b) Insulating the wall

5. Internal view of the test chamber

Figure A-5: Internal view of the test changer with different instruments

6. U-value of the wall

greenTEG

Measurement result:

Logger data:		**Mean measured values:**	
Serial No:	319553	Heat Flux (HF):	-0.6 W/m²
Type:	U-value measurement kit	Inside temp. (T1):	28.8 °C
Sensitivity:	16.8 uV/(W/m²)	Outside temp. (T2):	27.4 °C
		Measurement time (t):	88.50 h

U-value analysis using average method (Section 7.1, ISO 9869-1:2014):

Analysis start time:	2017-08-25 09:11:26	U-value w/o last 24h (U24):	0.54 W/(m²K)
Analysis end time:	2017-08-28 09:11:26	U-value first 2/3 (U2/3):	0.54 W/(m²K)
Analysis period:	72 h	U-value last 2/3 (U2/3):	0.53 W/(m²K)
U-value:	0.52 W/(m²K)	dU24:	-3.5 %
		dU2/3:	2.7 %
		dR24:	3.9 %
		dR2/3:	-3.0 %

Measurement data fulfils requirements of ISO 9869-1:2014 section 7.1.
Uncertainties due to improper installation or environmental influences must be estimated by user (see section 6.1).

Additional comments:

Measurement overview over t=88.50 h

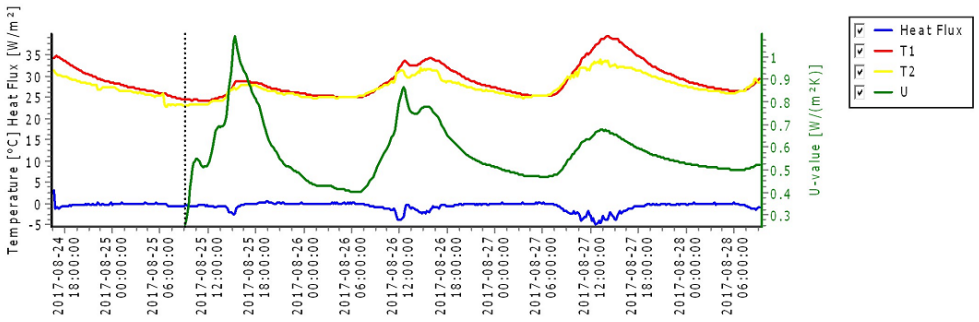

Figure A-6: Measured U-value of the test chamber's wall

BRIEF BIO-DATA OF THE AUTHOR

Mr. Sankar Barman is a research scholar in Centre for Energy and Environment, Malaviya National Institute of Technology (MNIT), Jaipur. He has received his Master of Technology (M. Tech.) degree in Energy Studies from Indian Institute of Technology Delhi (IIT-D) in 2011. He worked in the research and product development industries before joining in the Ph.D. programme, January 2015. His research interests are renewable energy system modeling and product development, energy efficiency, photovoltaic application in building, solar thermal technology, and energy storage system.

LIST OF PUBLICATIONS

1. **Sankar Barman,** Amartya Chowdhury, Sanjay Mathur, Jyotirmay Mathur, "Assessment of the efficiency of window integrated CdTe based semi-transparent photovoltaic module," **Sustainable Cities and Society,** vol. 37, pp. 250–262, 2018.

2. **Sankar Barman,** Amartya Chowdhury, Sanjay Mathura, Jyotirmay Mathura, Praloy Mondalb, Debajyoti Das, "A simplified approach for performance evaluation of semi-transparent photovoltaic window," **Energy Strategy Reviews** [Communicated, ESR-S-17-00419].

3. **Sankar Barman,** Amartya Chowdhury, Sanjay Chhettri, Sanjay Mathur, Jyotirmay Mathur, "Angular loss of window integrated semi-transparent photovoltaic modules- An analysis," **Sustainable Energy Technologies and Assessments Journal** [Communicated, SETA_2018_1].

4. **Sankar Barman,** Amartya Chowdhury, Sanjay Mathur, Jyotirmay Mathur, "Effects of window configuration and air ventilation strategy on energy generation of window integrated semi-transparent SPV module," **Solaris 2017**, a national conference on Renewable Energy Sources for Sustainable Climate, IIT BHU, 7-9 Feb, Varanasi, India.